

**REMOVAL OF ANIONIC CONTAMINANTS BY  
ENVIRONMENTAL-FRIENDLY ENGINEERED  
MATERIALS**

**WEI YUTING**

**NATIONAL UNIVERSITY OF SINGAPORE**

**2011**

**REMOVAL OF ANIONIC CONTAMINANTS BY  
ENVIRONMENTAL-FRIENDLY ENGINEERED  
MATERIALS**

**WEI YUTING**

*(M.Eng., Xi'an Jiaotong University)*

**A THESIS SUBMITTED FOR  
THE DEGREE OF DOCTOR OF PHILOSOPHY  
DEPARTMENT OF CIVIL AND ENVIRONMENTAL  
ENGINEERING  
NATIONAL UNIVERSITY OF SINGAPORE**

**2011**

## **ACKNOWLEDGEMENTS**

I would like to express my deep and sincere gratitude to everyone who has supported me to complete the doctoral study.

First and foremost, I am deeply grateful to my supervisor, Associate Prof. J. Paul Chen for his valuable advice and support all along my work. His scientific spirit, personal guidance and endless encouragement were a great help during the entire study. It is his constructive criticisms and numerous corrections in my manuscripts to get the thesis in present form.

Furthermore, I wish to express my gratitude to all my research group members who I have always collaborated with. Special thanks must also go out to Mr Zou Shuaiwen who has been an excellent guider patiently assisting me through the research methodology and experimental techniques throughout this period. I also want to sincerely thank Dr. Zheng Yuming, Ms. K.G.Nadeeshani Nanayakkara, Mr. Ma Yue, and Ms. Lim Soh Fong for their support, views, and friendless.

This study also benefited from endless technical support of the professional officers and laboratory staffs, especially Ms. Susan Chia, Mr. Sukiantor Bin Tokiman, Mr. Mohamed Sidek Bin Ahmad, of the Department of Civil and Environmental Engineering at the National University of Singapore.

On a personal level, I am deeply indebted to my family members. First, I wish to express my heartfelt gratitude to my grandma Lu Mingzhen, father Wei Lekui as well

## *Acknowledgements*

---

as mother Lei Zuhua for their deepest and endless love, care and encouragement. Then, my gratefulness is to my beloved husband, Zhang Xing, for his everlasting love, patience, trust, and care. I strongly believe that I wouldn't have come this so far without his accompany. Thanks very much for always bearing my stress and taking care of me during the bad days of my life. Next, I am sincerely thankful to my uncles, aunts, and cousins for their continuous support all the while.

The financial support from the National University of Singapore is greatly appreciated. Without their support, my desire to pursue doctoral study is difficult to be realized.

## **TABLE OF CONTENTS**

<b>ACKNOWLEDGEMENTS .....</b>	<b>I</b>
<b>TABLE OF CONTENTS .....</b>	<b>III</b>
<b>SUMMARY .....</b>	<b>X</b>
<b>LIST OF TABLES .....</b>	<b>XIII</b>
<b>LIST OF FIGURES .....</b>	<b>XV</b>
<b>LIST OF ABBREVIATIONS .....</b>	<b>XX</b>
<b>NOMENCLATURE.....</b>	<b>XXIV</b>
<b>CHAPTER 1 INTRODUCTION.....</b>	<b>1</b>
1.1 BACKGROUND.....	1
1.2 OBJECTIVES .....	4
<b>CHAPTER 2 LITERATURE REVIEW.....</b>	<b>7</b>
2.1 BORON .....	7
2.1.1 <i>Solution chemistry</i> .....	7
2.1.2 <i>Boron in aqueous environment</i> .....	9
2.1.3 <i>Toxic effects of boron and current regulations</i> .....	13
2.1.4 <i>Available treatment technologies</i> .....	15
2.1.4.1 Chemical precipitation .....	15
2.1.4.2 Liquid-liquid extraction .....	16

2.1.4.3 Electrocoagulation .....	16
2.1.4.4 Membrane filtration .....	18
2.1.4.5 Sorption.....	20
2.2 ARSENATE AND METHYLATED ARSENIC .....	23
2.2.1 <i>Arsenic species</i> .....	23
2.2.2 <i>Occurrence and sources of arsenic in natural water</i> .....	25
2.2.3 <i>Health effects and regulatory issues</i> .....	27
2.2.4 <i>Existing technologies for arsenic removal</i> .....	29
2.2.4.1 Coagulation/precipitation.....	29
2.2.4.2 Ion exchange .....	32
2.2.4.3 Membrane techniques .....	33
2.2.4.4 Biological processes.....	35
2.2.4.5 Sorption.....	37
2.4 MODELS FOR SORPTION EQUILIBRIUM .....	42
2.5 MODELS FOR SORPTION KINETICS.....	44
<b>CHAPTER 3 MATERIALS AND METHODS.....</b>	<b>48</b>
3.1 MATERIALS .....	48
3.2 PREPARATION OF CHITOSAN-BASED SORBENTS .....	49
3.2.1 <i>Preparation of crosslinked chitosan beads</i> .....	49
3.2.2 <i>Immobilization of the initiator on the crosslinked chitosan beads</i> .....	51
3.2.3 <i>Surface-initiated atom transfer radical polymerization</i> .....	51

3.2.4 Preparation of NMDG modified CTS-PGMA.....	51
3.3 SURFACE MODIFICATION OF CELLULOSE MEMBRANES .....	52
3.3.1 Pretreatment of RC membranes.....	52
3.3.2 Surface initiation.....	52
3.3.3 Surface-initiated polymerization on cellulose membranes.....	53
3.3.4 NMDG functionalization.....	53
3.4 PHYSICAL CHARACTERIZATIONS .....	53
3.4.1 Specific surface area.....	53
3.4.2 Surface charge density.....	54
3.4.3 Contact angle.....	54
3.5 BATCH EXPERIMENTS.....	55
3.5.1 Boron, arsenic, TOC, IC and pH analyses .....	55
3.5.2 Sorption of boron.....	55
3.5.3 Inorganic arsenic and methylated arsenic.....	57
3.5.4 Leaching tests.....	58
3.6 SPECTROSCOPIC ANALYSES.....	59
3.6.1 Microscope and Scanning Electron Microscopy.....	59
3.6.2 Fourier Transform Infrared Spectroscopy.....	59
3.6.3 Attenuated Total Reflection - Fourier Transform Infrared Spectroscopy .	60
3.6.4 X-Ray Photoelectron Spectroscopy.....	60
<b>CHAPTER 4 SURFACE MODIFICATION OF CHITOSAN VIA ATOM TRANSFER RADICAL POLYMERIZATION.....</b>	<b>62</b>

4.1 SORBENT PREPARATION.....	63
4.2 SURFACE MODIFICATION REACTIONS .....	66
4.2.1 Characterization of CCTS.....	66
4.2.2 Immobilization of the ATRP initiator on CCTS Surface.....	68
4.2.3 Surface Initiated ATRP from Chitosan Surface.....	71
4.2.4 Functionalization of CTS-PGMA surface.....	74
4.3 MATERIAL CHARACTERIZATION.....	76
4.3.1 Morphologies observation of the sorbent .....	77
4.3.2 Specific surface area.....	78
4.3.3 Surface charge density.....	80
4.3.4 Leaching study.....	81
4.4 SECTION SUMMARY.....	82
<b>CHAPTER 5 BORON SORPTION ONTO NMDG MODIFIED CHITOSAN SORBENT: SORPTION BEHAVIOR AND MECHANISM STUDY.....</b>	<b>83</b>
5.1 EQUILIBRIUM STUDIES .....	84
5.1.1 Effect of solution pH on boron sorption .....	84
5.1.2 Sorption isotherm.....	87
5.2 KINETICS STUDY .....	93
5.2.1 Boron sorption kinetics and its modeling simulation .....	93
5.2.2 Sensitivity analysis of the model parameters.....	94
5.3 EFFECT OF IONIC STRENGTH ON BORON REMOVAL .....	96



5.4 APPLICATION OF BORON REMOVAL FROM SIMULATED SEAWATER .....	98
5.5 MECHANISM STUDY .....	100
5.6 SECTION SUMMARY .....	104
<b>CHAPTER 6 ENHANCED SORPTION OF ARSENIC ONTO NMDG MODIFIED CHITOSAN SORBENT (I): INORGANIC ARSENIC.....</b>	<b>105</b>
6.1 EQUILIBRIUM STUDIES .....	106
6.1.1 <i>Effect of solution pH</i> .....	106
6.1.2 <i>Sorption isotherm</i> .....	109
6.2 SORPTION KINETICS UNDER DIFFERENT IONIC STRENGTH EFFECT .....	110
6.3 SIMULTANEOUS SORPTION OF ARSENATE AND NATURAL ORGANIC MATTER.....	113
6.4 COMPETITIVE SORPTION.....	115
6.5 FTIR ANALYSIS.....	117
6.6 XPS ANALYSIS .....	118
6.7 SECTION SUMMARY .....	120
<b>CHAPTER 7 ENHANCED SORPTION OF ARSENIC ONTO NMDG MODIFIED CHITOSAN SORBENT (II): METHYLATED ARSENIC .....</b>	<b>122</b>
7.1 EQUILIBRIUM STUDIES .....	123
7.1.1 <i>Effect of pH</i> .....	123
7.1.2 <i>Sorption isotherm</i> .....	126
7.2 SORPTION KINETICS UNDER DIFFERENT IONIC STRENGTH .....	129
7.3 EFFECT OF NATURAL ORGANIC MATTER .....	130

7.4 EFFECT OF COEXISTING ANIONS .....	132
7.5 SPECTROSCOPIC ANALYSIS .....	134
7.6 SECTION SUMMARY .....	136
<b>CHAPTER 8 FUNCTIONALIZATION OF REGENERATED CELLULOSE MEMBRANES FOR BORON REMOVAL .....</b>	<b>138</b>
8.1 MEMBRANE SURFACE MODIFICATION .....	139
8.2 SURFACE CHARACTERIZATION .....	140
8.2.1 ATR-FTIR analysis.....	140
8.2.2 XPS analysis.....	142
8.2.3 Water contact angle analysis.....	146
8.2.4 Surface morphology of membranes .....	148
8.3 BORON SORPTION .....	150
8.3.1 Effect of pH .....	150
8.3.2 Sorption isotherm.....	151
8.3.3 Ionic strength effect.....	152
8.4 MECHANISM STUDY .....	154
8.5 SECTION SUMMARY .....	155
<b>CHAPTER 9 CONCLUSIONS AND RECOMMENDATIONS .....</b>	<b>157</b>
9.1 CONCLUSIONS .....	157
9.2 RECOMMENDATIONS .....	161
<b>REFERENCES.....</b>	<b>163</b>

**PUBLICATIONS** ..... 186

## **SUMMARY**

In this study, two novel polymeric materials, chitosan-based polymeric sorbent (CTS-MG) and cellulose-based adsorptive membrane (RC-MG), were synthesized for an efficient sorption of boron and arsenic. Equilibrium and kinetic studies with these two materials were carried out under various physicochemical conditions. A comprehensive understanding of sorption mechanisms was conducted via instrumental analysis.

N-methyl-D-glucamine (NMDG) was immobilized onto crosslinked chitosan (CCTS) via electrostatic extrusion and surface polymerization techniques. Surface initiators were initially immobilized on CCTS through the interaction between surface hydroxyl and amine groups and 2-bromoisobutyrate bromide. Glycidyl methacrylate (GMA) polymer brushes were grafted to the surface-initiated chitosan at ambient temperature. Epoxide functional groups of the grafted poly(glycidyl methacrylate) (PGMA) further reacted with NMDG to create the affinity binding sites for boron.

The SEM and BET studies revealed that chemical modification resulted in a rough surface and porous structure compared to raw chitosan. It was demonstrated that boron uptake capacity of CTS-MG was significantly enhanced after surface modification. At the optimum neutral pH, the maximum sorption capacity was as high as 2.84 mmol/g, much higher than those of commercial boron selective resins (e.g. Amberlite IRA-743) and many other synthesized sorbents. Almost 90 % of boron sorption occurred within 8 h and the experimental data was well fitted by an

intraparticle surface diffusion model. Existence of sodium chloride and sodium nitrate had little effect on boron removal, implying formation of inner-sphere surface complexes on the sorbent. Furthermore, simulated seawater was employed to evaluate the actual application of the sorbent. The final boron concentration of less than 0.5 mg/L is achievable at the dose of sorbent > 1.2 g/L, of which the removal efficiency is above 90 %. The interaction between boron and surface functional groups on the novel sorbent was also explored by FT-IR and XPS. The oxygen in the form of secondary alcohol played an important role in boron sorption, and the tetrahedral B complexes were finally present on the surface of novel sorbent.

Laboratory experiments were also carried out to investigate sorption behaviors of inorganic arsenic as well as methylated arsenic species, monomethylarsonic acid (MMA) and dimethylarsinic acid (DMA) onto CTS-MG. Surface modification of crosslinked chitosan was found to increase the sorption capabilities and affinities of both inorganic and organic arsenic species. Arsenic sorption was highly pH-dependent and the maximum sorption capacities were 69.28 mg/g for arsenate (pH 3), 15.4 mg/g for MMA (pH 3.4) and 7.1 mg/g for DMA (pH 5), exhibiting competitive advantages with other reported materials. Affinity of these three species to CTS-MG decreased in the sequence of arsenate > MMA > DMA. Most of the arsenic was rapidly adsorbed in the first 5 h, followed by a relatively slow process. Results also showed that the uptake of MMA and DMA was sensitive to the existence of background electrolytes, suggesting that both inorganic and organic arsenic species formed outer-sphere complexes on the sorbent surface. Presence of natural organic matter was unfavorable for arsenic removal; simultaneous uptake of organic

contaminants such as humic acid was observed in this study as well. Effects of co-existing anions (e.g.  $F^-$ ,  $PO_4^{3-}$ ,  $SO_4^{2-}$ ) in natural water on arsenic removal decreased in the order of sulfate > phosphate > fluoride. Spectroscopic analyses also verified the successful attachment of both inorganic and organic arsenic species, which was mainly due to tertiary amine and polyhydroxyl functions on the surface of CTS-MG.

Cellulose-based adsorptive membrane was also prepared for efficient boron removal through a three-step surface modification of regenerated cellulose (RC) membranes. The pristine and modified membranes were characterized by ATR-FTIR, XPS, SEM and dynamic water contact angle measurement. Results show that the designed functional groups have been successfully grafted onto RC substrates, and surface functionalization contributes to higher boron binding capability. The optimal pH for boron sorption falls in a wide range from 4 to 8. Under neutral pH condition, the maximum sorption capacity of the modified membrane is determined to be 0.75 mmol/g, which is comparable with those of commercial resins. Studies of electrolytes influence indicate the formation of inner-sphere surface complexes on the membrane surface. The ATR-FTIR and XPS analyses also reveal the involvement of hydroxyl and amine functionalities of the adsorptive membrane for boron removal, as well as the presence of tetrahedral boron complexes in the membrane surface.

## **LIST OF TABLES**

Table 2.1 Boron concentration in water from different countries .....	10
Table 2.2 Relative tolerance of agricultural crops to boron.....	14
Table 2.3 Sorption of boron by different sorbents.....	21
Table 2.4 Structure and pK <sub>a</sub> values for various arsenic species .....	25
Table 2.5 Occurrence of arsenic in groundwater and estimated population in affected countries.....	26
Table 2.6 Arsenic sorption capacities of selected iron oxides/oxyhydroxide based sorbents .....	41
Table 4.1. Operational parameters of electrostatic extrusion for preparation of chitosan beads .....	64
Table 4.2. Assignment of IR bands for CCTS .....	67
Table 4.3 Binding energy and relative content of C and N in CCTS and CTS-Br.....	70
Table 4.4 Binding energy and relative content of C and O in CTS-PGMA and CTS-MG .....	74
Table 4.5 Leaching characteristics of CTS-MG at different pH.....	82
Table 5.1 Isotherm parameters for B sorption on CTS-MG, CCTS and Amberlite IRA-743. ....	89
Table 5.2 Comparison of boron sorption capacities on several synthesized materials	91

Table 5.3 Chemical composition of simulated seawater (pH = 8.1).....	98
Table 6.1 Isotherm parameters for arsenate sorption on CCTS and CTS-MG.....	110
Table 7.1 Parameters of the isotherm models.....	127
Table 7.2 Comparison of methylated arsenic sorption onto several sorbents reported in literature.....	128
Table 8.1 Elemental surface composition of pristine and modified RC membranes determined from XPS .....	142
Table 8.2 Binding energy and relative content of C in pristine and modified RC membranes.....	145



## LIST OF FIGURES

Figure 2.1. Schematic of basic electrocoagulation system .....	17
Figure 2.2. Eh-pH diagram for aqueous As species in the system As-O <sub>2</sub> -H <sub>2</sub> O at 25 °C and 1 bar total pressure .....	24
Figure 3.1. Electrostatic droplet generating system.....	50
Figure 4.1. Pictures of chitosan beads .....	64
Figure 4.2. Schematic diagram illustrating the preparation of CTS-MG via ATRP ..	65
Figure 4.3. FITR spectra of (a) CCTS, (b) CTS-PGMA, (c) CTS-MG.....	66
Figure 4.4. XPS (a) wide scan, (b) N 1s, and (c) C 1s core-level spectra of CCTS ...	68
Figure 4.5. XPS (a) wide scan, (b) Br 3d, (c) C 1s, and (d) N 1s core-level spectra of CTS-Br.....	69
Figure 4.6. XPS (a) wide scan, (b) C 1s, and (c) O 1s core-level spectra of CTS-PGMA .....	72
Figure 4.7. XPS (a) wide scan, (b) C 1s, and (c) O 1s core-level spectra of CTS-MG .....	76
Figure 4.8. Microscopic images in wet condition: (a) CCTS, (b) CTS-MG, and (c) lead of pencil (0.5mm).....	77
Figure 4.9. SEM in dry condition: (a) CCTS (×100), (b) CTS-MG (×100), (c) CCTS (×500), (d) CTS-MG (×500) , (e) CCTS (×1000), and (f) CTS-MG (×1000).....	78
Figure 4.10 Plot of BET model for CTS-MG .....	80

Figure 4.11 Surface charge density as a function of pH. Experimental conditions: $m = 0.5$ g/L, $T = 293$ K. ....	81
Figure 5.1. (a) Boron sorption capacity as a function of pH, (b) Effect of boron sorption on solution pH. Experimental conditions: $[B]_0 = 0.39$ mM, $m = 0.5$ g/L, $T = 293$ K, contact time = 3 d.....	85
Figure 5.2. Boron sorption isotherms on CTS-MG, CCTS and commercial resin Amberlite IRA-743. ● CTS-MG, ■ CCTS, ▲ Amberlite IRA-743, — Langmuir fitting, ---- Freundlich fitting. Experimental conditions: $m = 0.5$ g/L, $pH = 7.0 \pm 0.1$ , $T = 293$ K, contact time = 3 d.....	88
Figure 5.3. Determination of Langmuir and Freundlich equation's constants. ● CTS-MG, ■ CCTS, ▲ Amberlite IRA-743.....	90
Figure 5.4. Kinetics of boron sorption by CTS-MG. Experimental conditions: $m = 0.5$ g/L, $pH = 7.0 \pm 0.1$ , $[B]_0 = 0.45$ mM, $T = 293$ K .....	93
Figure 5.5. Sensitivity analysis of the kinetic model parameters: (a) diffusivity ( $D_s$ ); (b) external mass transfer coefficient ( $k_f$ ); (c) particle radius ( $a_p$ ).....	95
Figure 5.6. Effects of ionic strength on B removal and solution pH. Experimental conditions: $m = 0.5$ g/L, $pH = 7.0 \pm 0.1$ , $[B]_0 = 0.46$ mM, $T = 293$ K, contact time = 3 d.....	97
Figure 5.7. Comparative studies of boron removal from simulated seawater and pure boron solution. Experimental conditions: ● & ○ Simulated seawater, initial pH = 8.1, △ Pure boron solution, initial pH = 7.0, $T = 293$ K, contact time = 3 d.....	99
Figure 5.8. FT-IR spectra of sorbents before and after boron sorption .....	101
Figure 5.9. XPS (a) wide scan of boron-loaded sorbent, and (b) N 1s core-level spectra of pristine sorbent; (c) N 1s core-level spectra of boron-loaded sorbent .....	102
Figure 5.10. Schematic diagram of boron uptake .....	103

Figure 6.1. (a) Uptake of arsenate as a function of pH, (b) Effect of arsenate sorption on solution pH. Experimental conditions:  $[\text{As(V)}]_0 = 20 \text{ mg/L}$ ,  $m = 0.5 \text{ g/L}$ ,  $T = 293 \text{ K}$ ..... 108

Figure 6.2. Sorption isotherm of arsenate onto CCTS and CTS-MG. Experimental conditions:  $m = 0.5 \text{ g/L}$ ,  $\text{pH} = 3$ ,  $T = 293 \text{ K}$ ..... 110

Figure 6.3. Sorption kinetics of arsenate at different ionic strength. Experimental conditions:  $[\text{As(v)}]_0 = 20 \text{ mg/L}$ ,  $m = 0.5 \text{ g/L}$ ,  $\text{pH} = 3$ ,  $T = 293 \text{ K}$ ..... 111

Figure 6.4 Simultaneous sorption of arsenate and HA. Experimental conditions:  $[\text{As(v)}]_0 = 20 \text{ mg/L}$ ,  $m = 0.5 \text{ g/L}$ ,  $\text{pH} = 7$ ,  $T = 293 \text{ K}$ ..... 114

Figure 6.5. Images of CTS-MG before and after arsenate sorption in the presence of NOM ..... 115

Figure 6.6. Effects of co-existing anions on arsenate removal. Experimental conditions:  $[\text{As(v)}]_0 = 20 \text{ mg/L}$ ,  $m = 0.5 \text{ g/L}$ ,  $\text{pH} = 7$ ,  $T = 293 \text{ K}$ ..... 116

Figure 6.7. FTIR spectra: (a) pristine sorbent and (b) As-loaded sorbent. .... 118

Figure 6.8. XPS of As-loaded sorbent: (a) widescan and As3d core-level; (b) N 1s core-level spectra ( $\text{pH} = 7$ ); and (c) N 1s core-level spectra ( $\text{pH} = 3$ )..... 119

Figure 7.1. (a) Uptake of MMA as a function of pH, (b) Effect of MMA sorption using CTS-MG on solution pH, (c) Uptake of DMA as a function of pH, (d) Effect of DMA sorption using CTS-MG on solution pH. ( $[\text{As}]_0 = 20 \text{ mg/L}$ ;  $m = 0.5 \text{ g/L}$ ;  $T = 293 \text{ K}$ ; contact time = 3 d) ..... 124

Figure 7.2. Methylated arsenic sorption isotherms onto CTS-MG and CCTS (Experimental conditions:  $m = 0.5 \text{ g/L}$ ,  $\text{pH} = 3.4$  (MMA),  $\text{pH} = 5$  (DMA),  $T = 293 \text{ K}$ , contact time = 3 d) ..... 127

Figure 7.3. Sorption kinetics of MMA and DMA at different ionic strength (Experimental conditions:  $[\text{As}]_0 = 20 \text{ mg/L}$ ,  $m = 0.5 \text{ g/L}$ ,  $\text{pH} = 3.4$  (MMA),  $\text{pH} = 5$  (DMA),  $T = 293 \text{ K}$ , contact time = 3 d)..... 129

Figure 7.4. Effect of humic acid on the sorption of methylated arsenic: (a) MMA, (b) DMA (Experimental conditions:  $[As]_0 = 20$  mg/L,  $m = 1$  g/L,  $pH = 7$ ,  $T = 293$  K, contact time = 3 d) ..... 131

Figure 7.5. Images of CTS-MG before and after methylated arsenic sorption in the presence of NOM..... 132

Figure 7.6. Competitive sorption of co-existing anions with methylated arsenic (Experimental conditions:  $[As]_0 = 20$  mg/L,  $m = 1$  g/L,  $pH = 7$ ,  $T = 293$  K, contact time = 3 d)..... 134

Figure 7.7. XPS (a) As3d core-level spectra of MMA-loaded sorbent, (b) As3d core-level spectra of DMA-loaded sorbent..... 135

Figure 7.8. N1s core-level spectra of (a) pristine sorbent, (b) MMA-loaded sorbent, (s) DMA-loaded sorbent. .... 136

Figure 8.1. ATR-FTIR spectra of (a) RC, (b) RC-PGMA, (c) RC-MG ..... 141

Figure 8.2. XPS spectra of RC (a and c) and RC-Br (b and d)..... 143

Figure 8.3. XPS spectra of RPGMA (a and c) and RC-MG (b and d)..... 146

Figure 8.4. Water contact angle versus drop age for pristine and modified RC membranes ..... 147

Figure 8.5. SEM images of the top and cross-sectional views of RC (images a-d) and RC-MG membranes (images e-h)..... 149

Figure 8.6. Effect of pH on the boron removal by RC-MG (Experimental conditions:  $[B]_0 = 0.46$  mM,  $m = 0.5.0$  g/L,  $T = 293$  K, contact time = 7 d) ..... 151

Figure 8.7. Sorption isotherms of boron removal by pristine and modified RC membranes (Experimental conditions:  $pH = 7$ ,  $m = 0.5$  g/L,  $T = 293$  K, contact time = 7 d)..... 152

Figure 8.8. Boron sorption as a function of pH and ionic strength in NaClO<sub>4</sub> solution.  
..... 153

Figure 8.9. ATR-FTIR spectra of RC-MG membranes before and after boron sorption  
..... 154

Figure 8.10. XPS spectra of boron-loaded membranes ..... 155

## **LIST OF ABBREVIATIONS**

<b>Abbreviations</b>	<b>Full name</b>
USEPA	U.S. environmental protection agency
WHO	world health organization
MCL	maximum contaminant level
ATRP	atom transfer radical polymerization
FT-IR	Fourier transform infrared spectroscopy
XPS	x-ray photoelectron spectroscopy
SEM	scanning electron microscopy
BET	Brunauer-Emmett-Teller
WCA	water contact angle
DL	detection limit
HRL	health risk limits
BPO	N-Bis(2,3-dihydroxypropyl) octadecylamine
EC	electrocoagulation
ED	electrodialysis
NF	nanofiltration

RO	reverse osmosis
AC	activated carbon
GMA	glycidyl methacrylate
NMDG	N-methyl-D-glucamine
GMA-MMA-DVB	glycidyl methacrylate - methyl methacrylate - divinyl benzene
GMA-co-TRIM	glycidyl methacrylate-co-trimethylolpropane trimethacrylate
PS-DVB	poly(styrene-divinylbenzene)
Eh	redox potential
MMA	monomethylarsonic acid
DMA	dimethylarsinic acid
IARC	international agency for research on cancer
EU	European union
TDS	total dissolved solids
GAC	granular activated carbon
Fe-GAC	nano-iron hydroxide impregnated GAC
AB	activated Bauxsol
LPRM	liquid phase of red mud
NZVI	nanoscale zero-valent iron

RC	regenerated cellulose
EGDE	ethylene glycol diglycidyl ether
THF	tetrahydrofuran
2-BIB	2-bromoisobutyryl bromide
TEA	triethylamine
DMF	N-dimethylformamide
BPY	2-2'-bipyridine
EDTA	ethylenediaminetetraacetic acid disodium salt
IHSS	international humic substances society
DI water	deionized water
CCTS	crosslinked chitosan
CTS-Br	surface-initiated chitosan beads
CTS-PGMA	chitosan grafted with PGMA
CTS-MG	NMDG modified chitosan-g-PGMA
RC-Br	initiator functionalized membrane
RC-PGMA	regenerated cellulose membrane grafted with PGMA
RC-MG	NMDG modified RC-g-PGMA
ICP-ES	inductively coupled plasma emission spectrometer



TOC	total organic carbon
HDPE	high density polyethylene
HA	humic acid
ATR-FTIR	attenuated total reflection - Fourier transform infrared spectroscopy
BE	binding energy
HEP	2-hydroxyethylamino 2,3-propanediol
NOM	natural organic matter
zpc	point of zero charge

## NOMENCLATURE

<b>Symbol</b>	<b>Description</b>
$b$	Langmuir isotherm single component parameter, L/mg or L/mmol
$q_{eq}, q^*$	concentration in the solid phase, in equilibrium with $C_{eq}$ , mg/g or mmol/g
$q_{max}$	maximum sorption capacity, mg/g or mmol/g
$C_{eq}, C^*$	concentration in the liquid phase, in equilibrium with $q_{eq}$ , mg/L or mmol/L
$C_0$	initial concentration, mg/L or mmol/L
$V$	volume of solution, L
$K_f, n$	Freundlich isotherm constants
$t$	time, s
$q_t$	sorption capacity at time t, mg/g or mmol/g
$K_1$	pseudo-first-order rate constant, s <sup>-1</sup>
$K_2$	pseudo-second-order rate constant, g/mg.s
$D_s$	surface diffusivity, m <sup>2</sup> /s
$D_p$	pore diffusivity, m <sup>2</sup> /s
$\rho_p$	particle density, kg/m <sup>3</sup>

$\varepsilon_p$	porosity of the particle, dimensionless
$a_p$	radius of sorbent, m
$r$	radial distance from center of particle, m
$k_f$	external mass transfer coefficient, m/s
$c_A$	concentration of acid, M
$c_B$	concentration of base, M
$[H^+]$	concentration of $H^+$ , M
$[OH^-]$	concentration of $OH^-$ , M
$F$	Faraday's constant, 96490 C/mol
$S$	specific surface area of sorbent, $m^2/g$
$a$	concentration of sorbent, g/L
$P$	partial vapor pressure of nitrogen gas in equilibrium, kPa
$P_0$	saturated pressure of nitrogen gas at 77.3 K, kPa
$V_a$	volume of adsorbed gas at equilibrium, mL
$V_m$	volume of monolayer adsorbed gas, mL
$C_{BET}$	BET constant, dimensionless
$N$	Avogadro constant, $mol^{-1}$
$s$	adsorption cross section, $m^2$

*m*            Mass of sorbent, g

*I*            Ionic strength, M

*T*            Temperature, K

## **CHAPTER 1**

### **INTRODUCTION**

#### **1.1 Background**

Water is essential to sustain a variety of lives, e.g. plants, animals and human beings. Contamination in water ingested poses an increasing threat to any living thing; it thus makes sense that water must be clean and free of contaminants to ensure their health and survival. Boron and arsenic are found to exhibit certain chronic or acute toxicity to plants species and human beings, respectively.

Boron is widely distributed in our environments. It naturally exists in water, soils, plants, animals; and also can come from anthropogenic activities. Although boron is an essential micronutrient required by plants, animals and even human beings, elevated boron concentrations in irrigation water can be detrimental for many plant species. With the world's freshwater sources diminishing, seawater containing an average boron concentration of 5 mg/L, has attracted much more attention as a agricultural water supply in many arid areas. Consequently, water contamination by boron is of special concern and it is necessary to keep a permissible boron level in water for proper utilization.

Another worldwide issue which is always a challenge for researchers in water environment is arsenic, the world's most hazardous chemical. Many countries of the world have been identified with arsenic contamination including Bangladesh,

Argentina, Chile, China, India, Mexico, Taiwan, Vietnam and the United States. The ubiquitous presence of arsenic can lead to adverse health effects ranging from acute lethality to chronic and even carcinogenic effects (Bencko, 1977; Choong et al., 2007). One of the major sources of arsenic exposure by the general population is drinking water. To minimize the health risks, the U.S. Environmental Protection Agency (USEPA) and World Health Organization (WHO) have stringently reduced the maximum contaminant level (MCL) of arsenic in drinking water from 50 to 10  $\mu\text{g/L}$  (Zheng et al., 2009).

In view of their adverse effects described above, numerous research activities have been prompted to reduce the pollution of boron and arsenic over the past decade. Conventional physicochemical processes include chemical precipitation, coagulation, membrane filtration, electrochemical treatment, and sorption so on. Comparatively, sorption is considered to be one of the most extensively used techniques because of its superiorities such as better performance, ease in operation and low cost / energy consumption etc. Hence, researchers are dedicated to developing novel sorbents which can be applied in a more efficient and sustainable ways than the currently available materials for removal of boron and arsenic.

Chitosan is one kind of abundant, low-cost and environmental-friendly biopolymers. It is normally obtained from the deacetylation of chitin, a major component of shrimp, crab and other crustaceans. Cellulose, the major structural component of green plants, is also considered to be the most abundant and renewable biopolymer in nature. These naturally occurring polysaccharides have been widely applied as sorbents in water and wastewater treatment due to its favorable properties

such as availability, biodegradability, biocompatibility and non-toxicity. The hydroxyl and amine groups in chitosan and cellulose are well known as the main binding sites for heavy metal ions; however, these groups do not show good performances towards anionic removal from aqueous solution. A possible solution is to provide the native biopolymers with specific chemical functionality and then to enhance their sorption properties.

In recent years, surface modification/functionalization has become a popular technique and widely applied in various fields. Generally, parent materials may not possess suitable surface properties required for specific applications; however, surface modification/functionalization can endow these parent materials with desirable functions, such as physical, chemical, electrical, magnetic, mechanical, biocompatible and corrosion-resistant properties through the choice of different functional groups. Due to the diversity of functional groups, there is a wide range of possibilities to functionalize a surface for different applications, e.g. heavy metal removal, biomolecular recognition, molecular separation or enzyme catalysis etc. The covalent attachment of functions onto the substrate can provide long-term chemical stability of the introduced surface chemical properties.

Among the chemical modification techniques, atom transfer radical polymerization (ATRP) developed by Wang and Matyjaszewski, has rapidly attracted growing interests. ATRP can be performed with a wide range of vinyl monomers such as acrylonitrile, acrylates, methacrylates, and styrene (Yu et al., 2003). It also does not need stringent experimental conditions as in the anionic and cationic polymerization (Zheng and Stover, 2003; Yu et al., 2004; Jin et al., 2005). Till now, most studies

using ATRP have been done onto such substrates as carbon nanotubes (Wu et al., 2007), silicon (Yu et al., 2003; Yu et al., 2004), titanium (Zhang et al., 2007a), gold (Rakhmatullina et al., 2009; Yoon et al., 2009) and synthetic polymers (Zheng and Stover, 2003).

However, to the best of our knowledge, only a few studies involve modification of chitosan or cellulose substrates with surface initiated ATRP technique for environmental application. Therefore, it is of great interest to modify surfaces of these two environmental-friendly biopolymers via ATRP to develop innovative separation materials for efficient boron and arsenic removal.

## **1.2 Objectives**

The main aim of this work was to seek an alternative solution to minimize contamination of boron and arsenic which have already been proven by many researchers as both chronic and acute chemicals. Hence, this research is intended to explore the possibilities of immobilizing distinctive functions onto solid substrates, for instance, chitosan and cellulose for anionic contaminants removal from aqueous solution.

The work focuses on development of novel polymeric separation materials, evaluation of their boron/arsenic sorption performances under various physicochemical conditions as well as investigation of the sorption mechanisms. More specifically, this thesis is aimed to accomplish the following specific objectives:



1. To design and synthesize innovative separation materials including chitosan-based sorbent and cellulose-based adsorptive membranes via electrostatic extrusion and ATRP techniques.
2. To confirm the critical role of each step in the synthesis by Infrared Spectroscopy (IR) and X-Ray Photoelectron Spectroscopy (XPS).
3. To characterize the physicochemical properties of the developed materials by a suite of analytical techniques including microscopes, Scanning Electron Microscopy (SEM), Brunauer-Emmett -Teller (BET) Analyzer, and Water Contact Angle (WCA) etc.
4. To demonstrate the sorption behavior of boron/arsenic with varying parameters such as solution pH, initial concentration, contact time, ionic strength, co-existing ions etc.
5. To conduct mechanism studies via experimental approaches and instrumental analysis.

Therefore, the findings from this present study may have significant impact on providing alternatively new materials which possess high capability for boron and arsenic removal from water and wastewater. Furthermore, studies of the sorption behavior should also provide valuable information for further full-scale industrial applications. Mechanism study may contribute to the understanding of the interaction occurring at water/solid interface.

This chapter provides a brief introduction on boron and arsenic contamination, treatment technologies and surface modification/functionalization techniques, and introduces the motivation for the current study as well. A more detailed literature reviews will be presented in the next chapter (Chapter 2).

## **CHAPTER 2**

### **LITERATURE REVIEW**

This chapter presents detailed information about boron and arsenic including their chemistry, sources in the environment, toxic effects and corresponding regulations. In addition, this chapter reviews a survey of literature pertinent to studies on current boron and arsenic treatment technologies. Mathematical modeling in sorption equilibrium and kinetics is also reviewed.

#### **2.1 Boron**

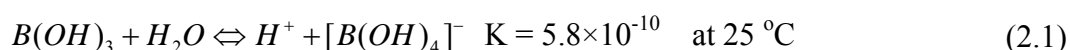
##### **2.1.1 Solution chemistry**

Boron atom has the electron configuration:  $1s^2, 2s^2, 2p^1$  and is located on periodic table in Group IIIA. All boron exists in trivalent valence state. It is a metalloid element having properties between the metals and the electronegative non-metals. The tendency for boron is to form anionic rather than cationic complexes (Muetterties, 1967).

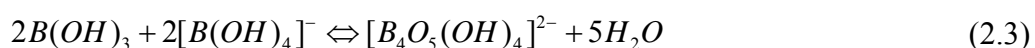
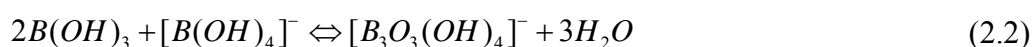
Although scientists refer to levels of “boron”, boron is never found free in nature. It often exists as various oxygen-containing compounds such as boric acid, its inorganic salts named borates, or borosilicate minerals. Actually, boron chemistry is a unique and complex discipline. It is impossible, nor intended, to describe all aspects of boron chemistry here. For the sorption of boron from aqueous solution, it is necessary to

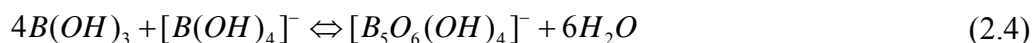
understand the chemistry of aqueous boric acid and borate equilibrium in the system of interest.

The chemistry of boron in aqueous solution is characterized by the existence of boric acid  $B(OH)_3$ , monomeric borates  $B(OH)_4^-$  and a series of polyborate anionic species. Boric acid with a trigonal geometry, normally behaves as a weak Lewis acid. It can accept hydroxyl ion from water and release a proton into solution according to the following dissociation reaction (Adams, 1964). The formed borate anion has a tetrahedral geometry.



The formation of different borate groups and their structures depend on solution pH, temperature as well as boron concentration. At extremely acidic or alkaline conditions, the predominant species in solution are boric acid or the mononuclear borate ion. In a dilute boric acid solution (less than 0.025 M), essentially only mononuclear species  $B(OH)_3$  and  $B(OH)_4^-$  are present. When boron concentration increases or temperature decreases, the possibility of forming polynuclear borates also increases (Salentine, 1983). However, existence of these polyborates in nature is very rare. Generally, boron is widely distributed in the form of boric acid and partially borate ions in our environment.





### 2.1.2 Boron in aqueous environment

Boron naturally occurs in surface water, groundwater as well as seawater. According to Mellor (Mellor, 1922), boron is the 10<sup>th</sup> most abundant element in oceanic salts, varying in concentration in seawater from 0.52 mg/L in the Baltic Sea to as much as 9.57 mg/L in the Mediterranean Sea. The global average, however, is around 4.6 mg/L.

The level of boron in surface water and groundwater bodies is highly location-specific. It depends on a variety of factors, the predominant one being geological circumstances in accordance with proximity to natural boron deposits and coastal regions, as well as on industrial and agricultural activities. Thus, there is insufficient data to generate a global mean value for boron concentration (Argust, 1998; Coughlin, 1998). In general, the natural boron content of groundwater and surface water is usually small (Table 2.1) (Xu et al., 2010).

In European surface water, the reported concentrations of boron generally ranges from the concentration under detection limit (DL) to a maximum recorded of 7.49 mg/L in Spain. Similar concentration ranges have been reported for water bodies within Pakistan, Russia, and Turkey with most values below 0.5 mg/L (Emiroglu et al., 2010). Concentrations of boron in freshwater in the U.S. tend to average about 0.1 mg/L. Nevertheless, in the western US where there are large masses of boron-rich formations and deposits, boron level tend to be higher (e.g. 5 - 15 mg/L) (Butterwick et al., 1989).

Table 2.1 Boron concentration in water from different countries

	Country	Sources	Sample number	Concentration range (mg/L)	Mean concentration (mg/L)
	Austria		30 <sup>a</sup>	< DL - 0.69	0.044
	Belgium		651 <sup>a</sup>	0.025 - 2.029	0.239
	Finland		463 <sup>a</sup>	<1 - 0.046	0.003
	France		25 <sup>a</sup>	< DL - 2.67	0.146
	Ireland		185 <sup>a</sup>	< DL - 1.63	0.026
	Italy	surface water	64 <sup>a</sup>	< DL - 0.894	0.114
Europe	Netherlands		9 <sup>a</sup>	0.038 - 0.878	0.111
	Portugal		8 <sup>a</sup>	0.030 - 3.86	0.367
	Spain		328 <sup>a</sup>	< DL - 7.49	0.137
	UK		147 <sup>a</sup>	< DL - 1.12	0.010 - 0.065
	Mediterranean	groundwater	6,400	> 0.3 (30 %), > 0.5 (23 %), > 1 (14 %)	
	Germany	surface water	197 <sup>a</sup>	< DL - 1.3	0.197
		groundwater			0.07
	Romania	groundwater from rural	60	0.02 -1.55	0.16 - 0.65
America	U.S.	rivers	76	0.01 - >2	0.10

		surface water	14		0.056
		groundwater	34		0.12
		public water supplies	989	0.005 - 2.0	0.15
	Canada	surface water		2.9 (max.)	0.16
	Argentina	surface water	8	0.25 - 0.32	0.29
		groundwater	10	0.35 - 1.64	0.72
		drinking water		0.31 - 15.2 <sup>b</sup>	
	Chile	groundwater		11.9 - 27.3	
		surface water		10.7 - 16.8	
Africa	Egypt	Lake water		0.249 - 1.14	
	Kashmir	drinking water	24	0.054 - 0.250	0.16
		surface water	76	0.003 - 0.246	0.04
Asia	China	groundwater	22	0.007 - 0.337	0.068
		overall	98	0.003 - 0.337	0.046

a: the number of the monitoring sites

b: boron concentration in soil was 900 mg/kg

Boron can be released into the aqueous environment by natural processes. The highest concentrations of boron are found in sediments and sedimentary rocks (Xu and Jiang, 2008). Weathering of boron-containing minerals or soils can slowly release boron into water. Boron in the atmosphere also can make its way to rainwater and eventually be introduced into the world's drinking water sources (Butterwick et al., 1989). The concentration of boron in thermal waters of western Anatolia, Turkey, was reported to be between 1 to 63 mg/L. The abundant-existing minerals such as sericite, illite and tourmaline were considered to be mainly responsible for the high boron contents in thermal waters. It caused environmental contamination in surface and ground water which was used for irrigation in the agricultural districts of western Anatolia (Gemici and Tarcan, 2002). The concentrations of boron in the aquifer of Bigadiç district also had a wide range of 0.054 mg/L and 391 mg/L, while the highest B level was detected at the mine areas (average 260 mg/L). The predominant aqueous species of B were undissociated boric acid (94 %) and the borate anion; and its origin was directly associated with the leaching of boron-containing rocks (Gemici et al., 2008). Besides, in the Gulf Coast aquifer of Texas, the total number of boron samples from 1990 to 2006 was 1117, while 393 of these samples were over the Health Risk Limits (HRL) of 600 µg/L. The measured B content was within 0.02 µg/L to 16,600 µg/L, the average of which was 901 µg/L. It was natural geologic source rather than oilfield discharge to contribute the high boron level (Glenn and Lester, 2010).

Other than that, boron contamination is in great part due to anthropogenic activities. At present, there is a wide variety of industrial and domestic applications



such as the use of borate-containing fertilizers, herbicides and detergents, the combustion of plant-based products (e.g. wood and oil etc.), and the release of wastes from borate mining and processing. Boron can also contaminate water when used as additives for borosilicate glass, cosmetics, ceramic, leather, textile and enamels so on (Ristic and Rajakovic, 1996; Ozturk and Kavak, 2004). For example, boron in Seine River at Paris was mainly related to boron discharge in urban effluents (65 % mean) (Chetelat and Gaillardet, 2005). Molina et al. also reported that in the Plioquaternary aquifer of southeastern Spain, the boron content was greater; which originated from three distinct components: marine intrusion, anthropogenic pollution and dissolution of evaporate deposits (Molina et al., 2003). Additionally, the U.S. in 2007 imported for consumption of boric acid, colemanite ( $\text{Ca}_2\text{B}_6\text{O}_{11}\cdot 5\text{H}_2\text{O}$ ), borax ( $\text{Na}_2\text{B}_4\text{O}_7\cdot 10\text{H}_2\text{O}$ ) and ulexite ( $\text{NaCaB}_5\text{O}_9\cdot 8\text{H}_2\text{O}$ ) were 186,000 tons; and the total consumption of all boron products increased by 3 % compared with that of 2006. The primary use of boron compounds were glass products and detergent products, followed by retardants and chemical fertilizers (Lyday, 2000). Among these, it is estimated that the majority of boron in wastewater effluent came from detergents and fertilizers (Dyer and Caprara, 1997).

### **2.1.3 Toxic effects of boron and current regulations**

Boron, as an essential micronutrient for plants, has been shown to play a critical role in carbohydrate metabolism, sugar transport, pollen germination, hormone development, nucleic acid synthesis, and membrane integrity (Howe, 1998; Parks and Edwards, 2005). Low levels of boron may be beneficial to various fruits and

vegetables; however, the ranges between boron deficiency and boron toxicity in plant are very narrow. When boron content is higher than a certain concentration, some toxicity symptoms will occur in plants including marginal and tip necrosis in leaves, followed by the loss in photosynthetic capacity and plant productivity (Parks and Edwards, 2005; Kabay et al., 2010). Irrigation water contaminated with boron is considered to be the most common cause of boron toxicity in plants. It is thus recommended that the maximum concentration of boron should not exceed the values as shown in Table 2.2., in order to protect the irrigated crops (Xu and Jiang, 2008).

Table 2.2 Relative tolerance of agricultural crops to boron

<b>Maximum concentration of B in irrigation water (mg/L)</b>	<b>Agricultural crops</b>
< 0.5	blackberry
0.5 - 1.0	peach, cherry, plum, grape, cowpea, onion, garlic, sweet potato, wheat, barley, sunflower, mung bean, sesame, lupin, strawberry, Jerusalem artichoke, kidney bean, lima bean
1.0 - 2.0	red pepper, pea, carrot, radish, potato, cucumber
2.0 - 4.0	Lettuce, cabbage, celery, turnip, kentucky bluegrass. Oat, corn, artichoke, tobacco, mustard, clover, squash, muskmelon
4.0 - 6.0	Sorghum, tomato, alfalfa, purple vetch, parsley, red beet, sugar beet
6.0 - 15.0	asparagus

In regard to animals and human beings, the effect of boron has not been identified so explicitly as was done for plants. Boron toxicity is difficult to be quantified

because it is related with the frequency, length, and level of exposure (Hilal et al., 2010). With the long-term oral exposure to boric acid or borax in laboratory animals (e.g. rats, mice, and rabbits), it was demonstrated that the male reproductive tract was a constant target of toxicity (WHO, 2004; Hilal et al., 2010) .

The WHO once set a guideline limit of 0.5 mg/L for boron in drinking water; lately, the revision of boron guideline value to 2.4 mg/L was suggested and will be incorporate into the Guidelines for Drinking-water Quality (4<sup>th</sup> edition) published in 2011 (Kabay et al., 2010). Although this new regulation is broadened for drinking water from the human health standpoint, the requirement of 0.5 mg/L is still kept for irrigation water by some utilities since boron shows the herbicidal effect.

#### **2.1.4 Available treatment technologies**

Boron must be removed from water and wastewater for various reasons, as mentioned previously, boron concentration is strictly regulated. This section reviews several typical physicochemical treatment processes which include chemical precipitation, liquid-liquid extraction, electrocoagulation, membrane filtration and sorption.

##### **2.1.4.1 Chemical precipitation**

Chemical precipitation process for boron removal is achieved by adding inorganic and organic precipitants including lime, metal salts, alumina-lime-soda and organic polyelectrolytes (e.g. polyvinyl alcohol, hydroxycarboxylic acid, dioxime etc.)

(Itakura et al., 2005; Remy et al., 2005; Garcia-Soto and Camacho, 2006). The treatment efficiency mainly depends on pH and a large amount of alkali is often required for adjustment. Another problem comes from the requirement of high chemical doses and other assistant coagulants in order to achieve high boron removal efficiency especially for low boron initial concentration (< 50 mg/L). Hence, this process often produces high volume of sludge, leading to disposal problems and increasing operation cost (Xu and Jiang, 2008).

#### **2.1.4.2 Liquid-liquid extraction**

Liquid-liquid extraction is another technology available for boron removal, in which certain organic-soluble chelating agents are adopted to extract boron, rather than direct extraction by an organic solvent. A wide range of reagents possessing vicinal-diol and/or tertiary amine functions have been used for boric acid extraction, e.g. aliphatic 1,2 and 1,3 diols, 2-butyl-2-ethyl-1,3-propandiol, N-Bis(2,3-dihydroxypropyl) octadecylamine (BPO) (Egneus and Uppstrom, 1973; Matsumoto et al., 1997; Bicak et al., 2003; Karakaplan et al., 2004). Despite relatively high removal efficiency for boron, this method is only applicable to relatively concentrated boric acid solutions.

#### **2.1.4.3 Electrocoagulation**

Electrocoagulation (EC) is an electrochemical treatment, in which the coagulants are generated in situ by the metal anode dissolution; simultaneously, hydrogen gas is

released from the cathodes, which would help float the flocculated particles out of the waste (Figure 2.1) (Xu and Jiang, 2008). Aluminum or iron electrodes are often used as anode materials in EC to remove boron. The efficiency of boron removal mainly depends on pH, current density, boron initial concentration, type and concentration of supporting electrolyte, electrolytic time (Bektas et al., 2004; Yilmaz et al., 2005). At optimal conditions, the percentage of boron removal from aqueous solution was reported to be higher than 90 % (Yilmaz et al., 2007; Yilmaz et al., 2008).

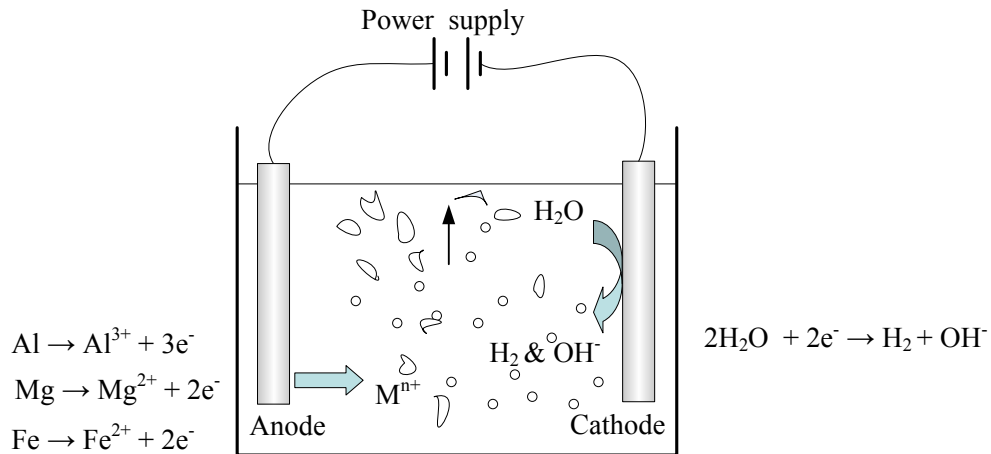


Figure 2.1. Schematic of basic electrocoagulation system

However, due to cathodic dissolution, the use of aluminum electrodes can cause the presence of residual aluminum in the treated water. This will create health problems as the USEPA guidelines suggest a maximum contamination of 0.05 - 0.2 mg/L. Vasudevan and the coauthors thus selected magnesium as an alternative anode and stainless steel as the cathode to remove boron from aqueous solution; and the results showed that the EC can achieve a maximum removal efficiency of 86.3 % (initial concentrations ranging from 3 - 7 mg/L) under a current density of 0.2 A/dm<sup>2</sup>

and pH of 7 (Vasudevan et al., 2010). Although electrocoagulation can efficiently remove boron without addition of chemical reagents, the drawbacks are elevated energy cost and corrosion problem during operations.

#### **2.1.4.4 Membrane filtration**

Membrane filtration used in boron removal often refers to electrodialysis (ED), nanofiltration (NF), and reverse osmosis (RO). As this review notes, these advanced processes usually have extreme difficulty in removing boron, and often require enhancements to achieve efficient removal such as polymer assisted filtration, multiple stage RO system etc. Nanofiltration by itself does not remove detectable levels of boron from water.

ED has been cited that it is usually capable of removing about 42 - 75 % of boron (Yazicigil and Oztekin, 2006). Boron removal by ED was mainly dependent on increasing solution pH and the degree of demineralization.  $B(OH)_3$  dissociation and speciation plays an important role in this process. If solution pH is below about 8 or 9, it appears that treatment efficiency falls off dramatically. For example, Kabay and the coworkers reported that percent removal of boron was only 20 % at pH 9.0; and it reached a value close to 80 % after pH increased to 10.5 (Kabay et al., 2008a). Banasiak and Schafer also found nearly 60 % of boron was removed from aqueous solution at pH 12 while less than 15 % of boron removal was obtained at pH 9 (Banasiak and Schafer, 2009). In order to achieve the desired removal efficiency, it is also required to remove the salts to extremely low levels, which may lead to

unfavorable energy consumption (Oren et al., 2006).

Although RO is very efficient to reject most of the salts in seawater (e.g. Na and Cl), boron removal is only between 40 % and 60 % under normal standard conditions due to the predominance of undissociated boric acid at acidic and neutral pH (Prats et al., 2000). The major obstacle of RO is severe pH limitation. It is reported that the rejection of boric acid is about 65 % while that of borate ion is 95 % (Nadav, 1999). Though increase of feed water pH can shift the equilibrium to the side of borate and obtain high rejection, it will cause immediate calcium carbonate and magnesium hydroxide scaling, associated corrosion and cost problems (Glueckstern and Priel, 2003).

As a single pass RO for seawater desalination is usually not good enough to produce treated water which satisfies the limit of 0.5 mg/L, “extra treatment” of such water has attracted considerable research so as to meet these standards. Several types of assisted or enhanced RO treatment have been tested. For example, if two- or three-stage RO is applied, pH can be raised after hardness ions are removed in the first stage, which allows better boron removal at higher pH and lower salinity and simultaneously avoids the scaling (Parks and Edwards, 2005; Oo and Song, 2009). However, low recovery and associated high cost become the major limitations. Alternatively, researchers adopted several polymeric sorbents to further purify the first pass RO permeate, e.g. fibrous sorbent based on polypropylene and viscose fibers grafted with polystyrene and glycidyl methacrylate and functionalized with N-methylglucamine (Parschova et al., 2007; Kabay et al., 2008b). Another approach

is to complex boron before membrane process through a variety of chemicals. The general idea is that, by generating a dissolved boron compound which has a charge or a larger molecular size, rejection of boron by the membrane can then be improved to acceptable levels (Parks and Edwards, 2005). Smith and the coworkers found that addition of polymer before NF improved boron rejection up to 80 %, but these levels of polymer are hundreds or thousands of times higher than are used in drinking water (Smith et al., 1995). Likewise, Geffen et al. reported on the complexation of boron with mannitol integrated with membrane system in their study; dosing of mannitol before NF or RO also led to 90 % and 97 % boron removal at pH 9 (Geffen et al., 2006).

#### **2.1.4.5 Sorption**

Boron sorption onto activated carbon (AC), AC impregnated with different compounds (e.g. calcium chloride, barium chloride, citric acid, tartaric acid and mannitol), activated alumina, zirconium dioxide, silica-aerosil, clays (bentonite, sepiolite and illite) and modified clays, neutralized red mud have been reported (Rajakovic and Ristic, 1996; Karahan et al., 2006; Cengeloglu et al., 2007; Kluczka et al., 2007a; Kluczka et al., 2007b). However, most sorbents do not exhibit good boron sorption capacity (Table 2.3).



Table 2.3 Sorption of boron by different sorbents

<b>Sorbent</b>	<b>Sorption capacity (mmol/g)</b>
AC	0.040
AC + CaCl <sub>2</sub>	0.072
AC + citric acid	0.093
AC + orthophosphoric (V) acid	0.097
AC + tartaric acid	0.203
AC + glucose	0.046
AC + mannitol	0.188
Bentomite	0.117
Sepiolite	0.034
Illite	0.058
Activated alumina	0.182
Zirconium dioxide	0.040
Neutralized red mud	0.555

In literature, polymers with vicinal polyalcohol functions are reportedly the most efficient ligands for complexation of boron in aqueous solutions. According to this chemistry, research has been widely conducted to date to develop boron-specific materials, most of which have common in the polyhydric functional group.

A sorbitol-modified poly(N-glycidyl styrene sulfonamide) with 1.22 mmol/g boron-loading capacity has been demonstrated to be an efficient and regenerable specific sorbent for removal of boron in ppm levels (Bicak and Senkal, 1998). Bicak and the coauthors also reported glycidyl methacrylate (GMA) based cross-link polymers containing N-methyl-D-glucamine (NMDG) with around 2.1 mmol/g boron

sorption capacities (Bicak et al., 2000). Glycidyl methacrylate (GMA)-methyl methacrylate (MMA)-DVB (divinyl benzene) terpolymer beads have been synthesized and used as support to introduce NMDG and aminodipropylene glycol groups. These polymer resins have 2.15 mmol/g and 3 mmol/g boron loading capacity, respectively (Bicak et al., 2001; Senkal and Bicak, 2003). Gazi and the coworkers prepared a new polymeric resin with glucose sulfonamide functions, which possesses a boron loading capacity of 2.365 mmol/g and showed reasonably rapid sorption ability (Gazi et al., 2004). MG modified macroporous poly(glycidyl methacrylate-co-trimethylolpropane trimethacrylate) (poly(GMA -co-TRIM)) has been developed and reported by (Wang et al., 2007). Results show that this sorbent has high sorption capacity (1.84 mmol/g) and fast kinetics. Gazi and the coauthors reported a novel hairy polymer resin with extremely rapid and selective boron sorption ability. 2-hydroxyalkylamino 2,3-propanediol was introduced into poly(styrene-divinylbenzene) (PS-DVB) microspheres. The hairy polymer with multi-hydroxyalkylamine functions is demonstrated to have the highest sorption capacity of 3.28 mmol/g (Gazi et al., 2008).

In addition to using synthetic polymers as substrates like PS-DVB, polyethylene, natural biopolymers has attracted much attention as excellent base substances due to their environmentally friendly characteristics. Chitosan derivatives incorporating saccharides have been investigated for the removal of boron (Matsumoto et al., 1999). Two forms of (powder and fiber) NMDG type cellulose derivatives were developed and the maximum value of the sorption capacities was 1.1 mmol/g at pH around 9 (Inukai et al., 2004). Sabarudin and the coworkers reported that chitosan resin derived

with NMDG exhibits high ability in boron sorption with capacity of 2.1 mmol/g and sorption kinetics was faster than that of the commercially available resins (Sabarudin et al., 2005).

Besides organic base materials, Rodriguez-Lopez et al. used mesoporous silica materials functionalized with saccharides to treat boron-containing water. These prepared solids have sorption capacity in the range of 0.49 - 1.85 mmol/g (Rodriguez-Lopez et al., 2004). Kaftan and the coauthors prepared a novel sorbent by modification of an inorganic support material, MCM-41 (silica mesoporous materials). The maximum amount of B is found to be 0.8 mmol/g of sorbent (Kaftan et al., 2005).

## **2.2 Arsenate and methylated arsenic**

### **2.2.1 Arsenic species**

Arsenic, a metalloid element (atomic number 33), ranks 20<sup>th</sup> in abundance of elements in the earth's crust, 14<sup>th</sup> in seawater and 12<sup>th</sup> in the human body (Mandal and Suzuki, 2002). In the environment, arsenic has an unusually complex geochemistry with sorption-desorption reactions, oxidation-reduction, precipitation-dissolution, ligand-exchange, biological transformation or all taking place (Jain and Ali, 2000).

Arsenic is stable in four oxidation states: +5, +3, 0 and -3. Among them, the elemental state is extremely rare; and -3 is only found at extremely reducing conditions. In most aquatic environments, arsenic occurs with two dominant

oxidation states: As(V) (arsenate) and As(III) (arsenite). These arsenic elements are found in both inorganic and organic forms and their speciation is mainly controlled by the solution chemistry such as redox potential (Eh) and pH (Figure 2.2) (Smedley and Kinniburgh, 2002). Of the inorganic arsenic species, pentavalent arsenate ( $\text{H}_2\text{AsO}_4^-$  and  $\text{HAsO}_4^{2-}$ ) is the dominant and stable inorganic form in the oxygen-rich environments (well-oxidized water), while trivalent arsenite mostly exists as  $\text{H}_3\text{AsO}_3^0$  and  $\text{H}_2\text{AsO}_3^-$  under reducing environments such as anaerobic groundwater. Organic arsenic species including monomethylarsonic acid (MMA) and dimethylarsinic acid (DMA) may be formed by biological activity, primary in surface waters, are rarely quantitatively important; however, their concentrations can not be neglected when waters are significantly contaminated through industrial or agricultural activities. The structure and  $\text{pK}_a$  values for arsenic species are stated in Table 2.4 (Lafferty and Loeppert, 2005).

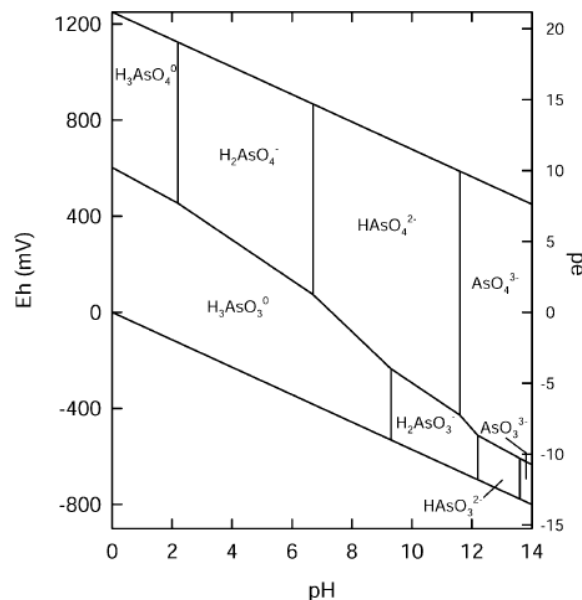
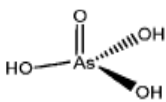
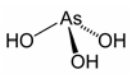
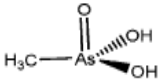
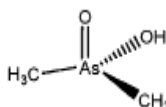


Figure 2.2. Eh-pH diagram for aqueous As species in the system As-O<sub>2</sub>-H<sub>2</sub>O at 25 °C and 1 bar total pressure

Table 2.4 Structure and pK<sub>a</sub> values for various arsenic species

Arsenic species	Structure	pK <sub>a1</sub>	pK <sub>a2</sub>	pK <sub>a3</sub>
As(V)		2.20	6.97	11.53
As(III)		9.22	12.13	13.4
MMA		4.19	8.77	--
DMA		6.14	--	--

### 2.2.2 Occurrence and sources of arsenic in natural water

Concentrations of arsenic in natural water bodies tend to be variable by several orders of magnitude, depending on the source of arsenic and the local geochemical environment. Typically, arsenic concentrations in freshwater are less than 10 ug/L, and frequently less than 1 ug/L (Smedley and Kinniburgh, 2002). For example, the baseline concentrations of arsenic in rainwater and snow in rural areas are invariably lower than 0.03 ug/L (Andreae, 1980).

However, a number of large aquifers in various parts of the world have identified with arsenic concentrations above 50 ug/L. Smedley and Kinniburgh wrote an excellent review of high-arsenic containing groundwater in many countries such as Argentina, Bangladesh, Chile, China, Hungary, West Bengal (India), Mexico, Romania, Taiwan, Vietnam and many parts of the USA, especially the south-west US (Smedley and Kinniburgh, 2002). The occurrence of arsenic in groundwater and

estimated population in affected countries are summarized in Table 2.5 (Smedley and Kinniburgh, 2002). It has been estimated that globally, millions of individuals are at risk due to exposure to excessive levels of arsenic; while Bangladesh and West Bengal (India) represent the most serious occurrences of arsenic in the world. Approximately 30 – 35 million people drinks water containing excessive arsenic in the Bengalesh; and up to 6 million people in West Bengal.

Table 2.5 Occurrence of arsenic in groundwater and estimated population in affected countries

<b>Country</b>	<b>Concentration (ug/L)</b>	<b>ranges</b>	<b>Estimated population exposed<sup>a</sup></b>
Argentina	< 1 - 5300		200, 000
Bangladesh	< 0.5 - 2500		30 millions
China	varied		5.6 millions
Hungary, Romania	< 2 - 176		29,000
Mexico	8 - 620		400,000
Northern Chile	100 - 1000		500,000
South-west USA	varied		350,000
Taiwan	10 - 1820		10,000
Vietnam	1 - 3050		> 1 million
West Bengal (India)	< 10 - 3200		6 millions

a: population exposed to drinking water with As > 50 ug/L.

Arsenic contamination in groundwater and surface water is globally ever-present from two principal sources: natural processes and anthropogenic inputs. In most cases, groundwater with high levels of arsenic is due to natural occurrences, e.g. oxidizing and reducing environment. The anthropogenic inputs may be locally severe but

occurrences are relatively rare.

Arsenic is mobilized naturally through a variety of processes such as weathering of arsenic-bearing rocks and sediments, volcanic emissions, atmospheric deposition, geochemical reactions as well as biological activity (Nriagu et al., 2007). It was reported that  $612 \times 10^8$  and  $2380 \times 10^8$  g/year of arsenic were contributed by soil erosion and leaching respectively, in dissolved and suspended forms in the ocean (Mohan and Pittman, 2007). Anthropogenic activities also release large quantities of arsenic to the water streams, such as mining activity, smelting and ore processing, combustion of fossil fuels as well as applications of arsenical pesticides, herbicides, crop desiccants and fertilizers. In general, the anthropogenic contribution to the aquatic environment was estimated to be 82,000 metric tons annually (Nriagu et al., 2007).

### **2.2.3 Health effects and regulatory issues**

Arsenic is of considerable environmental concern as a toxic and carcinogenic element. The severity of toxicity is basically dependent on its chemical form (e.g. inorganic or organic), oxidation state and solubility in the biological media (Subramanian and Sukumar, 1988). In general, arsenic toxicity decreases with increasing degree of methylation; and the trivalent forms are considered to be more toxic than the pentavalent forms (Jain and Ali, 2000). Of the four predominant arsenic species in the environment, arsenite is the most toxic followed by arsenate, MMA and DMA.

According to WHO, long-term exposure to arsenic in drinking-water is causally associated with cancer at several sites, particularly skin, bladder and lungs (WHO, 2004). Arsenic also linked to other non-carcinogenic symptoms, such as nausea, vomiting, diarrhea, abnormal heart rhythm, partial paralysis, blindness, hyperkeratosis, pigmentation changes, cardiovascular disease and nervy system disturbance (Jain and Ali, 2000; Choong et al., 2007).

Diseases induced by arsenic poisoning are no longer news but reported worldwide. Due to consumption of high arsenic-containing drinking water, more than 12 % of the individuals exhibited dermatological manifestations in Antofagasta; chronic arsenic poisoning was also reported in some regions of North Mexico, where the exposed population showed one of the cutaneous signs of chronic arsenic poisoning (Jain and Ali, 2000). In Taiwan, higher arsenic exposure via drinking water led to a unique peripheral vascular disease called “blackfoot disease” (Tseng et al., 2005). According to some estimates, over 200,000 deaths from cancer can be caused by drinking arsenic-containing water in Bangladesh. The problem of arsenic contaminated groundwater in West Bengal, India has been claimed as the biggest calamity in the world (Choong et al., 2007).

Arsenic is classified as a Group A carcinogen by the USEPA, WHO and International Agency for Research on Cancer (IARC). Cases of arsenic poisoning have prompted WHO in 2004 to regulate the maximum permissible limits for drinking water more strictly from an earlier value 50 to 10 ug/L (WHO, 2004). This reduced limit was also accepted by authorities of the European Union (EU) and



USEPA (Vaclavikova et al., 2008). In particular, under Directive 2000/60/CE, the European Community has already defined more strict restriction of 1.6 and 1.4  $\mu\text{g/L}$  for superficial water to be achieved within 2008 and 2015, respectively (Di Natale et al., 2008).

#### **2.2.4 Existing technologies for arsenic removal**

A variety of technologies for arsenic removal have been studied in literature, which can be mainly divided into five process categories: coagulation/precipitation, ion exchange, membrane filtration, biological process, and sorption. The technologies under review perform most effectively when treating arsenic in the form of As(V). For As (III), it is usually converted through pre-oxidation to As(V) by oxidants such as chlorine, hypochlorite, potassium permanganate, ozone, hydrogen peroxide, Fenton reagent and so on.

##### **2.2.4.1 Coagulation/precipitation**

Coagulation/precipitation either by alum or iron coagulants or lime softening is a commonly used and effective technique for arsenic removal on a large-scale treatment facility. The most widely used coagulants are aluminum salts (e.g. alum) and ferric salts (e.g. ferric chloride, ferric sulfate), which hydrolyze to form aluminum and iron hydroxide particulates, respectively; while lime softening apparently removes arsenic through co-precipitation of arsenic on calcium carbonate and hydrous magnesium oxide floc. The efficiency and economics of this process are highly dependent on the

type and dosage of chemical agents, initial arsenic concentrations and pH.

Removal of arsenic by coagulation/precipitation/filtration can be achieved via three primary mechanisms (Edwards, 1994). All these three mechanisms can independently contribute towards contaminant removal.

1) precipitation: formation of the insoluble compounds such as  $\text{Al}(\text{AsO}_4)$  or  $\text{Fe}(\text{AsO}_4)$

2) co-precipitation: incorporation of soluble arsenic species into a growing metal hydroxide phase

3) adsorption: the electrostatic binding of soluble arsenic to the external surfaces of the insoluble metal hydroxide.

Numerous studies have been performed to evaluate arsenic removal using alum and iron salts. According to the lab-scale tests, 99 % of arsenic can be removed by both iron or aluminum salts under optimal conditions, and the residual arsenic content is lower than 1  $\mu\text{g/L}$  (Cheng et al., 1994). Full-scale facilities typically demonstrate a somewhat lower efficiency, from 50 % to over 90 % removal. It was also reported that ferric and alum coagulation are equally effective for arsenic decontamination on a molar basis (Edwards, 1994). However, on a weight basis, alum performance is slightly lower than ferric salts for arsenic removal (Cheng et al., 1994; Scott et al., 1995; Hering et al., 1997). Such observation is primarily because iron hydroxide is less soluble than aluminum hydroxide over a wide range of pH (Hering et al., 1997).

Although it shows a good efficiency to treat water/wastewater with high levels of arsenic, coagulation/precipitation process may be difficult to consistently meet a

low-level MCL imposed by USEPA. Systems using lime softening may require secondary treatment to achieve that goal. Also, it produces a large amount of wet bulky sludge which contains toxic chemicals arsenic, and sludge disposal becomes a great concern, especially if nearby landfills are unwilling to accept such kind of sludge.

Electrocoagulation is a well known process for arsenic contaminated wastewater treatment (Lakshminathiraj et al., 2010); it has also been used to treat potable water containing arsenic (Melitas et al., 2002). EC involves complex chemical and physical processes containing many surface and interfacial phenomena. Typically, aluminum or iron plates are used as sacrificial anodes. Depending on the solution pH and exposure to oxygen, metal oxides, oxy-hydroxides and hydroxides are formed in the reaction medium.

Parga and the coworkers reported arsenic removal from contaminated groundwater in La Comarca Lagunera Mexico using air injection integrated EC process (Parga et al., 2005). Results suggest that magnetic particles of magnetite and amorphous iron oxyhydroxides produced during EC process could remove arsenite and arsenate from well water with an efficiency of over 90 % within 90 s or less. Combination of Al-Fe electrodes in EC has been applied by Gomes and the coauthors (Gomes et al., 2007). Such EC process showed that partial As(III) were found to convert to As(V) and the removal efficiency of total arsenic ranged from 78.9 % to over 99.6 % with different initial concentrations. Studies on the electrochemical decontamination of arsenic-containing wastewater were conducted by

Lakshmipathiraj and the coworkers (Lakshmipathiraj et al., 2010). Almost 95 % removal of the total arsenic was achieved within 5 min from its initial concentration of 10 mg/L. It can be seen that EC exhibits high removal efficiency towards arsenic; however, the energy consumption and electrode material loss pose a great pressure to electrochemical coagulation.

#### **2.2.4.2 Ion exchange**

Reportedly, several types of ion exchange resins have been developed for arsenic removal. Generally, these resins are based on a cross-linked polymer skeleton, namely matrix. Such matrix mostly consists of polystyrene cross-linked with divinylbenzene; through covalently bonded charged functional groups are linked to the matrix.

Calmon investigated arsenic removal using both cation and anion exchangers (Calmon, 1973). Cation exchangers were ineffective, but to some extent, several anion resins yielded removals in both batch equilibrium tests and column studies. Anion exchange resins are available in two basic forms, weak base and strong base. In many cases, the resins activated by hydroxyl groups can achieve significant arsenic removal due to Van der Waals bonding, ion exchange as well as electrostatic interaction. However, the removal capability largely relies on the presence of other competing species in solution such as sulfate, total dissolved solids (TDS), selenium, fluoride, phosphate and nitrate. Usually, up to 95 % of arsenate can be easily removed by ion exchange resins when sulfate content is low in waters; and treat ranges from hundreds to over a thousand bed volumes before the breakthrough occurs.

Consequently, it is recommended that ion exchange resins should not be applied in waters with high levels of sulfate and TDS.

#### **2.2.4.3 Membrane techniques**

Membrane techniques like NF, RO and ED are capable of rejecting almost all kinds of dissolved solids including arsenic from water. During this process, arsenic is separated from water by passing it through a membrane or semi-permeable barrier.

NF was found to be able to remove more than 90 % of pentavalent arsenic and the recoveries ranged between 5.6 to 15 % (Kosutic et al., 2005). Studies carried out by Figoli and the coauthors were to investigate the effects of operating parameters on arsenic removal by NF (Figoli et al., 2010). Their findings show that an increase of pH, a decrease of temperature and arsenic feed concentration led to higher arsenic rejection. Among all the parameters affecting arsenic removal, feed concentration plays a key role for the production of a permeate stream within the allowed limits imposed by WHO. Recently, Harisha and the coworkers used thin film composite NF membrane to remove arsenic from drinking water (Harisha et al., 2010). They found that the commercial membranes retained significant flux and was able to reject up to 99.8 % of arsenic and decrease arsenic concentration to the level stipulated by WHO; pH and presence of other ions affected the efficiency of this process.

RO is considered to be another alternative membrane technique for arsenate removal from water. It usually provides arsenic removal efficiencies of greater than 95 % when operating pressure is at ideal psi. Ning had reviewed the removal

mechanisms of arsenic by RO and concluded that arsenic in the commonly high oxidation states of (V) was very effectively removed by RO (Ning, 2002). With further attention to treating the weakly acidic As(III) species by operation of RO at sufficiently high pH made possible by newer antiscalants, practical processes can be developed with RO to remove all major species of arsenic from water.

Household reverse osmosis units were also set up in a Western U.S. region with high arsenic in groundwater to produce drinking water and performance of these 59 RO systems were examined (Walker et al., 2008). It was found that RO system was not working properly in 3 of the 59 households, while arsenic levels in treated water still exceeded 10 ppb in 18 of the 59 households. They attributed such observation to two main factors. First, arsenic concentrations were too high even though the rejection of RO could remove 95 % of arsenic. Second, trivalent arsenic was the dominant species in nearly 15 % of the wells and significantly reduced the efficiency.

NF and RO membrane techniques might be the technically superior technology to meet the regulation limit of arsenic. Besides, this process will not produce toxic sludge and can achieve simultaneous removal of other dissolved toxic contaminants. However, it still should be extensively considered before practical application due to the high initial investment, technological development costs and energy consumption. Also, low water recovery may be an issue in water-scarce region. Furthermore, prevention and maintenance techniques are usually required to solve the membrane fouling. The discharge of the concentrate may also be a concern.

ED is similar to RO except the driving force; an electric current is applied to draw

the ions through the semi-permeable membrane. It is also expected to achieve high removal efficiency of arsenic (Pedersen et al., 2005; Basha et al., 2008). Although it is easier to operate, ED may not be competitive with respect to costs and process efficiency when compared to NF and RO.

#### **2.2.4.4 Biological processes**

Biological treatment has substantial promise for removal of arsenic species. There are two main types of arsenic and microorganism interactions. One is direct bioaccumulation of arsenic species by different forms of microbial biomass; the other is using microbial oxidation to produce biogenic hydroxides or sulfides for subsequent arsenic sorption or precipitation (Wang and Zhao, 2009). Several factors may affect biological treatment performance including pH, contaminant concentration, available nutrients and temperature.

Three bacterial strains namely, *Ralstonia eutropha* MTCC 2487, *Pseudomonas putida* MTCC 1194 and *Bacillus indicus* MTCC 4374 were employed by Mondal and the coworkers to examine their arsenic removal efficiencies from simulated wastewater, which were 67 %, 60 % and 61 %, respectively (Mondal et al., 2008). Pokhrel and the coauthors investigated the potential of fungal biomass (*Aspergillus niger*) coated iron oxide-coated to remove arsenic from aqueous solution. Results showed that it was able to remove 95 % of As(V), 75 % of As(III), and 50 % of DMA from contaminated water at pH 6 (Pokhrel and Viraraghavan, 2006, 2008). Genetically engineering techniques has been reported to enhance cellular

accumulation of arsenic by Kostal and the coworkers (Kostal et al., 2004). It was found that the metalloregulatory protein ArsR, overpressed in engineered bacteria *Escherichia coli* accumulated 5- and 60-fold-higher levels of As(III) and As(V) than cells without ArsR overexpression. The level of arsenic accumulation was 1.47-2.2 nmol/mg dry weight, and the engineered cells could remove 98 % of 50 ug/L arsenite from contaminated water.

Arsenic can also be removed from solutions by sequestering as insoluble arsenic-sulfide complexes through the metabolic activity of anaerobic sulfate-reducing bacteria. A mixed culture of sulfate-reducing bacteria was employed by Teclu and the coworkers. to study the bioremoval of arsenic species from groundwater (Teclu et al., 2008). 77 % and 55 % of As(V) and As(III) removal was found respectively under the following conditions: pH 6.9, initial arsenic concentration (1 mg/L), 24 h contact time and biomass (2 g/L).

Recently, Hassan and the coauthors developed a combined bio-physicochemical treatment process for arsenic removal from groundwater (Hassan et al., 2009). During this system, several indigenous iron-oxidizing bacteria present in most groundwater can oxidize iron in the presence of organic matter and form complexes of multiple adsorbing solids. Arsenic was directly adsorbed on the biogenic iron oxides and subsequently precipitated. Moreover, microbiological oxidation of arsenite to arsenate occurred, which would lead to further improved overall removal efficiency. More than 95 % arsenic removal was reported for this combined system.

Biological treatment of arsenic may generate less sludge than conventional



coagulation/precipitation. However, such bioprocesses must compete with existing techniques in terms of efficiency and economy. High concentrations of arsenic could inhibit biological activity. The requirement of pretreatment to encourage the growth of key microorganisms as well as addition of nutrient may increase the costs.

#### **2.2.4.5 Sorption**

Arsenic sorption has been studied using a wide variety of materials such as AC, industrial / agricultural by-products or wastes, soils and constituents as well as metal-based sorbents.

AC is a commonly used material in arsenic treatment. Sorption of arsenic onto activated charcoal versus pH and temperature was studied by Eguez and Cho (Eguez and Cho, 1987). The capacity of As(III) was constant over the pH range of 0.16-3.5, while As(V) exhibited a maximum sorption at pH 2.35. Results suggest that physisorption occurred due to weak Van der Waals forces. Three activated carbons with different ash contents were studied for arsenic sorption: coconut shell carbon with 3 % ash, peat-based extruded carbon with 5 % ash and a coal-based carbon with 5-6 % ash (Lorenzen et al., 1995). As(V) was more effectively removed from water by carbon types with a high ash content.

To improve sorption capability of AC, researchers used different metal ions, mostly iron oxide to impregnate carbon. The chemically treated AC usually achieves higher arsenic removal compared with the non-impregnated one. Gu and the coworkers developed iron-containing granular activated carbon sorbents (As-GAC)

for arsenic removal from drinking water (Gu et al., 2005). Granular activated carbon (GAC) was used as a supporting medium for ferric ions which were impregnated by aqueous ferrous chloride and followed by hypochlorite chemical oxidation. It was found that As-GAC could remove arsenic most efficiently when the iron content was around 6 %; but further increases in iron was unfavorable for arsenic uptake. Recently, nano-iron (hydr)oxide impregnated GAC (Fe-GAC) samples were synthesized by Hristovski and the coworkers using two different preparative methods (Hristovski et al., 2009). The Fe-GAC developed via the permanganate method had almost an order of magnitude higher arsenic sorption capacity than that prepared by direct precipitation from alcohol (approx. 250 vs. 45 ug As/g dry media at pH 6.4).

In these studies, commercially available activated carbons were used; however, the commercial AC is not suitable for developing countries due to its relatively high cost (Choong et al., 2007). Other low-cost and abundant materials were thus utilized, such as industrial and agricultural by-products or wastes, soils, clay minerals and zeolites.

Red mud (Bauxol) is a waste material formed during the production of alumina when bauxite ore is subjected to caustic leaching. Seawater-neutralized red mud, activated Bauxsol (AB) by acid treatment or by combination with heat treatment, Bauxsol with added ferric sulfate or aluminum sulfate, and chemically modified AB-coated sand were all applied to arsenic removal (Mohan and Pittman, 2007). Arsenate removal from aqueous solution by using liquid phase of red mud (LPRM) was also reported (Altundogan and Tumen, 2003). Results suggested that it is

beneficial to use a waste material of red mud liquid phase in the treatment of arsenical wastewater, possibly combination with red mud solids as sorbent.

Agricultural wastes also have been explored as alternative sorbents for water purification or wastewater treatment, such as rice husk, coconut husk, amine modified coconut coir, orange juice residues and waste tea fungal biomass (Choong et al., 2007). Rice husk without any pretreatment was adopted by Amin and coworkers. for arsenic removal from groundwater (Amin et al., 2006). Complete removal (column methods) of arsenic was achieved under the following conditions: initial arsenic concentration (100 ug/L), rice husk amount (6 g), average particle size (780 and 510 um), flow rate (6.7 and 1.7 mL/min), and pH (6.5 and 6.0), respectively. The desorption efficiency treated with 1 M of potassium hydroxide was in the range of 71-96 %. Ghimire and the coworkers chemically modified orange juice residue for arsenic removal (Ghimire et al., 2002). Maximum sorption capacities of the prepared sorbent for arsenite and arsenate uptake were reported to be 0.91 and 0.94 mmol/g, respectively.

Due to their high affinity, metal-based sorbents, especially iron and its compounds have been widely studied and used to adsorb arsenic, including zero-valent iron Fe(0), bimetallic sorbent, iron oxides/oxyhydroxides and iron oxides/oxyhydroxides-based sorbents. Interactions such as ion exchange, specific sorption to surface hydroxyl functions or coprecipitation contribute to arsenic removal. Generally, the exposed surface area of Fe(0) usually plays an important role in both the sorption kinetics and capacities. Kanel and the coauthors synthesized nanoscale zero-valent iron (NZVI,

1–120 nm diameter) for As(V) removal from groundwater (Kanel et al., 2006). Arsenic removal was very fast and achieved within minutes by NZVI whereas it took hours to days for micron-sized iron. Instrumental analysis confirmed partial reduction of As(V) to As(III) and formation of an inner-sphere surface complex on the surface. The reaction mechanism was attributed to sorption and coprecipitation. Zhang and the coworkers investigated a Fe-Ce bimetal sorbent for arsenic sorption, which exhibited a significantly higher As(V) sorption capacity (2 mmol/g) than the individual Ce and Fe oxides (0.45 mmol/g for CeO<sub>2</sub> and 0.35 mmol/g for Fe<sub>3</sub>O<sub>4</sub>) prepared by the same procedure (Zhang et al., 2005). Recently, a zirconium-based magnetic sorbent (ZrO(OH)<sub>2</sub>·1.6Fe<sub>3</sub>O<sub>4</sub>·2.5H<sub>2</sub>O) was developed through a coprecipitation technology and its arsenic removal potential was investigated (Zheng et al., 2009). Results showed that the maximum sorption capacity of 45.6 mg/g was achieved. Spectra analysis indicated that hydroxyl groups played a major role in the arsenic uptake. Bimetal oxide magnetic nanomaterials (MnFe<sub>2</sub>O<sub>4</sub> and CoFe<sub>2</sub>O<sub>4</sub>) were synthesized and used for arsenic sorption as well (Zhang et al., 2010b). The maximum sorption capacities of arsenite and arsenate on MnFe<sub>2</sub>O<sub>4</sub> were 94 and 90 mg/g, and on CoFe<sub>2</sub>O<sub>4</sub> were 100 and 74 mg/g, respectively. Increase of surface hydroxyl (M-OH) species was reported to lead to higher sorption capabilities of this bimetal oxide sorbent compared to Fe<sub>3</sub>O<sub>4</sub>.

Several iron oxides/oxyhydroxides, such as amorphous hydrous ferric oxide (FeOOH), goethite ( $\alpha$ -FeOOH), akaganeite ( $\beta$ -FeOOH) and hematite ( $\alpha$ -Fe<sub>2</sub>O<sub>3</sub>) are promising sorbents for removing both As(V) and As(III) from aqueous solutions (Choong et al., 2007; Mohan and Pittman, 2007). Among them, amorphous hydrous

ferric oxide exhibits the highest sorption capacity due to the highest surface area (Mohan and Pittman, 2007). However, it usually tends to form crystalline iron oxides with low surface area during preparation, which significantly affects its performance. Moreover, most of the iron oxides exist as fine powders which are difficult to be separated from liquid in solid/ liquid separation. Therefore, researchers have proposed to include porous oxides/oxyhydroxides into a well organized host matrix; other types of sorbents based on iron oxides/oxyhydroxides are investigated for arsenic treatment as well, such as iron oxide-coated polymeric materials, iron oxide-coated sand, iron oxide-coated cement, iron-hydroxide coated alumina, iron-doped alginate gels. A comparison of the sorption capacities of selected sorbents based on iron oxides/oxyhydroxides towards arsenic is shown in Table 2.6 (Choong et al., 2007; Mohan and Pittman, 2007).

Other reported works on the metal based sorbents also include titanium, cerium as well as rare earth metal (e.g. lanthanum) (Biswas et al., 2008; Jing et al., 2009; Deng et al., 2010). Several recent studies are discussed. Arsenic sorption behavior was examined using lanthanum (III) and/or cerium (III)-loaded orange waste gels (Biswas et al., 2008). Results showed that arsenate sorption was more favorable over a pH range of 6-9.5 whereas arsenite was better adsorbed at pH 9-11. This chemically modified orange waste gels can effectively remove arsenate and arsenite with maximum sorption capacities of 42 and 43 mg/g, respectively. A novel Ce-Ti oxide sorbent was prepared by the hydrolysis-precipitation method and employed for arsenate removal from water (Deng et al., 2010). Spectroscopic investigations revealed that this sorbent was composed of some nanoparticles in the size range of

100-200 nm, which aggregated to form porous sorbents. At the equilibrium As(V) concentration of 10 ug/L, the average sorption capacity of this hybrid sorbent was up to 7.5 mg/g, indicating the high removal capability at low concentrations.

Table 2.6 Arsenic sorption capacities of selected iron oxides/oxyhydroxide based sorbents

Sorbent	Type of water	pH	Capacity (mg/g)	
			As(V)	As(III)
Fe-oxide coated sand	drinking	7.6	0.043	0.041
Fe(III) loaded chelating resin	aqueous solution	9.0 for As(III) 3.5 for As(V)	55.44	62.93
Fe(III) alginate gels	--	4.0	6.44	--
Fe-hydroxide coated alumina	drinking water	6.62-6.74 for As(III) 7.15-7.2 for As(V)	36.64	7.64
Iron oxide coated cement	drinking water	approx. 7	6.43	0.67
Bead cellulose loaded with iron oxyhydroxide	groundwater	7.0	33.2	99.6

## 2.4 Models for sorption equilibrium

In general, equilibrium model is mainly for batch sorption at equilibrium state. Langmuir and Freundlich isotherms are widely used due to their simplicity of the formulae and more importantly the models often provide good fitting results.

$$\text{Langmuir equation} \quad q_{eq} = \frac{bq_{max}C_{eq}}{1+bC_{eq}} \quad (2.5)$$

where  $q_{\max}$  and  $b$  are Langmuir constants, which reflect the maximum sorption capacity and the affinity between adsorbate and sorbent.  $q_{eq}$  and  $C_{eq}$  are the sorption capacity and the equilibrium concentration of adsorbate in solution, respectively.

The Langmuir equation was originally formulated based on theoretical assumptions: (1) the sorption can not proceed beyond monolayer coverage; (2) all surface sites are identical and energetically equivalent, and (3) there is no interaction among the molecules adsorbed (Ruthven, 1984; Cussler, 1997). However, in reality, the surface of sorbent is usually not uniform; and various sorption sites may coexist on the sorbent surface. Therefore, the assumptions of homogenous and monolayer sorption limited its use in more broad area.

Sometimes, the empirical Freundlich isotherm can describe the real sorption processes more accurately than the Langmuir equation, by assuming that the sorbent has heterogeneous surface sites with different energies for sorption (Onyango et al., 2004). The mathematical statement is given as:

$$\text{Freundlich equation} \quad q_{eq} = K_f C_{eq}^{1/n} \quad (2.6)$$

where  $K_f$  is Freundlich constant and  $1/n$  is sorption intensity constant or heterogeneity coefficient which has a lower value for more heterogeneous surfaces (Zhang et al., 2007b).

These two isotherms have been widely employed in liquid-solid sorption system.

Gupta and the coworkers showed the sorption isotherms of As(III) and As(V) on iron-chitosan composites obeyed the Langmuir equation (Gupta et al., 2009). This model also fitted best to arsenic(V) sorption onto chitosan at low concentration range of 25 to 2500 µg/L in the research study of Gerente and the coauthors (Gerente et al.). Sorption of As(III), As(V) and DMA from aqueous solutions onto polymeric Al/Fe modified montmorillonite was studied; and their data were best described by the Freundlich isotherm model (Ramesh et al., 2007). Bursali and the coworkers suggested that Freundlich models provided best conformity with the experimental data for boron sorption by invasive marine seaweed (*Caulerpa racemosa* var. *cylindracea*) as well (Bursali et al., 2009).

## **2.5 Models for sorption kinetics**

In the past decades, several mathematical models have been proposed to describe the sorption kinetics, which can generally be grouped into two major classes: empirical models and mechanistic models (Chen, 1997). The first group of models is essentially based on data fitting and not able to interpret the sorption experimental data (Chen and Lin, 2001a). The common empirical models include pseudo-first rate order and pseudo-second rate order, which can be presented as follows:

$$\text{Pseudo-first rate equation} \quad \frac{dq}{dt} = K_1 (q_{eq} - q_t) \quad (2.7)$$

$$q_t = 0 \text{ at } t = 0; \quad q_t = q_t \text{ at } t = t$$



$$\text{Pseudo-second rate equation } \frac{dq}{dt} = K_2 (q_{eq} - q_t)^2 \quad (2.8)$$

$$q_t = 0 \text{ at } t = 0; \quad q_t = q_t \text{ at } t = t$$

where  $q_{eq}$  and  $q_t$  are the sorption capacities at equilibrium time and time  $t$ , respectively.  $K_1$  and  $K_2$  are the pseudo-first-order rate constant and pseudo-second-order rate constant, respectively. Ho and McKay reviewed many research works and found that the highest correlation coefficients were obtained for the pseudo-second order kinetic model (Ho and McKay, 1999).

In recent years, numerous studies employed the pseudo-first order and pseudo-second order equations that have been applied to different kinds of sorption systems, such as the sorption of arsenic using modified calcined bauxite, surface modified carbon black, dolomite and synthetic siderite (Bhakat et al., 2006; Borah et al., 2008; Guo et al., 2010; Salameh et al., 2010), removal of boron by Siral samples and fly ash (Yurdakoc et al., 2005; Yuksel and Yurum, 2010), sorption of malachite green from aqueous solutions using oil palm trunk fibre (Hameed and El-Khaiary, 2008), the sorption of 4-nitrophenol onto a novel hyper-crosslinked polymer (Pan et al., 2007), as well as removal of phosphate from water by a Fe-Mn binary oxide sorbent (Zhang et al., 2009).

From a mechanistic point of view, it is important to explain the experimental data, for example, determination of the rate-limiting step during the sorption process. For a solid-liquid sorption, the transport of adsorbates is normally characterized by external

mass transfer or intraparticle diffusion or both.

The sorption kinetics is usually constructed on the basis of three consecutive steps (Lazaridis and Asouhidou, 2003; Qiu et al., 2009): (1) transport of adsorbates from bulk solution to the external surface of sorbents through liquid film; (2) transport within the particle, which is so-called intraparticle diffusion; and (3) sorption and desorption between the adsorbates and active sites. For many environmental applications, the overall rate of sorption is controlled by the slowest step, which would be either external transfer (film diffusion) or intraparticle diffusion. The common models contain two different intraparticle diffusion mechanisms: surface diffusion and pore diffusion, which are generally written as follows (Tien, 1994):

$$\begin{aligned} \text{Surface diffusion model} \quad \frac{1}{D_s} \frac{\partial q}{\partial t} &= \frac{1}{r^2} \frac{\partial}{\partial r} \left[ r^2 \frac{\partial q}{\partial r} \right] & (2.9) \\ 0 \leq r \leq a_p, t \geq 0 \end{aligned}$$

$$\begin{aligned} \text{Pore diffusion model} \quad \varepsilon_p \frac{\partial c}{\partial t} &= \frac{D_p}{r^2} \frac{\partial}{\partial r} \left[ r^2 \frac{\partial c}{\partial r} \right] - \rho_p \frac{\partial q}{\partial t} & (2.10) \\ 0 \leq r \leq a_p, t \geq 0 \end{aligned}$$

where  $c$  ( $\text{mol/m}^3$ ) and  $q$  ( $\text{mol/kg}$ ) are the concentrations of adsorbate in the bulk and solid phases, respectively;  $D_s$  and  $D_p$  ( $\text{m}^2/\text{s}$ ) are the surface diffusivity and pore diffusivity within the particles, respectively;  $\rho_p$  ( $\text{kg/m}^3$ ) is the particle density;  $r$  (m) is radius distance measured from the center of particle;  $a_p$  (m) is the particle radius;  $\varepsilon_p$  is the porosity of the sorbent, and  $t$  (s) is the time.

Chen and the coworkers used a diffusion-controlled model to predict the sorption kinetics at different pH (Chen et al., 1997; Chen and Lin, 2001a). Chen and Yang found that the surface diffusion controlled the biosorption kinetics when metal ions were adsorbed onto chemically modified seaweed (*Sargassum sp.*) (Chen and Yang, 2005). Conversely, pore diffusion model was reported by Xue and Sun to better describe the sorption of lysozyme using poly(vinyl alcohol)-based magnetic affinity support (Xue and Sun, 2001). Recently, a novel kinetic model was proposed by Choi and the coauthors for aqueous benzene sorption on activated carbon, based on mass conservation of benzene coupled with three-stage sorption: the first portion for an instantaneous stage or external surface sorption, the second portion for a gradual stage with rate-limiting intraparticle diffusion, and the third portion for a constant stage in which the aqueous phase no longer interacts with activated carbon (Choi et al., 2007).

## **CHAPTER 3**

### **MATERIALS AND METHODS**

#### **3.1 Materials**

Flake-type chitosan ( $\geq 85$  % deacetylated) from Sigma Co. were used to prepare chitosan beads. Regenerated cellulose membranes (RC) with 47 mm diameter, and 1.0  $\mu\text{m}$  average pore diameter were purchased from Whatman, Inc. Acetic acid from Merck and Ethylene glycol diglycidyl ether (EGDE) from Sigma-Aldrich were used for preparation of crosslinked chitosan beads. Tetrahydrofuran (THF, HPLC grade) and methanol (HPLC grade) from TEDIA, 2-Bromoisobutyryl bromide (2-BIB,  $> 97$  %) from Fluka as well as triethylamine (TEA,  $> 99$  %) from Sigma-Aldrich were used for the introduction of polymerization initiator. Glycidyl methacrylate (GMA,  $\geq 97$  %) supplied by Fluka was used in the surface graft polymerization on chitosan beads and RC membranes. Chemicals used for GMA polymerization included N, N-dimethylformamide (DMF, HPLC grade) from TEDIA, 2,2'-bipyridine (BPY,  $\geq 99$  %), and copper (I) bromide (CuBr, 98 %) from Sigma-Aldrich, ethylenediaminetetraacetic acid disodium salt (EDTA, 99 %) from J.T.Baker. N-methyl-D-glucamine (NMDG,  $\geq 97$  %) from Fluka and acetone (HPLC grade) from TEDIA were used for further fictionalization of grafted polymers.

Other chemicals for sorption experiments were listed as below. Boric acid ( $\text{H}_3\text{BO}_3$ , 99.6 %) from Fisher Scientific was used to prepare boron stock solution. Sodium

hydrogen arsenate heptahydrate ( $\text{Na}_2\text{HAsO}_4 \cdot 7\text{H}_2\text{O}$ ,  $\geq 98\%$ ) from Fluka, disodium methylarsenate ( $\text{CH}_3\text{AsNa}_2\text{O}_3$ ,  $98\%$ ), one of MMA species from Chem Service as well as sodium cacodylate ( $(\text{CH}_3)_2\text{AsNaO}_2$ ,  $\geq 98\%$ ), one sodium salt of DMA from Sigma-Aldrich were used to prepare inorganic and organic arsenic stock solutions, respectively. Sodium chloride ( $\text{NaCl}$ ,  $\geq 99.5\%$ ), sodium nitrate ( $\text{NaNO}_3$ ,  $\geq 99\%$ ), sodium perchlorate ( $\text{NaClO}_4$ ,  $98\%$ ), sodium fluoride ( $\text{NaF}$ ,  $\geq 99\%$ ), sodium dihydrogen phosphate monohydrate ( $\text{NaH}_2\text{PO}_4 \cdot 7\text{H}_2\text{O}$ ,  $\geq 99\%$ ) and sodium sulfate ( $\text{Na}_2\text{SO}_4$ ,  $\geq 99\%$ ) were analytical grades purchased from Sigma-Aldrich. Suwannee River humic acid was obtained from the International Humic Substances Society (IHSS). Nitric acid ( $\text{HNO}_3$ ,  $\geq 65\%$ ) and sodium hydroxide ( $\text{NaOH}$ ,  $\geq 99\%$ ) from Merck were used for pH adjustment.

### **3.2 Preparation of chitosan-based sorbents**

#### **3.2.1 Preparation of crosslinked chitosan beads**

Chitosan beads were prepared by electrostatic extrusion method. Setups for droplet generation experiments were conducted as shown in Figure 3.1. A variable high voltage power supply machine from Matsusada containing a step up transformer was assembled to convert an AC 240 V input into a desired output voltage. The positively charge high voltage output line was connected directly to the needle on the syringe. The syringe was placed on the syringe pump to disperse chitosan solution. This syringe pump had an integrated digital flow rate controller. A collection Petri plate was placed directly below the needle position and on top of a magnetic stirrer.

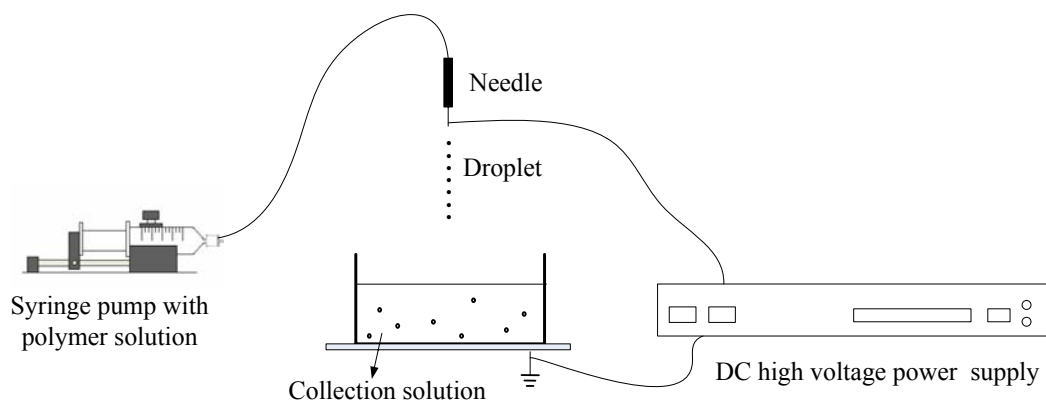


Figure 3.1. Electrostatic droplet generating system

Chitosan flakes were initially dissolved in acetic acid solution. The solution subsequently dripped through the positively charged needle and formed droplets at the end of the needle. These droplets were pulled off by electrostatic force and dropped into alkaline collection solution which had been grounded. Size of droplets was mainly controlled by the voltage and flow rate of chitosan solution. Thus, the nascent beads were immediately formed. Subsequently, the beads formed were left in the solution overnight to ensure the completion of the gelling process. The wet beads were finally collected and extensively rinsed with deionized (DI) water until the pH of solution became the same as the fresh DI water, and then stored in DI water for future use.

The chitosan beads were suspended in a water solution. EGDE was then added into the chitosan suspension. The mixture was shaken for 6 h for crosslinking reaction. After the reaction was completed, the mixture was cooled down to room temperature and then washed with sufficient DI water until the pH became the same as the fresh DI water. The crosslinked chitosan (hereafter referred to CCTS) beads were finally

dried in freeze dryer for two days and stored in a desiccators.

### **3.2.2 Immobilization of the initiator on the crosslinked chitosan beads**

CCTS particles were weighed and added into a solution containing triethylamine and THF, followed by slowly dropwise addition of 2-BIB in THF over 20 min. The mixture was firstly gently stirred at 0 °C for several hours and then at room temperature overnight. Finally, the surface-initiated chitosan beads (designated as CTS-Br) were collected and washed successively with THF, methanol and DI water; and finally dried by a freeze drier for two days.

### **3.2.3 Surface-initiated atom transfer radical polymerization**

For the polymerization of GMA on the initiated chitosan surface, GMA, CuBr and BPY were added into a round-bottom flask containing a mixed solvent of DMF and DI water. The solution was stirred and bubbled with argon gas for around 30 min. The surface-initiated beads were then added into the mixture.

The flask was tightly sealed and reaction mixture was shaken at room temperature for a predetermined time. After polymerization, the chitosan beads grafted with PGMA were separated and washed with excess acetone, EDTA and DI water; finally dried with a freeze drier for 2 days. The collected particles were significantly bigger than the initial size and were designated as chitosan-g-PGMA (CTS-PGMA).

### **3.2.4 Preparation of NMDG modified CTS-PGMA**

The prepared CTS-PGMA particle was reacted with NMDG in DMF. At the end, the mixture was cooled, filtered, washed with methanol and DI water, respectively. The products were dried at freeze dryer for 2 days to obtain NMDG modified chitosan-g-PGMA (hereafter referred to CTS-MG).

### **3.3 Surface modification of cellulose membranes**

#### **3.3.1 Pretreatment of RC membranes**

RC membranes were prewetted with methanol for 10-15 min to remove glycerine, which is used as a structural “preservative” for these membranes; and then were rinsed with ultrapure water twice for 10 min each rinse to remove methanol.

#### **3.3.2 Surface initiation**

RC were immersed in anhydrous THF for 10 min before initiation. Thereafter, the membranes were removed from THF and dried for 5 min before placing into the solution for initiation. The initiator 2-BIB was immobilized by reaction with hydroxyl groups of RC membranes to covalently immobilize bromoester initiator groups to the membrane surface. A typical solution consisted of RC membranes, 2-BIB, TEA, and anhydrous THF, in which the molar ratio of 2-BIB to TEA was kept 1:1. The reaction mixture was gently stirred at 0 °C for several hours, and then at room temperature overnight. The initiator functionalized membranes (refer to RC-Br) were washed thoroughly with methanol and ultrapure water.



### **3.3.3 Surface-initiated polymerization on cellulose membranes**

For the surface initiated ATRP, the initiators, GMA, BPY were added to a mixed solvent of DMF and ultrapure water. The mixture was degassed with argon with 30 min; and then CuBr was introduced to the reaction mixture. The flask was sealed and the ATRP reaction proceeded for predetermined period of time. After polymerization, RC membranes with surface grafted poly(glycidyl methacrylate) (denoted as RC-PGMA) was removed from the solution and washed thoroughly with excess acetone and ultrapure water.

### **3.3.4 NMDG functionalization**

The NMDG modified RC-g-PGMA (denoted as RC-MG) was prepared by treatment of RC-PGMA surface with excess NMDG in DMF. At the end, the mixture was cooled and washed with ultrapure water.

## **3.4 Physical characterizations**

### **3.4.1 Specific surface area**

Specific surface area was determined using nitrogen adsorption / desorption and the Brunauer-Emmett-Teller (BET) algorithm on A NOVA 4200e BET Analyzer (Quantachrome Instrument, U.S.A). Prior to the measurements, the samples were degassed at 70 °C overnight under flowing nitrogen. The specific surface area was calculated via computational treatment of the BET Equations.

### 3.4.2 Surface charge density

The surface charge density ( $\sigma_0$ ) of the sorbent is defined by the uptake of protons by the surface. It is determined by the potentiometric titration experiments, and calculated from the following equation (Chen and Lin, 2001b).

$$\sigma_0 = \frac{(c_A - c_B + [OH^-] + [H^+])F}{Sa} \quad (3.1)$$

where  $c_A$  and  $c_B$  (M) are the concentrations of acid and base needed to reach a point on the titration curve.  $[H^+]$  and  $[OH^-]$  (M) are the concentrations of  $H^+$  and  $OH^-$ ,  $F$  is Faraday's constant (96490 C/mol),  $S$  ( $m^2/g$ ) is the specific surface area of sorbent, and  $a$  (g/L) is the concentration of sorbent.

The surface charge density of the sorbent was obtained by an acid-base titration. 50 mg of sorbent was shaken with 100 ml  $CO_2$ -free aqueous solution for 1 day in an air-tight bottle. A recorded volume of 0.01 M / 0.1 M  $HNO_3$  or 0.01 M NaOH was added into the mixture. Time interval between each addition was maintained around 20 minutes to stabilize the solution pH and then pH value of the mixture was then recorded. The pH values were measured by ORION 920Aplus pH meter. During the titration, the solution were shaken and bubbled with nitrogen gas in order to prevent  $CO_2$  from being adsorbed from the atmosphere. Experiments were conducted at room temperature. The acid and base titration experiments were carried out separately.

### 3.4.3 Contact angle

Water contact angles of the membranes were measured and calculated in dynamic mode at ambient temperature. The automated contact angle goniometer (DSA20B, Kruss) was equipped with software-controlled dosing system and contact angles determination software. For each measurement of contact angle value, at least three points from different parts of the membrane surface were recorded and averaged. The curves of contact angle versus drop age was plotted to compare the relative hydrophilicity of the membranes at different reaction stage.

### **3.5 Batch experiments**

#### **3.5.1 Boron, arsenic, TOC, IC and pH analyses**

The concentrations of boron and arsenic were measured by an inductively coupled plasma emission spectrometer (ICP-ES; Perkin-Elmer Optima 3000, USA). Before analysis, all the samples were filtered through 0.45  $\mu\text{m}$  membrane filter. Total organic carbon (TOC) was used to evaluate the degree of natural organic matter sorption, which was measured using a TOC analyzer (Shimadzu TOC Analyzer, Japan). The chemical compositions of simulated seawater were determined by ion chromatography system (ICS-2000 RFIC, Dionex) and TOC analyzer. pH values of the solutions were measured by an ORION 920Aplus pH meter

#### **3.5.2 Sorption of boron**

Batch equilibrium sorption experiments were performed to investigate the characteristics of boron removal from aqueous solution. The sorption capacity ( $q_{\text{eq}}$ ) is

defined as:

$$q_{eq} = \frac{V(C_0 - C_{eq})}{m} \quad (3.2)$$

where V, C<sub>0</sub>, C<sub>eq</sub> and m are volume of solution, initial concentration, equilibrium concentration, and weight of sorbent, respectively.

The stock solutions of boron used in sorption experiments were prepared from H<sub>3</sub>BO<sub>3</sub>. Initially, stock solutions containing 1000 mg/L boron were prepared by dissolving 5.72 g of H<sub>3</sub>BO<sub>3</sub> in 1 L of DI water. Experimental solutions were diluted freshly from these stock solutions as required.

In the pH effect study, boron solutions at various initial pH values were adjusted by HNO<sub>3</sub> and NaOH. The sorbents / membranes were added to boron solution with a known concentration. All mixtures were shaken at room temperature for 3 days. Samples were taken at the end of the experiments to analyze boron concentration by ICP-ES. Both initial and equilibrium pH values were recorded.

Sorption isotherm experiments were conducted by adding a dosage of 0.5 g/L sorbents / membranes in high density polyethylene (HDPE) bottles with various initial boron concentrations. Initial pH of the solution was adjusted to 7.0. All bottles were shaken at room temperature for 3 days to reach equilibrium. At the end of the experiments, 20 ml samples were collected for ICP analysis. CCTS, RC and commercial resin Amberlite IRA-743 were also tested for their uptake capacities for boron. The procedures were the same as the above.

Sorption kinetic experiments were conducted to determine the equilibrium time for boron sorption. The initial pH was adjusted to the optimum value of 7.0. Desired amount of sorbents was added to boron solution with a known concentration. Samples were taken at appropriate time intervals and boron concentrations were analyzed by ICP-ES.

In order to test the effects of co-existing anions, ionic strength ranged from 0 mM to 100 mM with NaCl and NaNO<sub>3</sub>. Solution pH was initially adjusted to 7.0 before the sorbent was added. Moreover, simulated seawater was prepared to do a batch run. Different doses of sorbents were added into boron solution, ranging from 0 g/L to 2 g/L. Other procedures were the same as those used in the abovementioned pH effect experiments.

### **3.5.3 Inorganic arsenic and methylated arsenic**

Stock solutions of arsenate, MMA and DMA were prepared by dissolving a certain amount of Na<sub>2</sub>HAsO<sub>4</sub>·7H<sub>2</sub>O, CH<sub>3</sub>AsNa<sub>2</sub>O<sub>3</sub> and (CH<sub>3</sub>)<sub>2</sub>AsNaO<sub>2</sub>, respectively, in ultrapure water. The stock solution was then diluted to prepare arsenic solution with different desired concentrations. The sorption capacity ( $q_{eq}$ ) can be determined by Equation 3.2.

In the pH effect study, arsenic solutions with initial pH ranging from 2 to 11 were used at a constant concentration of 20 mg/L. Both initial and equilibrium pH values were recorded. Total arsenic concentrations before and after sorption were analyzed by the ICP-ES.

Sorption isotherm experiments were used to evaluate arsenic removal efficiency, which were conducted by varying initial arsenic concentrations with a dosage of 0.5 g/L sorbents. Initial pH of the solution was adjusted to 3.4, 4.0 and 5.0 for arsenate, MMA and DMA, respectively. CCTS (before modification) was also used to test the uptake capacities for both inorganic and organic arsenic species.

During batch kinetic sorption, arsenic solution of 20 mg/L was prepared; and NaClO<sub>4</sub> were selected as ionic strength backgrounds, ranging from 0 mM to 50 mM. Solution pH was initially adjusted to the desired pH level before the sorbent was added. The solution was then stirred at a constant rate. Samples were taken at predetermined time intervals to measure arsenic concentration by ICP-ES.

Effect of natural organic matter on arsenic removal was investigated with varying concentrations of humic acid (HA) at a constant arsenic concentration of 20 mg/L. The TOC analyzer was used to determine the concentrations of HA before and after the sorption. In order to test the effects of co-existing anions, concentrations of three different anions (fluoride, phosphate and sulfate) were adjusted from 0 mM to 1 mM. Solution pH was initially adjusted to 7.0 for both inorganic and organic arsenic species. All batch experiments were performed at room temperature; and all mixture were shaken for 3 days, a duration long enough to achieve equilibrium concentrations.

#### **3.5.4 Leaching tests**

The leaching experiments were performed in order to determine whether metal

(e.g. copper) leaching would result in a secondary pollution in the treated water. 20 mg of the pristine sorbents were immersed in 40 ml ultrapure water with initial pH adjusted to different values. After shaking for several days to achieve equilibrium, the solution was filtered to do ICP analysis to determine the metal elution.

### **3.6 Spectroscopic analyses**

#### **3.6.1 Microscope and Scanning Electron Microscopy**

The microscope (Carl Zeiss Microimaging GmbH, Germany) and scanning electron microscopy (SEM, JEOL, JSM-5600V, Japan) were employed to inspect the surface morphology of the polymeric sorbent. Morphology of membranes before and after functionalization was also investigated by SEM. During the SEM analysis, the samples were initially mounted on the sample studs using double-sided adhesive tapes, and then coated with platinum for production of electrical conductivity during test. The SEM analysis enables the direct observation of the changes in the surface microstructures due to chemical modification.

#### **3.6.2 Fourier Transform Infrared Spectroscopy**

Fourier Transform Infrared Spectroscopy (FT-IR) was used to determine the characteristics and changes of functional groups in the sorbents during synthetic reaction and sorption process. Each sample was mixed with pure potassium bromide which acts as background and then grounded into powder in an agate mortar at an approximate mass ratio of 1/100. The resulting mixture was then pressed at 10 tons

for 5 mins to form pellets. The pellets were characterized with infrared transmission spectra using FTS-135 (Bio-Rad, USA) spectrometer in the wavenumber range of 400 to 4000  $\text{cm}^{-1}$ . The background obtained from the scan of pure KBr was automatically subtracted from the sample spectra. All the spectra were plotted in the same scale on the transmittance axis.

### **3.6.3 Attenuated Total Reflection - Fourier Transform Infrared Spectroscopy**

A Fourier transfer infrared attenuated total reflection spectrometer (ATR-FTIR) was used to provide information on the surface chemistry of unmodified, initiator-functionalized, GMA grafted, and NMDG modified membranes. It was also employed to elucidate the sorption mechanism of NMDG modified membranes. The instrument was IRPrestige-21 (Shimadzu) equipped with a single reflection ATR accessory with ZnSe crystal. The spectra were recorded within the range of 600 - 4000  $\text{cm}^{-1}$  with a resolution of 4  $\text{cm}^{-1}$  over 32 scans.

### **3.6.4 X-Ray Photoelectron Spectroscopy**

Different types of materials were analyzed using X-ray photoelectron spectroscopy (Kratos XPS system-Axis His-165 Ultra, Shimadzu, Japan), with a monochromatized Al  $K\alpha$  X-ray source (1486.7 eV) working at 150 watt, 15 kV and 10 mA and base pressure of  $3 \times 10^{-8}$  Torr in the analytical chamber. For wide scan spectra, an energy range from 0 to 1100 eV was used with pass energy of 80 eV and step size of 1 eV. The high-resolution scans were conducted according to the peak being examined with pass energy of 40 eV and step size of 0.05 eV. To compensate



for the charging effects, all spectra were calibrated with graphitic carbon as the reference at a binding energy (BE) of 284.6 eV.

The XPS results were collected in binding energy forms and fitted using a nonlinear least-square curve fitting program (XPSPEAK41 Software). The XPS spectra were deconvoluted with the subtraction of linear or Shirley background. Linear type background was used for non-metal elements, while Shirley type background was applied for transition metals. The line-width (full width at half-maximum) of those spectra was fixed constant between 1 and 2. The percentage of Lorentzian-Gaussian was set at 0 for all the deconvoluted spectra. Surface compositions for each element were determined from the deconvoluted peaks area ratios.

## **CHAPTER 4**

### **SURFACE MODIFICATION OF CHITOSAN VIA ATOM TRANSFER RADICAL POLYMERIZATION**

Recently, more attention has been paid to surface modification of various solid substrates. The motivation for immobilizing a variety of functional groups onto the solid surfaces stems from the desire to provide parent materials with specific properties for practical application. ATRP developed by Wang and Matyjaszewski, is one of the most investigated controlled graft polymerization techniques, and it has been proven to be an effective method to achieve this purpose. Till now, studies on surface initiated polymerization from different types of substrates have been conducted; however, there have been no studies involving the surface initiated ATRP to modify chitosan substrates for boron removal application.

Among a variety of functional groups which can be integrated into polymers, the epoxide group becomes increasingly more attractive as it can be readily modified with different compounds (Bayramoglu et al., 2009). Through ring opening reaction, it is easily converted into various functional groups including hydroxyl, amine, and carboxyl groups (Yu et al., 2004). GMA, a commercially interesting functional monomer, was selected in our study because the presence of epoxide group can offer numerous possibilities for further functionalization (Canamero et al., 2004).

Most of the research on boron has provided information that chemical compounds containing vicinal polyhydroxyl groups tend to react with boric acid or borates, producing either neutral boron ester or anionic borate complexes; and the amine capability of retaining a proton is also favorable for boron chelation (Bicak et al., 2001; Geffen et al., 2006). In accordance with this chemistry, NMDG possessing an amine group and five hydroxyl functions can have exceptionally high boron binding capabilities. Therefore, it is of great interest to modify chitosan surfaces with GMA and further with NMDG to develop innovative sorbents, which can enhance boron removal from aqueous solution.

In this chapter, we report on the graft polymerization of GMA on chitosan surfaces via surface-initiated ATRP and further functionalization by NMDG. Materials at different surface modification steps were characterized with FT-IR and XPS, in order to elucidate the synthetic reaction mechanisms. The overall morphology of raw chitosan and modified chitosan were explored using microscopes and SEM. In addition, the novel sorbent was characterized via BET, potentiometric titration and leaching test.

#### **4.1 Sorbent Preparation**

The novel sorbent was synthesized according to the method described in previous chapter. Briefly, chitosan beads were initially prepared through electrostatic extrusion technique (Zhou et al., 2005): chitosan-acetic acid solution was dropped through a positively charged needle into alkaline solution under gentle stirring. The solidified

beads were formed and then reacted with crosslinking reagent (see Figure 4.1). The instrumental parameters used are listed in Table 4.1.

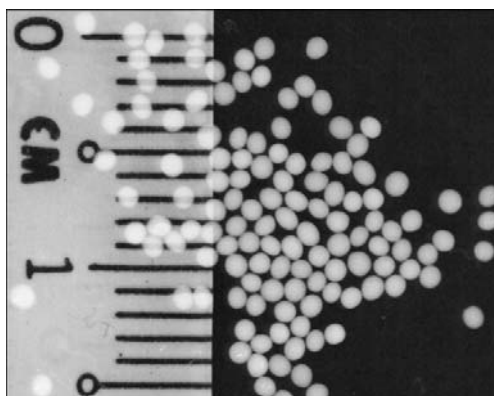


Figure 4.1. Pictures of chitosan beads

Table 4.1 Operational parameters of electrostatic extrusion for preparation of chitosan beads

Applied voltage	10 kv
Flow rate	1 ml/min
Needle size	25 G
Electrode spacing	4 cm
Chitosan concentration	1.5 % w/v
Gelling ion concentration	2 M
Polarity of dropping device	Positively charged needle

The pathway of preparing NMDG modified chitosan-g-PGMA can be outlined as in Figure 4.2, which mainly consists of three steps: surface initiation, GMA polymerization and NMDG functionalization. Briefly, initiators (hereafter referred to CTS-Br) were immobilized onto CCTS through the interaction between surface hydroxyl and amine groups and 2-bromoisobutyrate bromide; second, polymerization

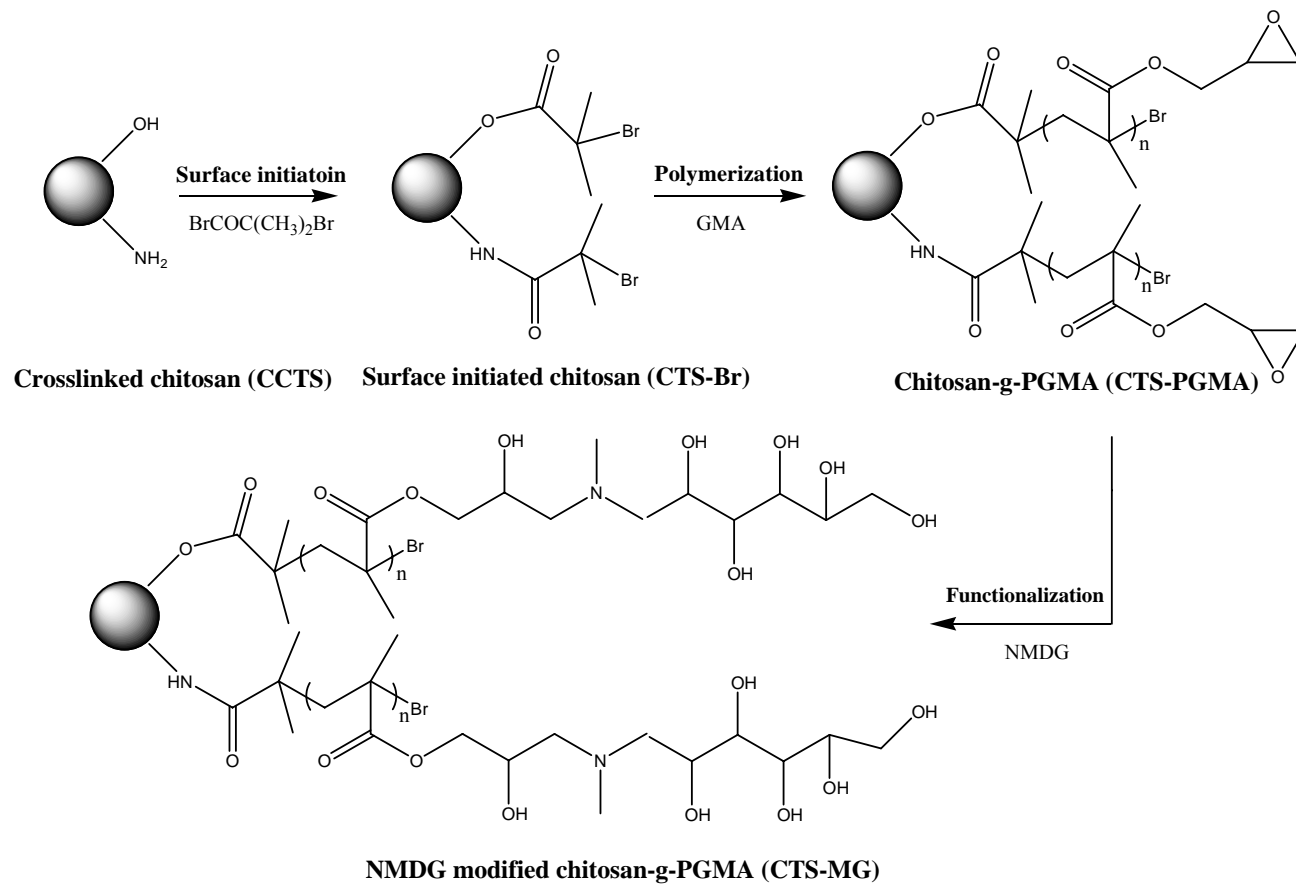


Figure 4.2. Schematic diagram illustrating the preparation of CTS-MG via ATRP

of GMA started from the initiator sites and then increased with time at ambient temperature; and the product was designated as CTS-PGMA; finally, epoxide functions of the grafted PGMA reacted with NMDG to create the affinity binding sites through ring-opening reactions.

## 4.2 Surface modification reactions

### 4.2.1 Characterization of CCTS

The FTIR spectrum in Figure 4.3a shows the major characteristic peaks for CCTS, which can be assigned in Table 4.2 (Socrates, 2000; Anirudhan et al., 2010). These peaks indicate the existence of hydroxyl and amine functional groups in chitosan.

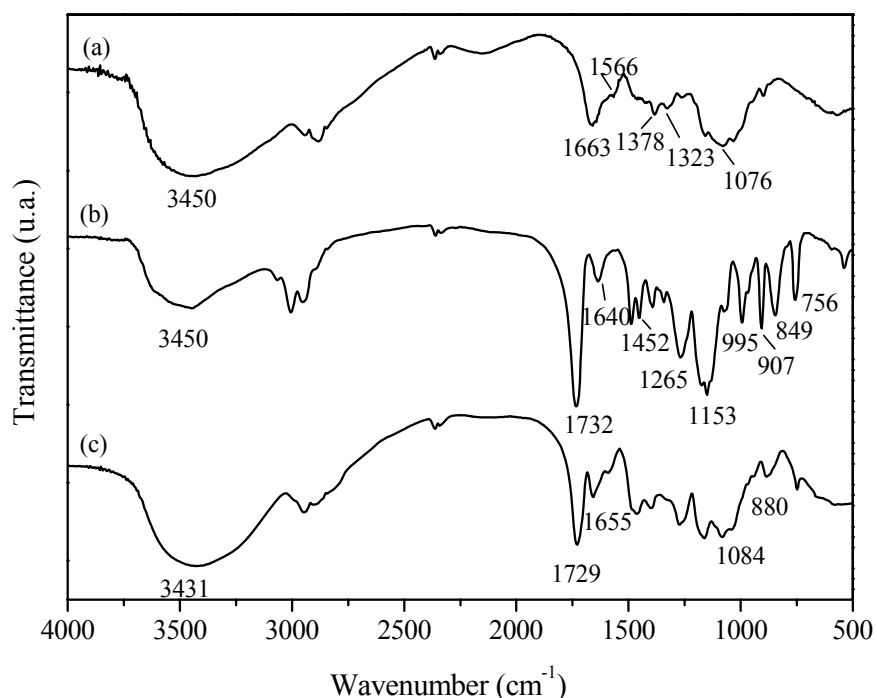


Figure 4.3. FTIR spectra of (a) CCTS, (b) CTS-PGMA, (c) CTS-MG

Table 4.2 Assignment of IR bands for CCTS

Wavenumber (cm <sup>-1</sup> )	Functional groups
1076 cm <sup>-1</sup> , 1323 cm <sup>-1</sup>	-CO and -CN stretching vibrations
1566 cm <sup>-1</sup>	-NH bending vibrations from amine
1663 cm <sup>-1</sup>	amide in N-acetylated chitin
3450 cm <sup>-1</sup>	-OH and -NH stretching vibrations

The chemical composition of CCTS surfaces was also determined by XPS. Figure 4.4a shows three peak components in the XPS wide scan spectrum: C 1s (286 eV), N 1s (399 eV), and O 1s (533 eV). For the N 1s core-level spectrum in the Figure 4.4b, it consists of two major component peaks at BEs of 399.5 eV and 400.2 eV, attributable to the primary amine (-NH<sub>2</sub>) and amide (-NH-C=O), respectively (Liu et al., 2008b). Chitosan is a polysaccharide consisting of D-glucosamine and N-acetyl-D-glucosamine, the amide groups can thus be found in CCTS. The relative content of nitrogen in the amide form to the total nitrogen is determined to be around 14.3 % through curve fitting analysis (Table 4.3). It is in good agreement with the degree of chitosan deacetylation, which is minimum 85 % deacetylation provided by the supplier.

The corresponding high resolution C 1s core-level spectrum can be deconvoluted into four individual component peaks, which come from the different groups and overlap on each other, as shown in Figure 4.4c. The peaks at BEs of 284.6, 285.5, 286.4, and 287.8 eV, are attributable to the C atom in the forms of C-C / C-H, C-N of amine, C-OH / C-O-C of hydroxyl and ether, NH-C=O of amide and chitosan's sugar residues, respectively (Liu et al., 2008b). Therefore, the functional groups in the

CCTS are well reflected by the above assignments.

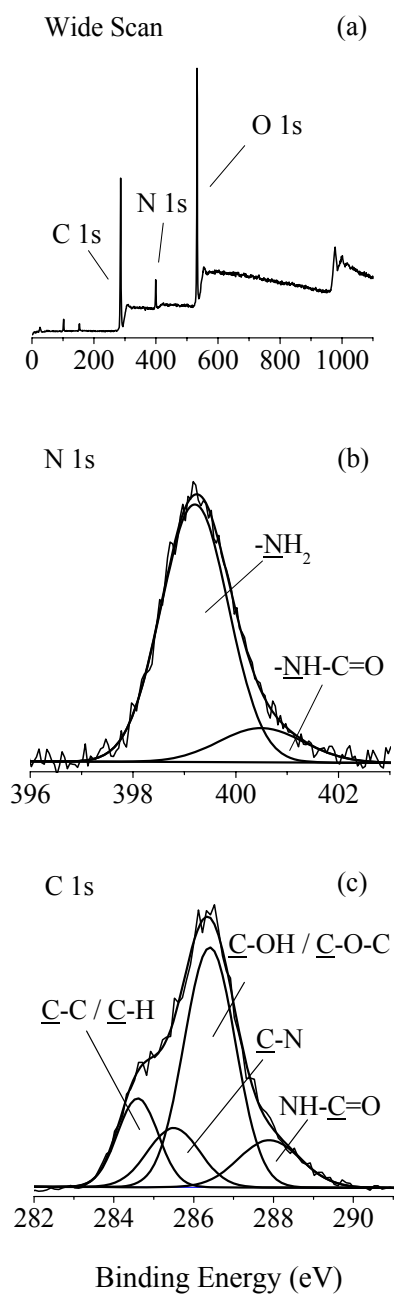


Figure 4.4. XPS (a) wide scan, (b) N 1s, and (c) C 1s core-level spectra of CCTS

#### 4.2.2 Immobilization of the ATRP initiator on CCTS Surface



To modify the CCTS for boron sorption, the initiators are indispensable to be immobilized on the CCTS surface. To evaluate whether the initiators were immobilized on the CCTS, FTIR and XPS spectroscopy analyses were conducted. Compared with the FTIR spectrum of CCTS, no obvious changes are observed (figure not shown), which may be due to the low amount of immobilized BrCOC(CH<sub>3</sub>)Br. In the wide scan XPS spectrum, besides the BE peaks at 286 eV for C 1s, 399 eV for N 1s, 533 eV for O 1s in initiated chitosan surfaces (see Figure 4.5a), the Br 3d peak at a BE of 70.5 eV, attributable to the covalently bonded bromide species, is also detected as shown in Figure 4.5b (Yu et al., 2003).

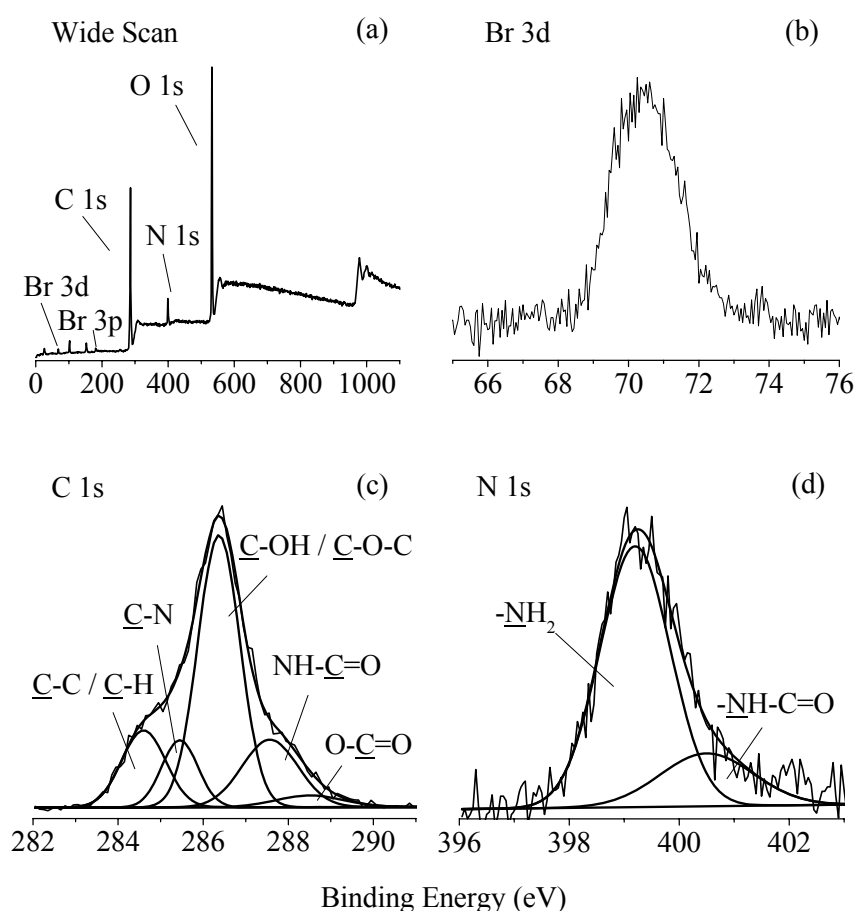


Figure 4.5. XPS (a) wide scan, (b) Br 3d, (c) C 1s, and (d) N 1s core-level spectra of CTS-Br

**Chapter 4: Surface Modification of Chitosan  
via Atom Transfer Radical Polymerization**

The deconvolution of the C 1s spectrum in Figure 4.5c produced five peaks with BEs at demonstrated 284.6, 285.5, 286.4, 287.7, and 285.5 eV. These peaks can be assigned by the above sequence to the C atom in the forms of  $\underline{\text{C}}\text{-C}$  /  $\underline{\text{C}}\text{-H}$ ,  $\underline{\text{C}}\text{-N}$ ,  $\underline{\text{C}}\text{-OH}$  /  $\underline{\text{C}}\text{-O-C}$ ,  $\text{NH-}\underline{\text{C}}\text{=O}$  and  $\text{O-}\underline{\text{C}}\text{=O}$  groups, respectively (Tang et al., 2009). Compared with Figure 4.4c, it is clear that a new peak at 288.5 eV appears in the C 1s core-level spectrum of CTS-Br. As for the N 1s core-level spectrum in the Figure 4.4d, it is still composed of two major component peaks of primary amine ( $\text{-}\underline{\text{N}}\text{H}_2$ ) and amide ( $\text{-}\underline{\text{N}}\text{H-C=O}$ ) at BEs of 399.5 eV and 400.2 eV, respectively.

Table 4.3 Binding energy and relative content of C and N in CCTS and CTS-Br

Valence state	Proposed components	CCTS		CTS-Br	
		Binding energy (eV)	Relative content (%)	Binding energy (eV)	Relative content (%)
C 1s	$\underline{\text{C}}\text{-C}$ / $\underline{\text{C}}\text{-H}$	284.6	16.3	284.6	15.5
	$\underline{\text{C}}\text{-N}$	285.5	15.1	285.5	11.1
	$\underline{\text{C}}\text{-OH}$ / $\underline{\text{C}}\text{-O-C}$	286.4	55.5	286.4	52.5
	$\text{NH-}\underline{\text{C}}\text{=O}$	287.8	13.2	287.7	17.3
	$\text{O-}\underline{\text{C}}\text{=O}$	----	----	288.5	3.60
N 1s	$\text{-}\underline{\text{N}}\text{H}_2$	399.2	85.7	399.2	79.8
	$\text{NH-C=}\underline{\text{O}}$	400.5	14.3	400.5	20.2

The relative contents of C 1s and N 1s in different forms are summarized in Table 4.3. It shows that the relative quantity of  $\underline{\text{C}}\text{-N}$  and  $\underline{\text{C}}\text{-OH}$  slightly decreases after surface initiated reaction. On the other hand, the content of  $\text{NH-}\underline{\text{C}}\text{=O}$  and  $\text{O-}\underline{\text{C}}\text{=O}$  increases from 13.2 % to 17.3 %, 0 to 3.6 %, respectively. The similar trend is clearly

observed in the quantity of  $-\underline{\text{N}}\text{H}_2$  (85.7 % vs 79.8 %) and  $\underline{\text{N}}\text{H}-\text{C}=\text{O}$  (14.3 % vs 20.2 %). These changes suggest that partial hydroxyl and amine groups are involved in the surface initiated reaction.

Consequently, the occurrence of Br 3d and the  $\text{O}-\underline{\text{C}}=\text{O}$  peak in the C 1s core-level spectrum implies that 2-bromoisobutyrate has been successfully immobilized on the surface of CCTS for the subsequent ATRP. This point can also be substantiated by the changes in the contents of hydroxyl and amine groups.

#### **4.2.3 Surface Initiated ATRP from Chitosan Surface**

The immobilization of initiators was followed by polymerization of GMA on the initiated CCTS surface. After polymerization, the FTIR spectrum of CTS-PGMA in Figure 4.3b shows some noticeable changes. The peak at  $1640\text{ cm}^{-1}$  represents the amide  $\text{C}=\text{O}$  stretching vibrations in  $-\text{NHCO}-$ . The vibrations at around  $1265\text{ cm}^{-1}$ ,  $1452\text{ cm}^{-1}$  and  $1732\text{ cm}^{-1}$  represent the ester configuration of PGMA, which are usually assigned to C-O symmetric stretching band of carbonyl groups,  $-\text{CH}_2$  scissoring band of PGMA and ester  $\text{C}=\text{O}$  stretching vibrations in carbonyl group, respectively (Arica et al., 2008; Barringer et al., 2009).

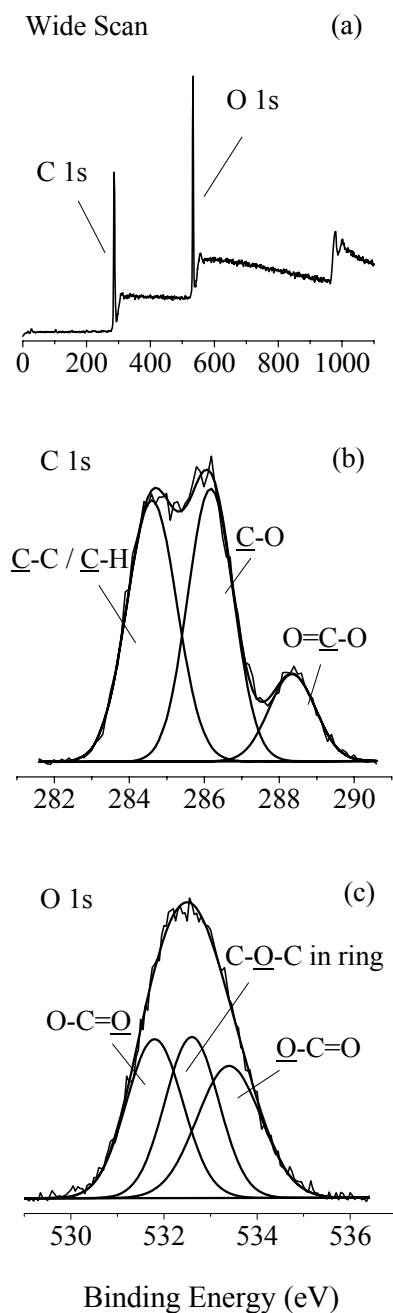


Figure 4.6. XPS (a) wide scan, (b) C 1s, and (c) O 1s core-level spectra of CTS-PGMA

Other than that, new peaks at  $907\text{ cm}^{-1}$ ,  $849\text{ cm}^{-1}$  and  $756\text{ cm}^{-1}$  which are the characteristic bands of epoxide groups, also confirm the presence of PGMA on the

surface of chitosan particles (Chan and Gleason, 2005; Ma et al., 2005). Meanwhile, it is clear that the intensity of peak at  $3450\text{ cm}^{-1}$  related to  $-\text{OH}$  group is significantly weakened. These results confirm the successful polymerization of GMA onto the surface of the initiated CCTS.

The presence of grafted GMA polymer on the chitosan surface was ascertained by XPS analysis as well. As shown in Figure 4.6a, the wide spectrum of CTS-PGMA is dominated by the C 1s and O 1s signals. Compared to the wide spectrum of CTS-Br, the disappearance of N 1s signal is due to the fact that the thickness of PGMA brushes was larger than the sampling depth of XPS technique (about 7.5 nm in organic matrix). The C 1s core-level spectrum of the CTS-PGMA surface in Figure 4.6b can be curve-fitted with three peak components at BE of about 284.6, 286.2, 288.5 eV, assigned to  $\underline{\text{C}}-\text{C} / \underline{\text{C}}-\text{H}$ ,  $\underline{\text{C}}-\text{O}$ , and  $\text{O}-\underline{\text{C}}=\text{O}$  species, respectively (Yu et al., 2004). On the other hand, for the O 1s core-level spectrum (see Figure 4.6c), three peak components of 531.8, 532.6, 533.6 eV can be assigned to  $\text{O}-\underline{\text{C}}=\underline{\text{O}}$ ,  $\text{C}-\underline{\text{O}}-\text{C}$  in ring and  $\underline{\text{O}}-\text{C}=\text{O}$ , respectively (Mao and Gleason, 2004).

Table 4.4 lists the relative contents of C 1s and O 1s in different forms for CTS-PGMA and CTS-MG. The  $[\underline{\text{C}}-\text{C} / \underline{\text{C}}-\text{H}]:[\underline{\text{C}}-\text{O}]:[\text{O}-\underline{\text{C}}=\text{O}]$  ratio of CTS-PGMA, obtained from the curve-fitted analysis, is about 3.2:3.1:1 (44.0 %:42.3 %:13.7 %), in good agreement with the corresponding theoretical ratio (3:3:1). Besides, fairly good agreement between XPS-derived and theoretical surface composition is also achieved for the  $[\text{O}-\underline{\text{C}}=\underline{\text{O}}]:[\text{C}-\underline{\text{O}}]:[\underline{\text{O}}-\text{C}=\text{O}]$  ratio, which is determined to be 1:1:1 (34.3 %:32.1 %:33.6 %). Therefore, these rational ratios suggest the epoxies functional groups of GMA are successfully grafted onto chitosan surface during the ATRP process, which

is also consistent with the findings in FTIR.

Table 4.4 Binding energy and relative content of C and O in CTS-PGMA and CTS-MG

Valence state	Proposed components	CTS-PGMA		CTS-MG	
		Binding Energy (eV)	Relative content (%)	Binding energy (eV)	Relative content (%)
<b>C 1s</b>	<u>C</u> -C / <u>C</u> -H	284.6	44.0	284.6	22.1
	<u>C</u> -N	----	----	285.5	21.9
	<u>C</u> -O	286.2	42.3	286.2	48.9
	O- <u>C</u> =O	288.5	13.7	288.6	7.1
<b>O 1s</b>	O-C= <u>O</u>	531.8	34.3	531.8	13.7
	C- <u>O</u>	532.6	33.1	532.4	73.6
		(C-O-C in ring)		(C-OH)	
	<u>O</u> -C=O	533.6	32.6	533.6	12.7

#### 4.2.4 Functionalization of CTS-PGMA surface

The last step of the modification was the grafting of NMDG on the surface of CTS-PGMA. An important feature of CTS-PGMA surface is the preservation of the reactive epoxide groups, which can readily and irreversibly react with the nucleophilic groups for subsequent surface functionalization (Yu et al., 2004). It is known that NMDG possessing specific functional groups can react with boron to form neutral or anionic complexes. Therefore, reaction of the CTS-PGMA surfaces with NMDG was conducted in order to obtain sorbents with high boron binding capabilities.

After functionalization with NMDG, the significant disappearance of typical bands for epoxide group at  $907\text{ cm}^{-1}$ ,  $849\text{ cm}^{-1}$  and  $756\text{ cm}^{-1}$ , is observed in the spectrum in Figure 4.3c, indicating the successful conversion of epoxide groups. Besides, new peak at  $1084\text{ cm}^{-1}$  appears which is assigned to tertiary amine C-N stretching vibrations (Socrates, 2000). Compared to CTS-PGMA, the broadening and intensification of absorption bands are also found in the region of  $3100\text{-}3700\text{ cm}^{-1}$ , which is related to the stretching vibrations of  $\text{-OH}$  groups. All results indicate the successful introduction of multiple-hydroxyl and tertiary amine functional groups via ring-opening reactions.

Further evidence of the subsequent chemical functionalization of CTS-PGMA can be obtained in the wide scan, C 1s and O 1s core-level spectra of CTS-MG in Figure 4.7. A new N 1s signal at the BE of 399 eV, assigned to the tertiary amine nitrogen is observed in the wide scan. Besides, in comparison with the C 1s core-level spectrum of CTS-PGMA, a new peak component at 285.5 eV, attributable to the  $\text{C-N}$  species, appears in the C 1s core-level spectrum of CTS-MG (Yu et al., 2003).

As shown in Table 4.4, the relative content of  $\text{C-N}$  has increases to approximately 21.9 % after NMDG modification which is indicative of successful ring opening reactions by the nucleophilic groups  $\text{-NH}$ . In addition, the  $[\text{C-O}]:[\text{O-C=O}]$  ratio of CTS-MG surface, determined from XPS analysis of O 1s core-level spectrum, is approximately 5.8:1 (73.6 %:12.7 %), which increases greatly from the 1:1 (33.1 %:32.6 %) for the original CTS-PGMA surface. Such findings clearly support the FT-IR analysis that polyhydroxyl functional groups have been successfully introduced

to the chitosan surface via ring opening of epoxide groups.

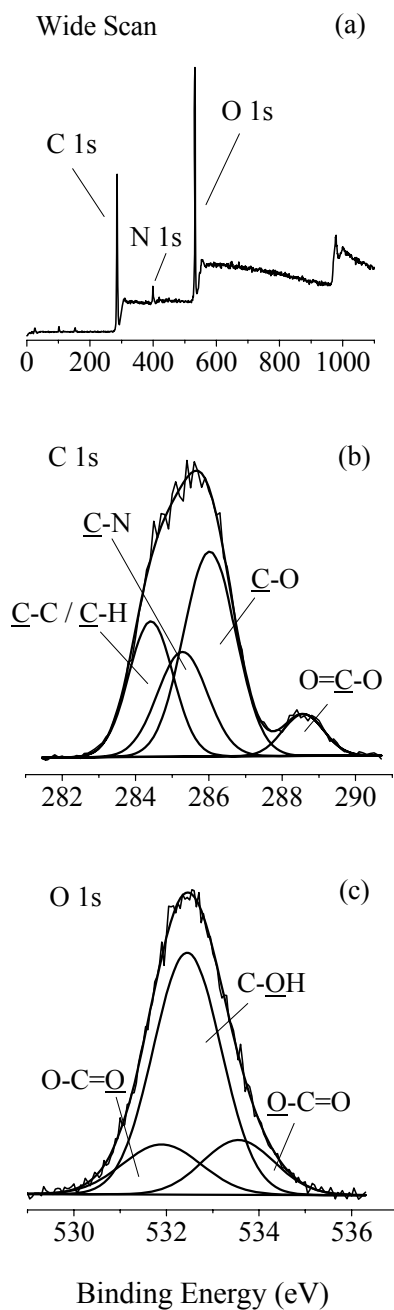


Figure 4.7. XPS (a) wide scan, (b) C 1s, and (c) O 1s core-level spectra of CTS-MG

### 4.3 Material characterization



### 4.3.1 Morphologies observation of the sorbent

A microscope was used to observe the overall morphology of CCTS and CTS-MG under wet condition. Microscopic images are shown in Figure 4.8.

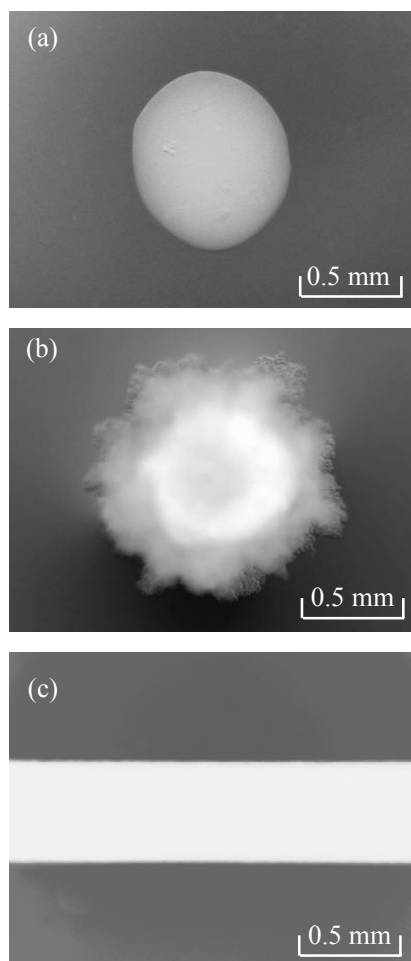


Figure 4.8. Microscopic images in wet condition: (a) CCTS, (b) CTS-MG, and (c) lead of pencil

Clearly, CCTS have white color with a mean diameter of around 1 mm. After modification, two distinct layers can be seen. At the shell of the particle, there is an existence of a hairy polymer layer. Such hairy layer is grafted onto the CCTS which serves as the core of the macrosphere.

## Chapter 4: Surface Modification of Chitosan via Atom Transfer Radical Polymerization

The SEM images in Figure 4.9 also demonstrate that the particles are significantly larger than the initial size after modification. Moreover, the surface of CCTS is relatively smooth and less porous, while abundant protuberances are present in the surface of CTS-MG. In other words, surface modification contributes to a rough surface and relatively porous structure of the sorbent, which can facilitate the diffusion of boric acid or borate ions during sorption.

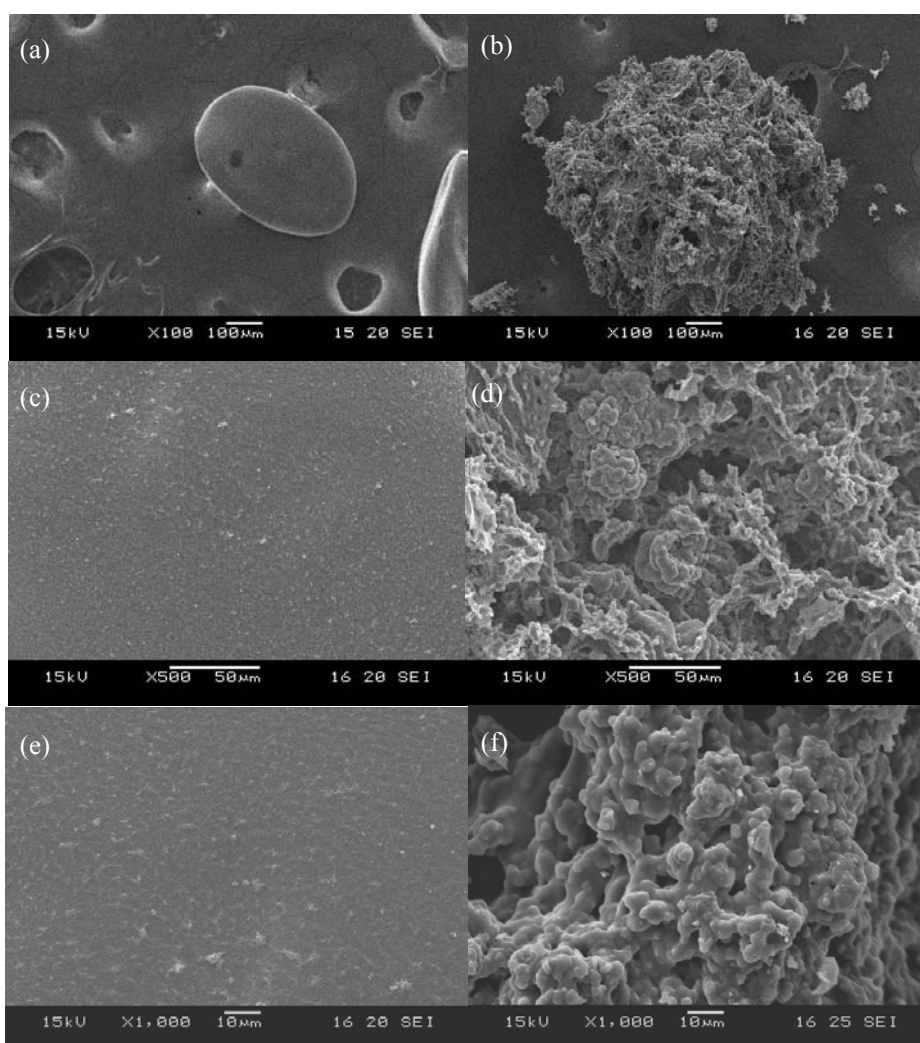


Figure 4.9. SEM in dry condition: (a) CCTS ( $\times 100$ ), (b) CTS-MG ( $\times 100$ ), (c) CCTS ( $\times 500$ ), (d) CTS-MG ( $\times 500$ ), (e) CCTS ( $\times 1000$ ), and (f) CTS-MG ( $\times 1000$ )

### 4.3.2 Specific surface area

The surface area of CTS-MG is obtained via instrumental analysis of nitrogen adsorption onto the sorbent at low temperature (around 77.3 K). The BET model (Equation 4.1) is used to analyze the adsorption data to determine their specific surface area. The BET model is expressed by the following equation (Brunauer et al., 1938)

$$\frac{1}{V_a \left[ \frac{P_0}{P} - 1 \right]} = \frac{C_{BET} - 1}{V_m C_{BET}} \left( \frac{P}{P_0} \right) + \frac{1}{V_m C_{BET}} \quad (4.1)$$

where  $P$  is partial vapor pressure of nitrogen gas in equilibrium (kPa),  $P_0$  is saturated pressure of nitrogen gas at 77.3 K (kPa),  $V_a$  is volume of adsorbed gas at equilibrium (mL), and  $V_m$  is volume of monolayer adsorbed gas (mL).  $C_{BET}$  is dimensionless BET constant. The values of slope and intercept of the linear plot of  $1/V_a \left[ \frac{P_0}{P} - 1 \right]$  versus  $P/P_0$  (Figure 4.10) are used to calculate the BET constant,  $C_{BET}$  and  $V_m$ . The BET constant,  $C_{BET}$  and  $V_m$ , obtained are 2.80 and 0.005. Hence, specific surface area,  $S$  ( $\text{m}^2/\text{g}$ ) is calculated using Equation (4.2).

$$S = \frac{V_m N s}{m \times 22400} \quad (4.2)$$

where  $N$  is Avogadro constant,  $s$  is adsorption cross section,  $m$  is mass of sorbent (g).

According to the BET analysis, CTS-MG has a specific surface area of  $16.7 \text{ m}^2/\text{g}$ , which is nearly 14 times higher than that of CCTS ( $1.2 \text{ m}^2/\text{g}$ , around the equipment DL). The results of BET also support the abovementioned indication that modified

chitosan is more porous compared to unmodified ones.

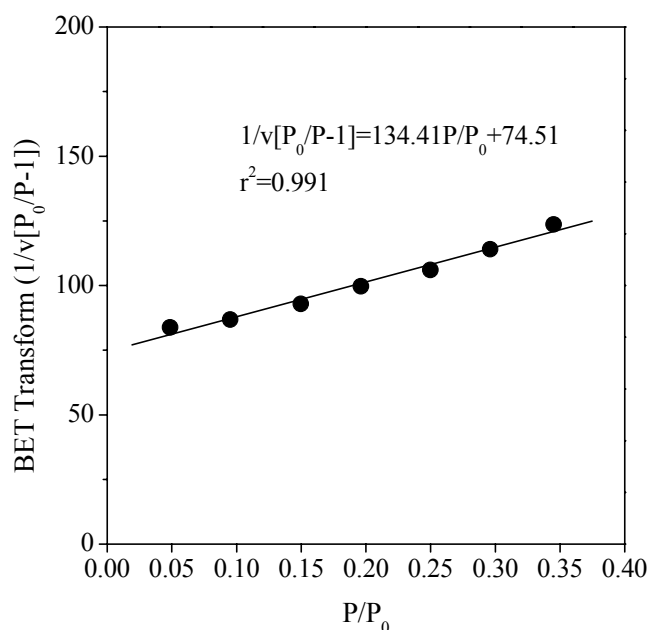


Figure 4.10. Plot of BET model for CTS-MG

### 4.3.3 Surface charge density

Figure 4.11 depicts the surface charge density as a function of solution pH. It decreases as pH increases, following the similar trend as other materials reported in literature (Lim et al., 2008).  $pH_{zpc}$  (point of zero charge) of 7.8 is determined.

At  $pH < 7.8$ , the surface charge density is positive, indicating a higher affinity for anions; at  $pH > 7.8$ , the surface is negatively charged and thus unfavorable for anions removal. Such affinity plays an important role in nonspecific sorption of ions through electrostatic interaction between ions and sorbent; however, it is less important in specific sorption (e.g. surface complexes formation).

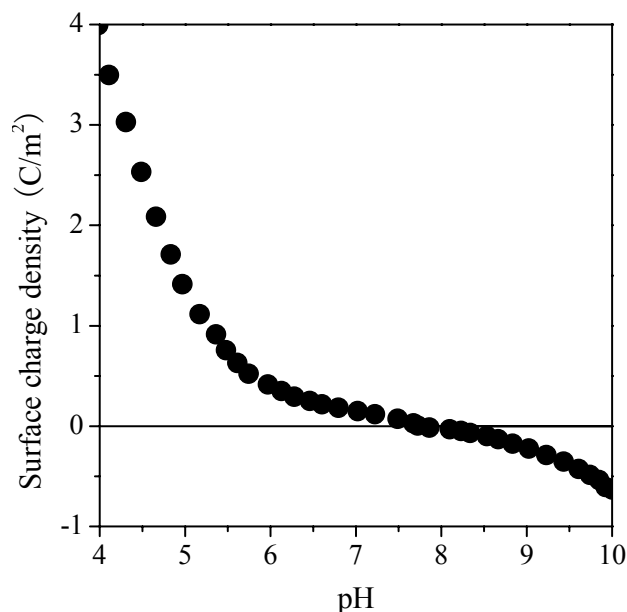


Figure 4.11. Surface charge density as a function of pH. Experimental conditions:  $m = 0.5$  g/L,  $T = 293$  K.

#### **4.3.4 Leaching study**

Results from the leaching tests are presented in Table 4.5 (equipment DL for Cu and Ca:  $< 0.1$  mg/L). The type of metal tested and pH conditions are also indicated in the table. It was observed that the concentration of  $\text{Ca}^{2+}$  is only 2.66 ppm even at pH 0.1. Release of alkaline earth metal ions  $\text{Ca}^{2+}$  of CCTS increases with a decrease of pH. The exchange between calcium in chitosan and hydrogen ions possibly contributes to such changes. However, after surface modification, no calcium ions are found in leaching solution, which can not cause any problem in water hardness.

Copper salts, as the catalysts used for ATRP reaction, it is therefore necessary to evaluate whether copper leaching occurs and results in a secondary pollution in the treated water. In almost all cases, copper leaching from CTS-MG is not observed

**Chapter 4: Surface Modification of Chitosan  
via Atom Transfer Radical Polymerization**

---

except that the leachate concentration is 0.37 mg/L at pH 0.1. Although copper tends to leach out, it is usually found at extremely acidic condition which is not selected for sorption process. On the other hand, the level is too low to cause the issue of secondary contamination. Hence, it is safe to conclude that no dangerous level of metal leaching would occur during sorption.

Table 4.5 Leaching characteristics of CTS-MG at different pH

	pH = 4.0		pH = 1.0		pH = 0.1	
	CCTS	CTS-MG	CCTS	CTS-MG	CCTS	CTS-MG
<b>Cu (mg/L)</b>	--	<DL	--	<DL	--	0.37
<b>Ca (mg/L)</b>	0.7	<DL	2.42	<DL	2.66	<DL

#### 4.4 Section summary

PGMA can be grafted from the CCTS via surface polymerization at ambient temperature and the grafted PGMA brushes can be further functionalized by NMDG via reaction of the epoxide rings. Both FT-IR and XPS studies confirm the successful immobilization of initiator by 2-bromoisobutyrate bromide, formation of PGMA polymer brushes, as well as further NMDG modification on CCTS surface. Chemical modification leads to significant changes in both particle size and surface morphology. Microscope observation demonstrates the existence of two distinct layers in the sorbent. Chitosan serves as the core, while a hairy polymer layer is the shell of macroshpere. The polymeric sorbent has a mean diameter of 0.6 mm, specific surface area of 16.7 m<sup>2</sup>/g and pH<sub>zpc</sub> of 7.8. Leaching tests demonstrate that no secondary contamination can be caused by CTS-MG.

## **CHAPTER 5**

# **BORON SORPTION ONTO NMDG MODIFIED CHITOSAN SORBENT: SORPTION BEHAVIOR AND MECHANISM STUDY**

Polymers with vicinal polyalcohol functions are reportedly the most efficient ligands for complexation of boron in aqueous solutions. Amberlite IRA-743, a commercial boron-specific resin with N-methylglucamine functions, emerged in the 1960s (Gazi. et al., 2008). Despite its high specificity to boron, this resin exhibits somewhat low in boron uptake capability. Regeneration cost and capacity loss during regeneration also make the process unsatisfactory. In addition, a variety of synthetic procedures have been carried out through surface modification of both inorganic and organic substrates, aiming to develop new materials for boron removal (Bicak et al., 2001; Inukai et al., 2004; Kaftan et al., 2005; Sabarudin et al., 2005; Wang et al., 2007). However, most polymer-supported resins are based on the copolymers of styrene and divinylbenzene. Application of styrene / divinylbenzene resins is often limited by their strong hydrophobic properties (Wang et al., 2007).

In this chapter, a series of batch sorption experiments were carried out to better understand boron sorption behavior of the novel polymeric sorbent (CTS-MG). The sorption isotherm, pH effect, kinetics, effect of ionic strength, and boron removal from simulated seawater were studied. The sorption isotherm and kinetics were fitted by

isotherm equations and intraparticle diffusion model, respectively. Sensitivity analysis on the kinetic model's parameters was carried out. Through these studies, the sorption properties were well understood. Furthermore, instrumental analyses by FT-IR and XPS were also conducted to investigate the interaction between boron and sorbent surface. Finally, a conceptual model was proposed to illustrate the sorption process.

## **5.1 Equilibrium studies**

### **5.1.1 Effect of solution pH on boron sorption**

It has been reported that below total concentration of 25 mmol boron, the major species present would be only  $\text{H}_3\text{BO}_3$  and  $\text{B}(\text{OH})_4^-$  without polyanionic species (Choi and Chen, 1979). A chemical equilibrium program (MINEQL+, Version 4.5) was used to calculate the distribution of boron species in aqueous solution as a function of pH (Figure 5.1a). As can be seen, the fraction of borate anion is negligible compared to that of boric acid when pH is below 8; while pH increases to above 10.5, only free ionic forms of boron are present in solution.

Since pH value will affect boron speciation and surface properties of sorbent, it is an important impact factor for the interaction between boron and the sorbent. Figure 5.1a illustrates the pH influences on boron sorption. As shown, boron in aqueous solution can be removed not only as borate ion but also as boric acid. Boron uptake on the material exhibits a typical parabolic sorption envelope. Under acidic condition, increasing pH results in rising sorption capacity. However, after a maximum sorption is



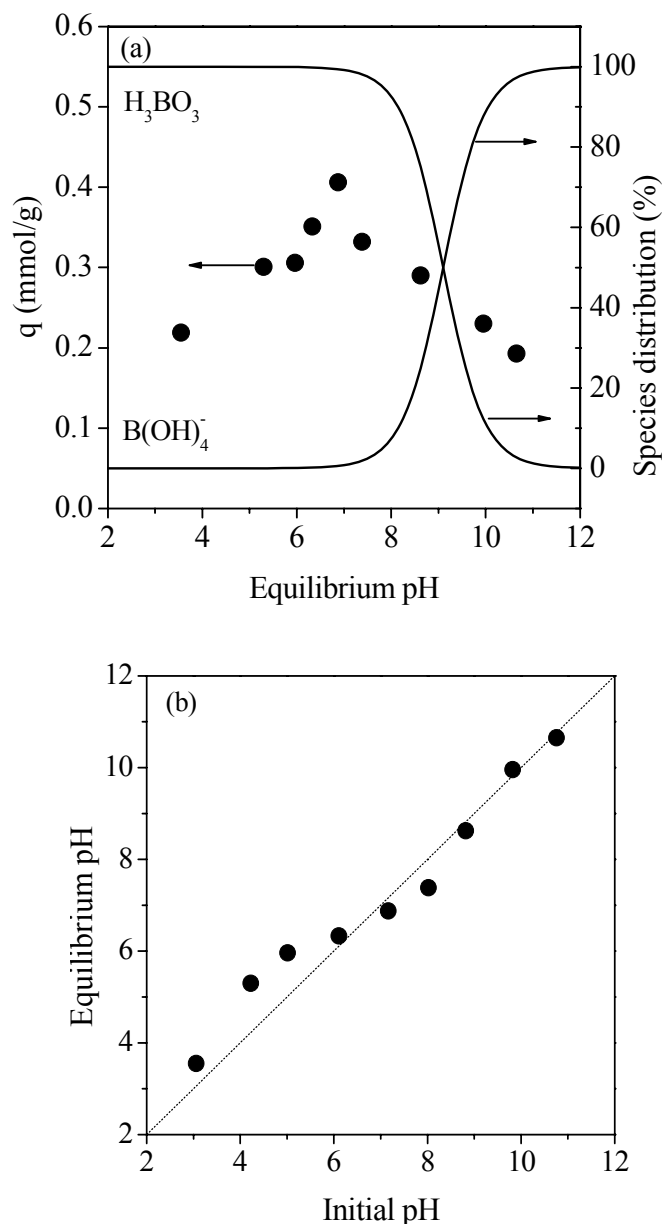


Figure 5.1. (a) Boron sorption capacity as a function of pH, (b) Effect of boron sorption on solution pH. Experimental conditions:  $[B]_0 = 0.39$  mM,  $m = 0.5$ g/L,  $T = 293$  K, contact time = 3 d

achieved at an intermediate pH, a subsequent decrease of sorption capacity is observed in the curve. It is clear that the sorption peak occurs near neutral pH, implying that this sorbent can be applied in the majority of water supplies with a pH range of 6.5 - 8.5 (Zhang et al., 2007c). Therefore, solution pH of all subsequent experiments was

adjusted to around 7.0. Similar trend can also be found in other reported literature studies (Goldberg et al., 1993; Qi et al., 2002; Wang et al., 2007; Xu and Peak, 2007; Liu et al., 2009a).

The dependence of boron uptake on pH is mainly related to the surface functional groups of CTS-MG. At lower pH, both the tertiary amine and hydroxyl sites on surface are under protonation and thus result in net positively charged surface. Meanwhile, the predominant species of boron in aqueous solution is neutral boric acid  $B(OH)_3$ . Boric acid can complex with polyhydroxyl to release  $H_2O$  and/or  $H^+$ . As pH increases, decrease of hydrogen ion is thought to increase the chances of boric acid to complex with surface functional groups; thus more boric acid is removed (Su and Suarez, 1995; Simonnot et al., 2000).

At higher pH values, borate anions become the dominant species in aqueous solution. Besides, deprotonation dominates and contributes to the net negatively surface charge. Increasing pH enhances the repulsive electrostatic interactions between  $B(OH)_4^-$  and sorbent surface. Meanwhile, when pH rises, more hydroxyl ions are present which also show certain different affinity for hydroxyl functional groups (e.g. alkoxide formation) (Garcia-Soto and Camacho, 2005). Strong competition for active sites possibly makes boron complex reaction more difficult; thus the amount of sorption is dropped.

Figure 5.1b demonstrates that pH changes during sorption are not very significant. The final pH is slightly higher than initial pH in acidic region but becomes a bit lower

under base conditions. On one hand, the retainment of hydrogen ions by tertiary amine and hydroxyl sites mainly leads to the rise of pH after sorption. On the other hand, at high pH region, competition of hydroxyl ions with borate anions for active sites contributes to lower final pH.

### **5.1.2 Sorption isotherm**

Efficiency of a sorbent is generally determined by its sorption capacity of a particular sorbate. Figure 5.2 shows the sorption isotherms of CTS-MG, CCTS and commercial resin Amberlite IRA-743 as well as the fitted results according to different isotherm equation. Generally, boron uptake increases with initial concentrations for these three materials; however, boron sorption on CCTS is very low, ranging from 0 to 0.4 mmol/g. The equilibrium sorption capacities of boron on CTS-MG are always greater than those on CCTS and commercial resin Amberlite IRA-743, indicating that grafting of multi-hydroxyl functional groups onto CCTS definitely improves boron removal capability.

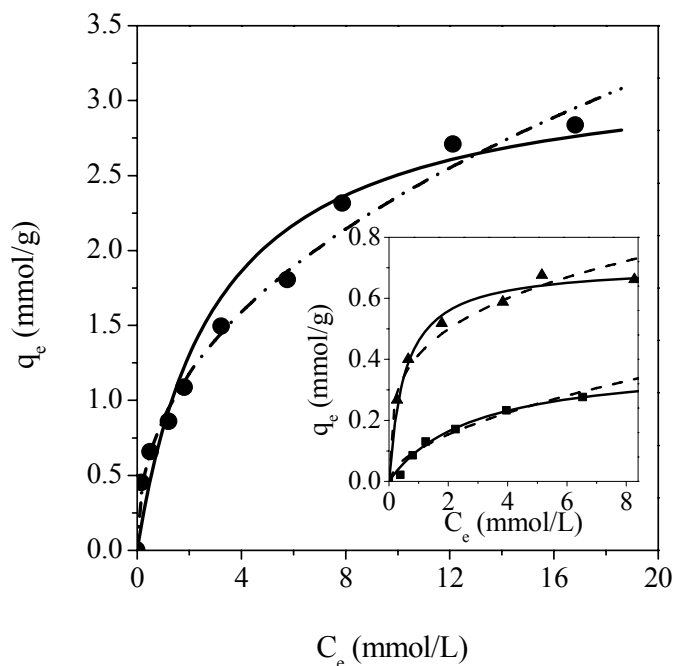


Figure 5.2. Boron sorption isotherms on CTS-MG, CCTS and commercial resin Amberlite IRA-743. ● CTS-MG, ■ CCTS, ▲ Amberlite IRA-743, — Langmuir fitting, ---- Freundlich fitting. Experimental conditions:  $m = 0.5 \text{ g/L}$ ,  $\text{pH} = 7.0 \pm 0.1$ ,  $T = 293 \text{ K}$ , contact time = 3 d

Besides, Langmuir and Freundlich (Equation 2.5 and 2.6 in Chapter 2) were used to describe the sorption performance. The analysis of experimental data using linearized model is represented in Figure 5.3; and the equilibrium constants are tabulated in Table 5.1, respectively.

Both isotherms well describe the sorption with high  $R^2$  values. Slightly higher  $R^2$  value in the fitting by Freundlich isotherm for the CTS-MG indicates that the sorption may be heterogeneous. However, the sorption by CCTS and IRA-743 may be homogenous because of slightly higher  $R^2$  values in the fitting by Langmuir isotherm.

Direct graphic maximal removal capacity (corresponding to the isotherm plateau) is 2.84 mmol/g for CTS-MG. In addition, according to the Langmuir fitting, the maximum

**Chapter 5: Boron Sorption onto NMDG Modified Chitosan Sorbent:  
Sorption Behavior and Mechanism Study**

sorption capacity of boron on CCTS and Amberlite IRA-743 are determined to be 0.39 mmol/g ( $R^2 = 0.995$ ), 0.71 mmol/g ( $R^2 = 0.996$ ), respectively.

Table 5.1 Isotherm parameters for B sorption on CTS-MG, CCTS and Amberlite IRA-743.

		<b>CTS-MG</b>	<b>CCTS</b>	<b>Amberlite IRA-743</b>
	$q_{\max}$ (mmol/g)	3.25	0.39	0.71
<b>Langmuir</b>	b (L/mmol)	0.33	0.35	1.86
	$R^2$	0.968	0.995	0.996
	$K_f$	0.87	0.10	0.41
<b>Freundlich</b>	1/n	0.43	0.55	0.27
	$R^2$	0.991	0.971	0.951

In literature, other researchers also have reported boron removal by various materials and the corresponding sorption capacities are between 0.49 to 3.28 mmol/g (Table 5.2). It can be said that the synthesized CTS-MG greatly outperforms most of sorbents and resins for boron removal from aqueous solutions.

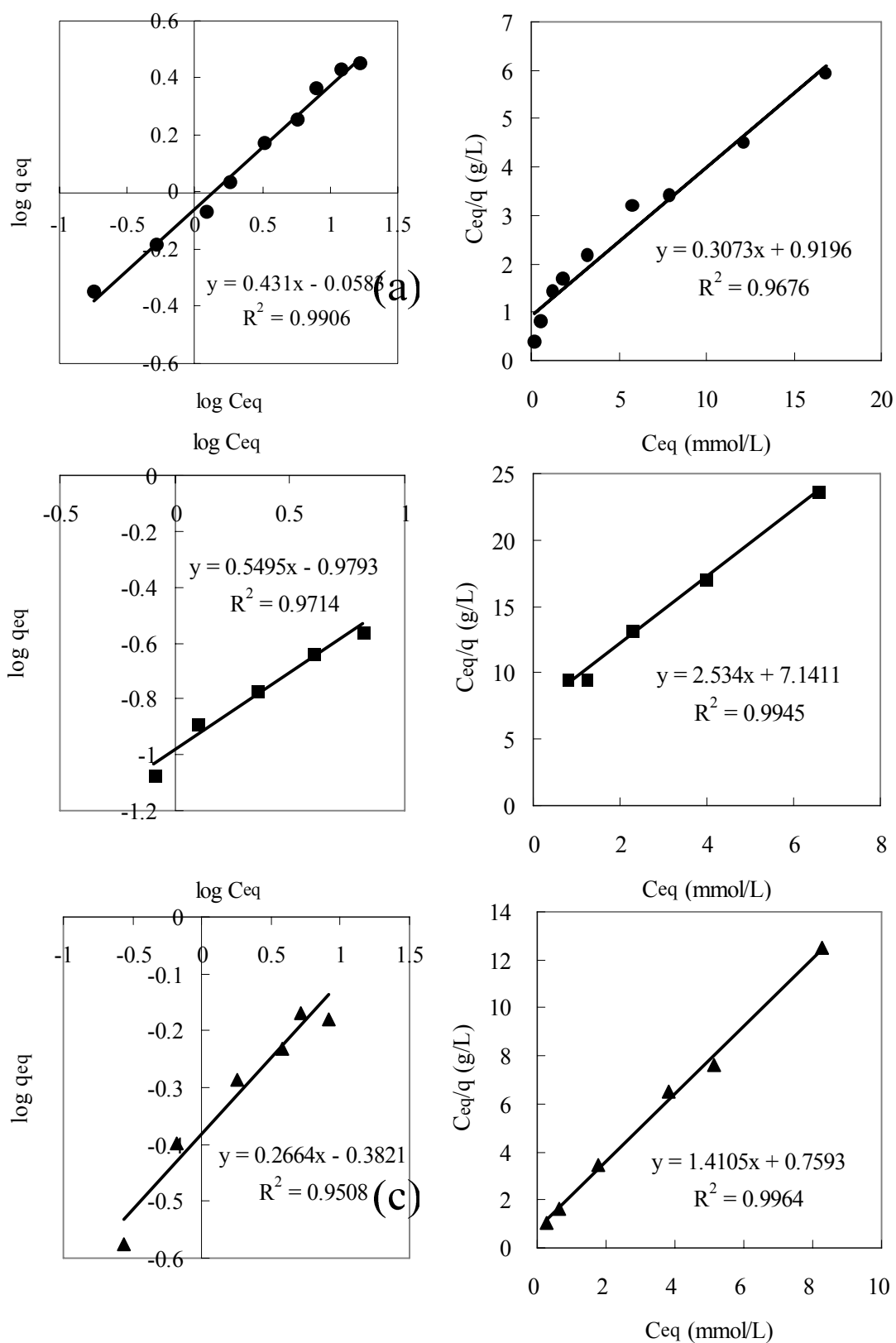


Figure 5.3. Determination of Langmuir and Freundlich equation's constants. ● CTS-MG, ■ CCTS, ▲ Amberlite IRA-743

Table 5.2 Comparison of boron sorption capacities on several synthesized materials

	<b>Synthesized materials</b>	<b>Base Material</b>	<b>Moiety</b>	<b>q(mmol/g)</b>	<b>References</b>
<b>Biopolymer based materials</b>	CTS-MG	CCTS	NMDG	2.84	This work
	NMDG-type cellulose derivatives	cellulose	NMDG	1.1	(Inukai et al., 2004)
	CCTs-NMDG	CCTS	NMDG	2.1	(Sabarudin et al., 2005)
<b>Organic based materials</b>	Amberlite IRA-743	polystyrene	NMDG	0.7	This work
	Diaion CRB02	PS-DVB	NMDG	$\geq 0.9^a$	(Hilal et al., 2010)
	DOWEX BSR-1	PS-DVB	NMDG	$0.7^a$	(Hilal et al., 2010)
	Purolite S108	PS-DVB	NMDG	$0.6^a$	(Hilal et al., 2010)
	Polymer supported iminodipropylene glycol	GMA-MMA-DVB	glycidol	3	(Senkal and Bicak, 2003)
	poly(styryl sulfonamide) based resin	PS-DVB	glucamine hydrochloride	2.365	(Gazi et al., 2004)
	Polymer supported 2-hydroxyethylamino proplene glycol	GMA-MMA-DVB	2-hydroxyethylamino propylene glycol	1.82	(Gazi and Bicak, 2007)
	poly(GMA-co-TRIM)-NMDG	poly(GMA-co-TRIM)	NMDG	1.84	(Wang et al., 2007)
Multi-hydroxyl functional hairy polymer	PS-DVB	HEP	3.28	(Gazi et al., 2008)	

<b>Synthesized materials</b>	<b>Base Material</b>	<b>Moiety</b>	<b>q(mmol/g)</b>	<b>References</b>
<b>Inorganic based materials</b>	Functionalized mesoporous solid	mesoporous silica	glucose fructose galactose mannose	0.67 0.76 0.49 1.85 (Rodriguez-Lopez et al., 2004)
	NMDG-MCM-41	MCM-41	NMDG	0.8 (Kaftan et al., 2005)
	Polyol-grafted SBA-15	SBA-15 (silica mesoporous materials)	glucose	0.63 (Wang et al., 2006)

a: capacity unit (eq/L)



## 5.2 Kinetics study

### 5.2.1 Boron sorption kinetics and its modeling simulation

Figure 5.4 illustrates the kinetic results of boron sorption by CTS-MG. The sorption kinetics initially involves a fast sorption, followed by a slightly slow process. It can be observed that more than 90 % of the ultimate sorption amount can be reached within 8 h and it takes up around 12 h to achieve the sorption equilibrium.

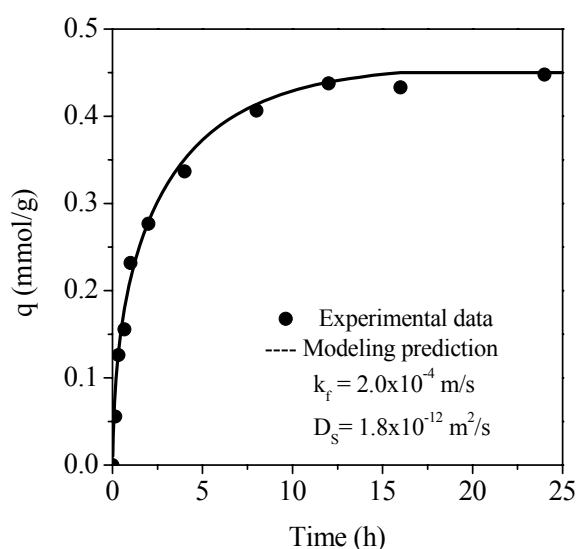


Figure 5.4. Kinetics of boron sorption by CTS-MG. Experimental conditions:  $m = 0.5 \text{ g/L}$ ,  $\text{pH} = 7.0 \pm 0.1$ ,  $[\text{B}]_0 = 0.45 \text{ mM}$ ,  $T = 293 \text{ K}$

Simulation of boron sorption kinetics was performed by the intraparticle diffusion model with an assumption of a “two-step mass transport mechanism”. Boron acid molecules first transfer through the external liquid film from the bulk solutions and subsequently diffuse inside the sorbent before finally being adsorbed by functional groups. Constant physical properties are assumed. The mathematical equation and its corresponding initial and boundary conditions are expressed as follows (Tien, 1994):

$$\frac{1}{D_s} \frac{\partial q}{\partial t} = \frac{1}{r^2} \frac{\partial}{\partial r} \left[ r^2 \frac{\partial q}{\partial r} \right] \quad 0 \leq r \leq a_p, t > 0 \quad (5.5)$$

The initial and boundary conditions may be specified as:

$$\frac{\partial q}{\partial r} = 0 \quad \text{at } r = 0 \quad (5.6)$$

$$D_s \rho_p \frac{\partial q}{\partial r} = k_f (C - C^*) \quad \text{at } r = a_p \quad (5.7)$$

$$q = 0 \quad \text{at } t = 0 \quad (5.8)$$

where  $C$  (mol/m<sup>3</sup>) and  $q$  (mol/kg) are the concentrations of boron in the bulk and solid phases, respectively;  $C^*$  (mol/m<sup>3</sup>) is the aqueous phase concentration at the particle surface, in equilibrium with the corresponding concentration in the solid phase  $q^*$  (mol/kg);  $D_s$  (m<sup>2</sup>/s) is the surface diffusivity within the particles;  $\rho_p$  (kg/m<sup>3</sup>) is the particle density;  $r$  (m) is radius distance measured from the center of particle;  $a_p$  (m) is the particle radius;  $k_f$  (m/s) is the external mass transfer coefficient, and  $t$  (s) is the time.

As shown in Figure 5.4, this model can well describe the experimental data. Constants were determined by the best-fitting between experimental data and the modeling prediction. The external mass transfer coefficient and the surface diffusivity are in ranges of  $10^{-4}$  m/s and  $10^{-12}$  m<sup>2</sup>/s, respectively.

### 5.2.2 Sensitivity analysis of the model parameters

**Chapter 5: Boron Sorption onto NMDG Modified Chitosan Sorbent:  
Sorption Behavior and Mechanism Study**

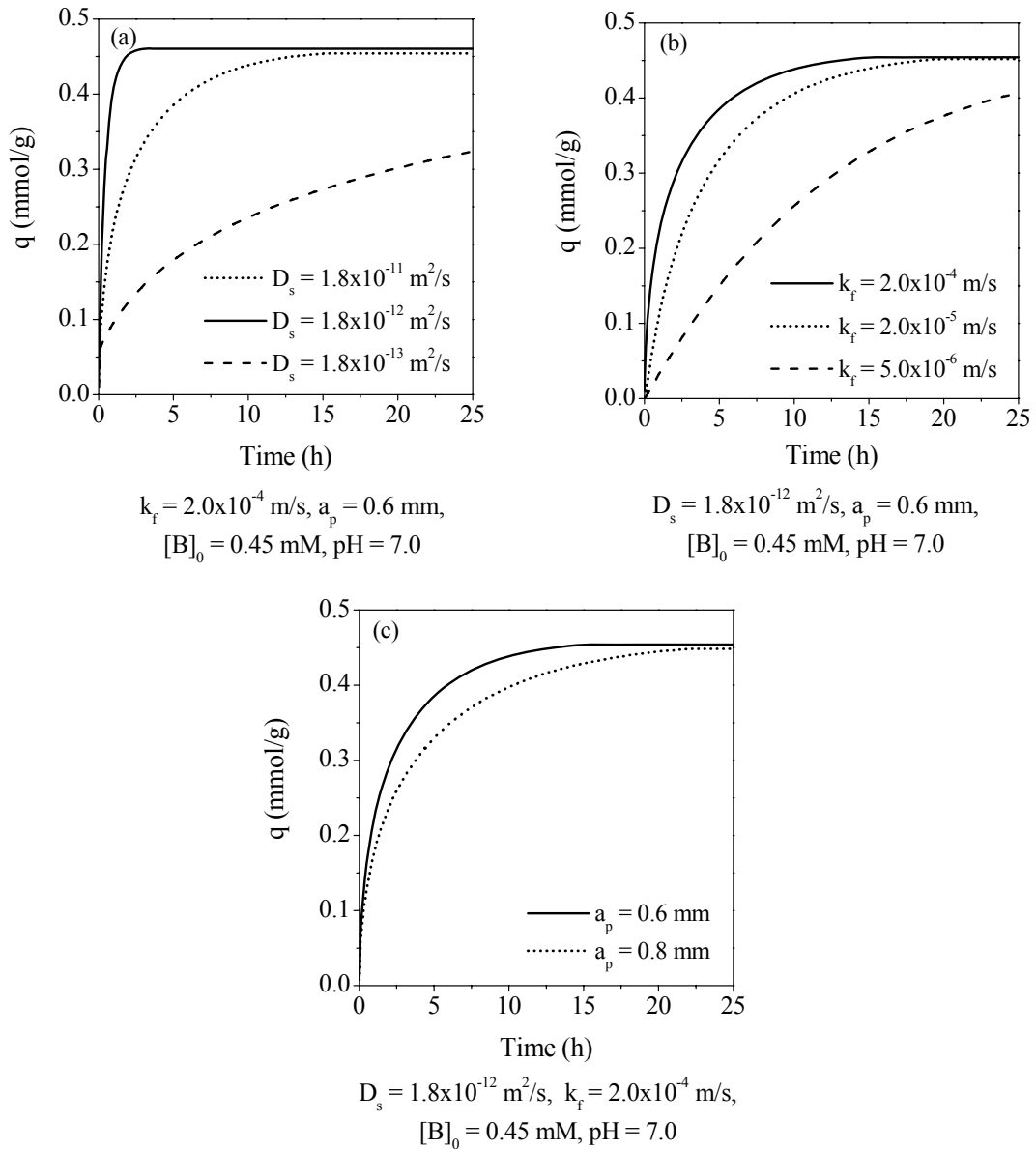


Figure 5.5. Sensitivity analysis of the kinetic model parameters: (a) diffusivity ( $D_s$ ); (b) external mass transfer coefficient ( $k_f$ ); (c) particle radius ( $a_p$ )

A series of calculations were carried out to test the sensitivity of the model parameters, including the diffusivity ( $D_s$ ), external mass transfer coefficient ( $k_f$ ) and the size of sorbent particles ( $a_p$ ). The analyses will be helpful in modeling studies of boron sorption kinetics by other sorbents. When the sensitivity of analysis on one

parameter was conducted, other parameters remained the same.

As illustrated in Figure 5.5a and 5.5b, the diffusivity and external mass transfer coefficient play important roles in the sorption rate. The external mass transfer coefficient affects the initial shorter sorption phase and leads to most of boron removal. On the other hand, the diffusivity determines the rate of sorption in the second longer phase.

Effect of particle size is shown in Figure 5.5c. The slowdown in the sorption kinetics is limited, even though the particle size ( $a_p$ ) increases from 0.6 mm to 0.8 mm (e.g. 33 % increment). According to the calculations, the radius of sorbent is less important in the kinetics. Increase of the diffusivity and external mass transfer coefficient as well as decrease of particle size can result in rapid sorption.

### **5.3 Effect of ionic strength on boron removal**

Boron binding on the CTS-MG was studied in the presence of the common electrolyte backgrounds (Figure 5.6). NaCl and NaNO<sub>3</sub> were used in the experiment due to the existence of large amount of salts in seawater. Ionic strength was varied from 0 mM to 100 mM.

Clearly, CTS-MG exhibits little ionic strength dependence in its sorption behavior for both NaCl and NaNO<sub>3</sub>. No obvious change of boron uptake is observed under low ionic strength. Higher boron removal occurs when the electrolyte concentration increases to 50 mM or 100 mM. Such observation of positive influences on boron

**Chapter 5: Boron Sorption onto NMDG Modified Chitosan Sorbent:  
Sorption Behavior and Mechanism Study**

---

sorption is possibly due to the compression of electrical double layer (EDL), which allows closer approach of boron to the surface sites (Chen and Lin, 2001b). These results indicate that boron may be adsorbed in a strong inner-sphere surface complex. Similar findings were reported by Goldberg et al. that boron sorption on goethite, gibbsite and kaolinite also showed little sensitivity to the solution ionic strength (Goldberg et al., 1993; Goldberg, 2005).

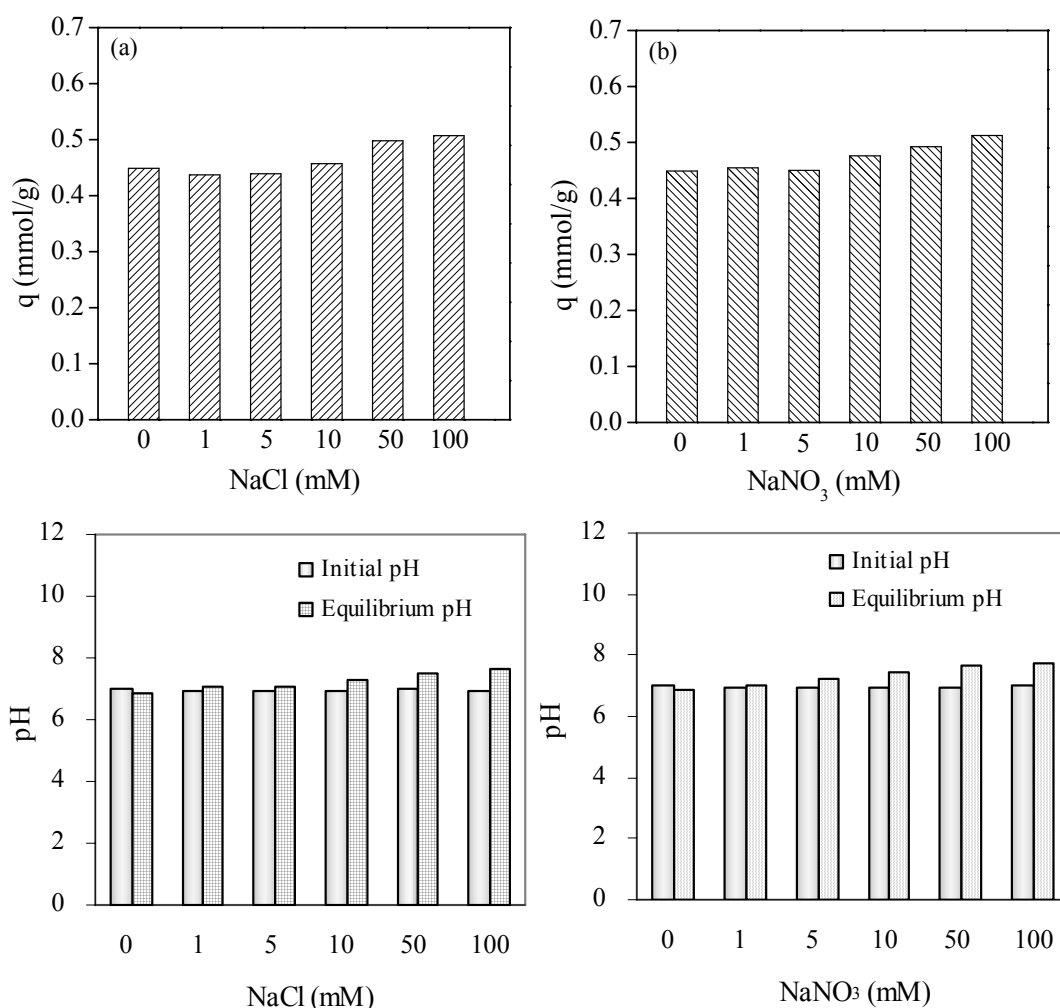


Figure 5.6. Effects of ionic strength on B removal and solution pH. Experimental conditions:  $m = 0.5\text{g/L}$ ,  $\text{pH} = 7.0 \pm 0.1$ ,  $[\text{B}]_0 = 0.46\text{ mM}$ ,  $T = 293\text{ K}$ , contact time = 3 d

**Chapter 5: Boron Sorption onto NMDG Modified Chitosan Sorbent:  
Sorption Behavior and Mechanism Study**

---

Besides, without presence of salts, pH decreases a bit after boron sorption. However, when salinity increases, equilibrium pH becomes higher than initial pH (e.g., 10 % increment most). It has been reported that higher ionic strength can cause the lower  $pK_a$  value; more borate will be present at higher salinity than that at lower salinity and same pH (Oo and Song, 2009). It is likely that in addition to boric acid, the shift of  $pK_a$  value results in the form of borate anions, which can react with surface sites of sorbents to release  $OH^-$  and cause a slight increase of solution pH.

#### **5.4 Application of boron removal from simulated seawater**

In this work, simulated seawater was prepared for batch sorption experiments so as to understand the efficiency of the novel sorbent in terms of sorption performance and applicability to the natural water samples. The chemical compositions of the simulated seawater are listed in Table 5.3; initial concentration of boron in simulated seawater is around 4.8 mg/L (0.44 mM).

Table 5.3 Chemical composition of simulated seawater (pH = 8.1)

<b>Species</b>	<b>Concentration (mg/L)</b>	<b>Species</b>	<b>Concentration (mg/L)</b>
Cl <sup>-</sup>	17567.0	Na <sup>+</sup>	9794.8
SO <sub>4</sub> <sup>2-</sup>	2243.4	K <sup>+</sup>	281.7
B	4.8	Ca <sup>2+</sup>	294.1
IC	21.8	Mg <sup>2+</sup>	1038.8
TOC	3.1		

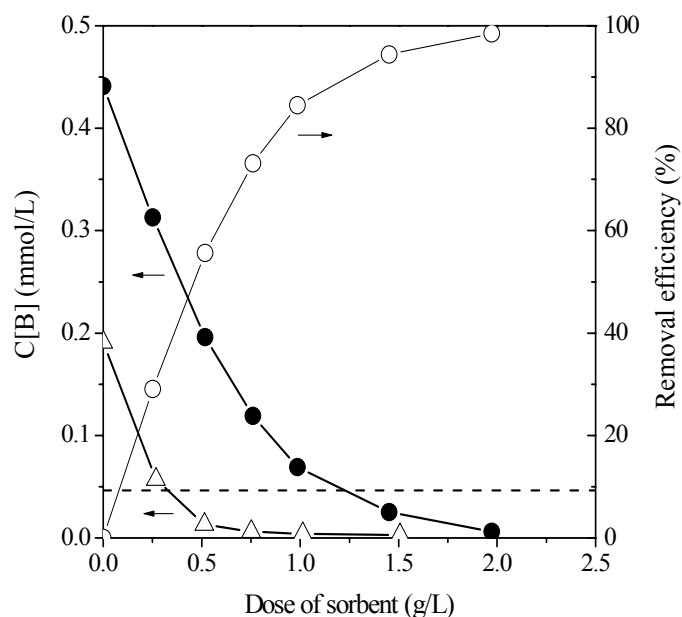


Figure 5.7. Comparative studies of boron removal from simulated seawater and single-species boron solution. Experimental conditions: ● & ○ Simulated seawater, initial pH = 8.1, △ Pure boron solution, initial pH = 7.0, T = 293 K, contact time = 3 d

As can be seen in Figure 5.7, boron equilibrium concentration can be reduced to be lower than 0.5 mg/L (0.046 mM) when the dose of sorbent increases to around 1.2 g/L and the removal efficiency can be achieved as high as 90 %. Results suggest that this polymeric sorbent can be directly used to remove boron from seawater.

Generally the present membrane for seawater desalination can remove 60 - 80 % of boron in the first stage (Jacob, 2007). It means after first stage RO treatment, boron concentration would be between 1 and 2 mg/L in the permeate (considering  $[B]_0 = 5$  mg/L). It should make more sense if substituting a second stage RO with the sorption unit. For example, assuming the initial boron concentration in permeate is around 2 mg/L (0.19 mM) and also assuming all other electrolytes were practically removed by RO, boron level in the effluent can be reduced to 0.5 mg/L (0.046 mM) when dose of

sorbent is around 0.3 g/L (see Figure 5.7). Such combination can reduce the overall capital operating cost as well as lower recovery problems in comparison with an “all RO” strategy.

### **5.5 Mechanism Study**

Sorption of boron causes the changes in surface functional groups of CTS-MG; and these changes can be observed through FT-IR study shown in Figure 5.8. For the pristine sorbent spectrum, the peak at  $880\text{ cm}^{-1}$  is mainly due to the -CCO stretching vibration in secondary alcohols, indicating the presence of multi-hydroxyl functional groups (-CHOH) (Socrates, 2000). After boron sorption, a noticeable feature is that the peak at  $880\text{ cm}^{-1}$  disappeared. Simultaneously, a new band appeared in the  $958\text{ cm}^{-1}$  region, which is attributable to the tetrahedral B asymmetric stretching band (Su and Suarez, 1995; Peak et al., 2003).

Besides, a minor peak shift can be observed in the absorption band of both -OH and -CO group. The -OH bond shifts from  $3396$  to  $3419\text{ cm}^{-1}$  after boron sorption, which is attributed to the attachment of boron on -OH group. The C-N stretching vibration in tertiary amine and C-O stretching vibration in secondary alcohol also shifts to a lower frequency (from  $1084\text{ cm}^{-1}$  to  $1077\text{ cm}^{-1}$ ), which can be due to the involvement of the amine group for boron removal. All these changes imply that partial multi-hydroxyl functional groups (-CHOH) are consumed after reaction with boron, and the tetrahedral B is present on the sorbent surface.



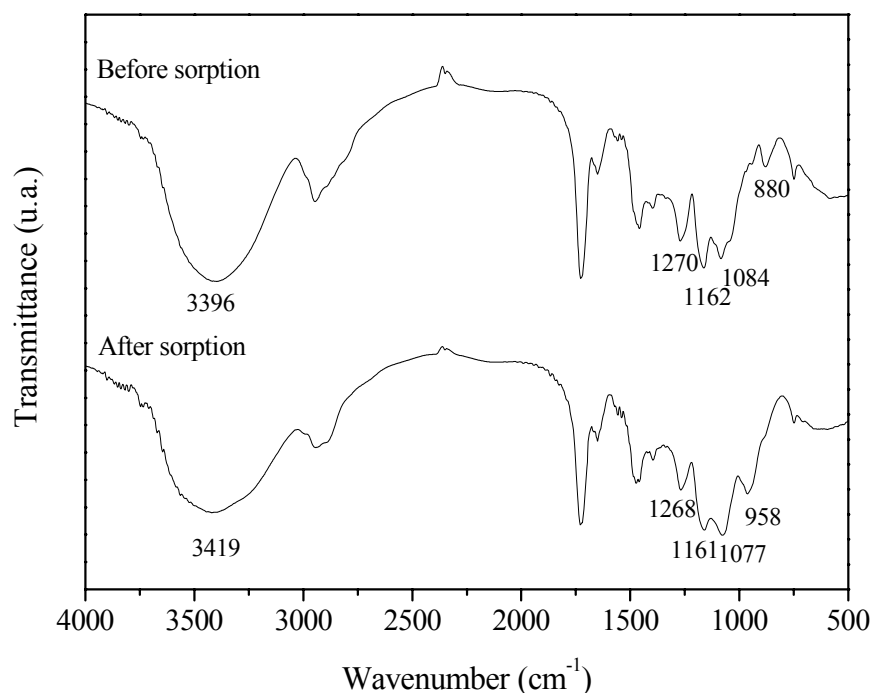


Figure 5.8. FT-IR spectra of sorbents before and after boron sorption

To investigate the interactions between boron and CTS-MG in the sorption process, XPS studies of the sorbent before and after boron sorption were also conducted (Figure 5.9 a-c).

The wide scan clearly in Figure 5.9a shows a new peak around 190 eV in boron-loaded sorbent, implying the accumulation of boron on the sorbents. Besides, it can be observed that in Figure 5.9b and 5.9c the ratio of the positively charged nitrogen atoms ( $-N^+$ , 401.8 eV) to the neutral nitrogen atoms ( $-N$ , 399.0 eV) in tertiary amine increases from 0.21 to 1.03 at pH 7.0, which indicates that certain amine groups are protonated during boron sorption (Moulder, 1992; Yu et al., 2004; Xu et al., 2005). The tertiary amine sites under protonation usually cause a slight increase of solution pH; however, according to the earlier findings in pH effect study,

**Chapter 5: Boron Sorption onto NMDG Modified Chitosan Sorbent:  
Sorption Behavior and Mechanism Study**

---

the equilibrium pH actually decreased a bit. Such opposite trend can be explained by the interaction between boric acid and surface hydroxyl functions, which can release the proton to solution and produce B complexes on the surface as well. Peak and the coauthors (Peak et al., 2003) reported few pathways for boric acid sorption; and their findings were consistent with what we observed in this study. It can also be supported by the early observation in FT-IR analysis that -CHOH groups were involved in boron sorption and the tetrahedral boron complexes formed on the sorbent surface.

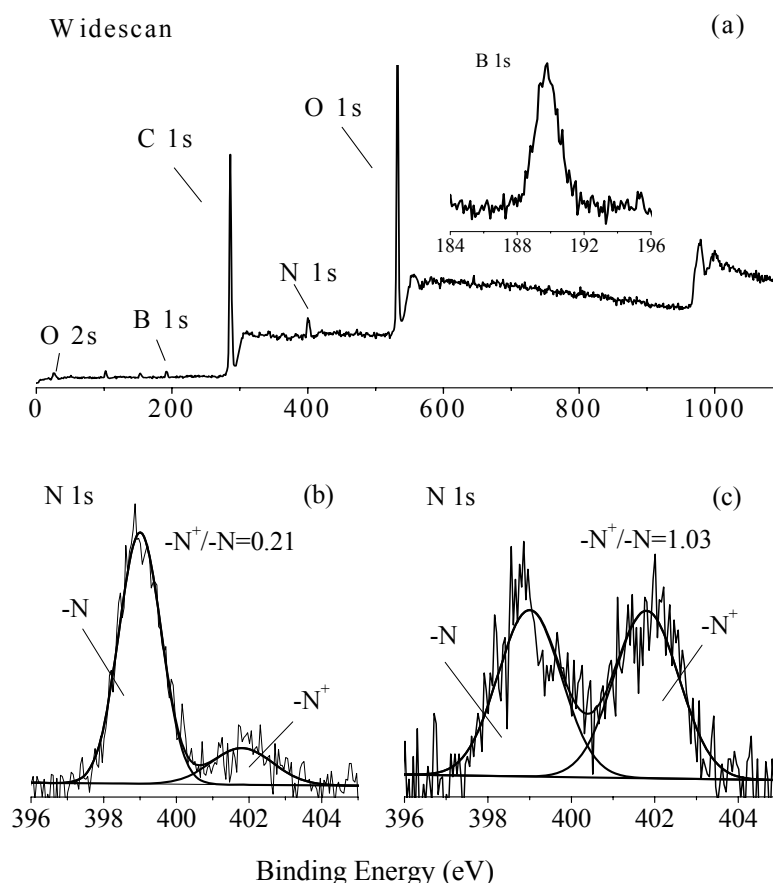


Figure 5.9. XPS (a) wide scan of boron-loaded sorbent, and (b) N 1s core-level spectra of pristine sorbent; (c) N 1s core-level spectra of boron-loaded sorbent

*Chapter 5: Boron Sorption onto NMDG Modified Chitosan Sorbent:  
Sorption Behavior and Mechanism Study*

Based on the previous studies, sorption mechanisms in Figure 5.10 are proposed to discuss the reactions of trigonal boric acid with hydroxyl groups on CTS-MG. As boric acid is considered to be a Lewis acid (electron pair acceptor), it has the affinity for Lewis base oxygen (electron pair donator) of polyhydroxyl functional groups and bound water on the sorbent interface; and the acid / base pairing continues to be stabilized by hydrogen bonding. An outer-sphere intermediate is initially formed between boric acid and the surface of sorbent; a proton is then released and the tetrahedral boron complexes formed on the sorbent surface (Peak et al., 2003).

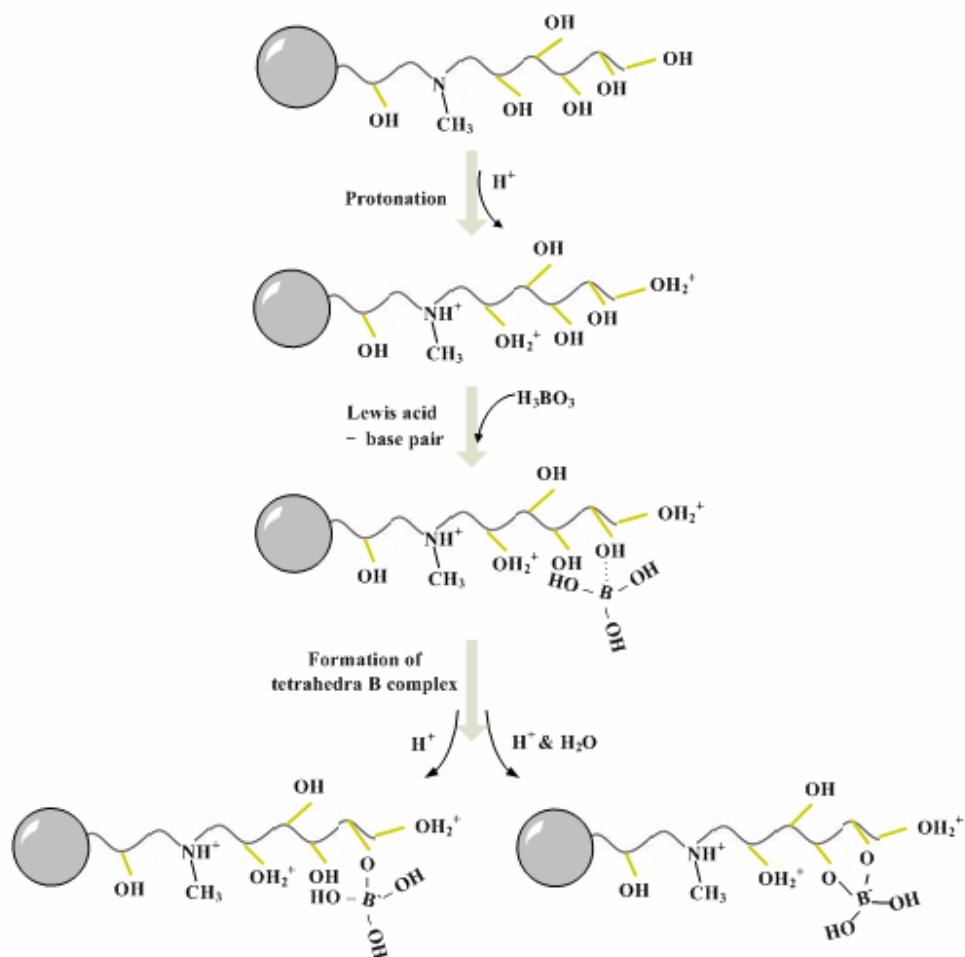


Figure 5.10. Schematic diagram of boron uptake

## **5.6 Section summary**

In this study, CTS-MG exhibits a considerably high ability for boron removal with the maximum capacity of 2.84 mmol/g, much higher than those of commercial resins and many other materials previously reported. Another advantage of the sorbent is that the optimal sorption occurs near neutral pH regions; and then it is applicable in the majority of water supplies without pH adjustment. Boron sorption is suppressed by hydrogen ions at low pH and weakened by electrostatic repulsion at high pH. The kinetic study indicates that 90 % of boron is adsorbed within 8 h and the experimental results are well described by an intraparticle surface diffusion model. The presence of sodium chloride and sodium nitrate does not affect boron sorption, implying formation of inner-sphere complexes at the water/solid interface. This sorbent also exhibits promising applicability for boron removal from natural water bodies such as seawater. The sorption chemistry investigated via FT-IR and XPS, suggest that the oxygen in the form of secondary alcohol (-COH) is mainly involved in boron sorption. Trigonal boric acid is converted to tetrahedral B complexes on the surface of sorbent. Furthermore, a conceptual model for the sorption of boron is proposed to illustrate the mechanisms.

## **CHAPTER 6**

### **ENHANCED SORPTION OF ARSENIC ONTO NMDG**

### **MODIFIED CHITOSAN SORBENT (I): INORGANIC**

### **ARSENIC**

Arsenic contamination in the water has been recognized as a great concern because of its high mobility and toxicity. A wide range of metal or metal oxide based sorbents have been developed and applied for the sorption of arsenic; they can be naturally derived or synthesized such as zero valent iron (Su and Puls, 2001; Mak et al., 2009), iron oxides (Jeong et al., 2007; Zhang et al., 2007e), titanium dioxide (Dutta et al., 2004; Pena et al., 2005) and zirconium (Peraniemi et al., 1994; Zheng et al., 2009). These aforementioned sorbents are effective for arsenic uptake due to their high affinity toward inorganic arsenic species; however, they usually exist as powders and have to be impregnated or loaded on porous host materials for industrial application owing to the poor physical properties such as weak mechanical strength or difficulty in post-treatment. On the other hand, rare earth metals based materials (e.g. lanthanum and cerium) (Wasay et al., 1996; Biswas et al., 2008) are considered to be a new sorption medium for removal of hazardous anions in aqueous solution; however, high cost in use of rare earth compounds comprises their applicability.

Several commercial resins are reportedly used for treatment of arsenic (Dambies et al., 2004); however, very limited studies are reported on the development of novel

## ***Chapter 6: Enhanced Sorption of Arsenic onto NMDG Modified Chitosan Sorbent (I): Inorganic Arsenic***

---

polymeric sorbents with NMDG moiety for arsenic sorption. NMDG moiety is known for its ability to remove boron and arsenic (Dambies et al., 2004; Inukai et al., 2004; Alexandratos, 2007; Wang et al., 2007).

This study focused on the investigation of inorganic arsenic sorption performances onto the novel sorbent with NMDG moiety. A series of batch sorption experiments were conducted as a function of such operational conditions as pH, initial arsenic concentrations, ionic strength, and competitive anions and presence of HA. FT-IR and XPS instruments were used to fully explore the interactions between arsenate anions and the sorbent.

### **6.1 Equilibrium studies**

#### **6.1.1 Effect of solution pH**

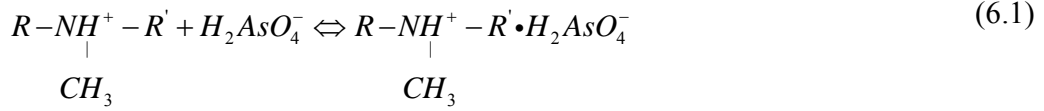
The pH effect on arsenate sorption onto CTS-MG is given in Figure 6.1. It is clear in Figure 6.1a that the optimum sorption occurs at a relatively narrow pH of 4 to 6. Under acid condition (pH 2 – 5), arsenate removal increases with an increase in pH. After a maximum sorption is reached at pH 5, a subsequent decrease in arsenate uptake is found.

The pH-dependent performance in the sorption can be explained as follows. As the surface hydroxyl sites exhibit amphoteric properties, they can be protonated or deprotonated through the addition or release of hydrogen ions (Zheng et al., 2009). On the other hand, according to the species distribution of arsenate at different pH,  $\text{H}_2\text{AsO}_4^-$  is the dominant species in the solution with a pH range of 3 – 6 (Figure 6.1a).

**Chapter 6: Enhanced Sorption of Arsenic onto  
NMDG Modified Chitosan Sorbent (I): Inorganic Arsenic**

---

The monovalent anions may be bound onto the sorbent, which can be expressed in the following reactions:



where  $R-\underset{\text{CH}_3}{\text{N}}-R'$  and  $R^*OH$  represent the two functional groups on the sorbent

With an increase in pH, the number of protonated amine and hydroxyl groups decreases; and then reduces the electrostatic interaction between protonated surface sites and anions. As a consequence, the sorption amount of CTS-MG for arsenate is reduced. When pH further increases to above  $pH_{zpc}$  of 7.8, the CTS-MG becomes negatively charged according to the results of potentiometric titration in Chapter 4. The uptake of arsenate is then retarded owing to the electrostatic repulsive forces. On the other hand, more hydroxyl ions are present at a rising pH, and demonstrate affinity for multiple-hydroxyl functional groups (e.g. alkoxide formation) as shown in Equation 6.3 (Garcia-Soto and Camacho, 2005). Stronger competition for active sites possibly makes arsenate removal more difficult.



Moreover, a buffering effect occurs during the sorption as shown in Figure 6.1b. The equilibrium pH is much higher than the initial pH values at acidic solution; while it decreases to lower values under alkaline conditions. Such findings also verify the

**Chapter 6: Enhanced Sorption of Arsenic onto  
NMDG Modified Chitosan Sorbent (I): Inorganic Arsenic**

protonation or deprotonation of surface groups on the CTS-MG during sorption process. Similar phenomena have been reported for arsenic removal by alginate-encapsulated magnetic sorbent as well as magnetite-doped activated carbon fiber (Lim and Chen, 2007; Zhang et al., 2010a).

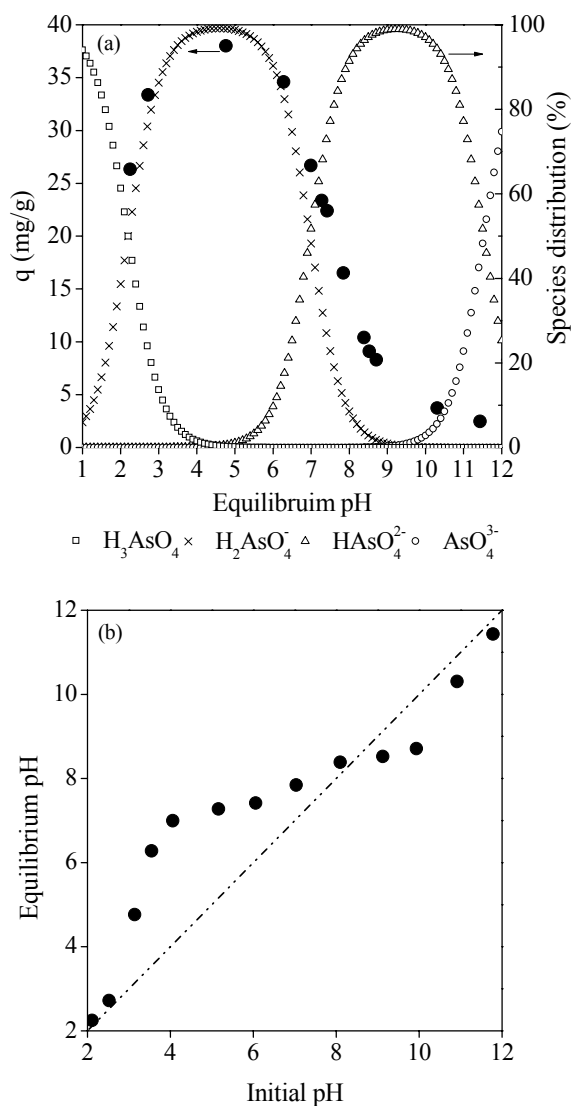


Figure 6.1. (a) Uptake of arsenate as a function of pH, (b) Effect of arsenate sorption on solution pH. Experimental conditions:  $[As(V)]_0 = 20$  mg/L,  $m = 0.5$  g/L,  $T = 293$  K



### **6.1.2 Sorption isotherm**

Experiments of arsenate sorption isotherm onto CTS-MG and CCTS were carried out to evaluate the maximum arsenate sorption capacity. Both Langmuir and Freundlich equations described by Equation 2.5 and 2.6 in Chapter 2 were used to fit the experimental results. The experimental data and modeling fitting are shown in Figure 6.2; the corresponding parameters for the isotherms are given in Table 6.1.

It is found that Freundlich equation is more applicable to describe sorption behavior of arsenate on CTS-MG, (correlation coefficient,  $R^2 = 0.993$ ). As shown in Figure 6.2, the maximal removal capacity (corresponding to the isotherm plateau) is 69.3 mg/g for CTS-MG, whereas the experimental results for CCTS exhibit the best fit to Langmuir model, implying the possible formation of monolayer coverage of adsorbate on the surface of CCTS. According to fitting results, the maximum sorption capacity of CCTS is 61.1 mg/g, respectively. It means the chemical modification of CCTS improves the arsenate sorption by nearly 13 %.

The initial gradient of the sorption isotherm curve (b) is another important parameter as it indicates the sorbent affinity at low concentrations. A high value of the affinity constant is usually desirable. The corresponding affinity values of the CTS-MG and CCTS are 1.09 and 0.06 L/mg, respectively; this clearly suggests the affinity of CTS-MG is much stronger than unmodified chitosan. It can be therefore concluded that the CTS-MG is more favorable for arsenate uptake than CCTS.

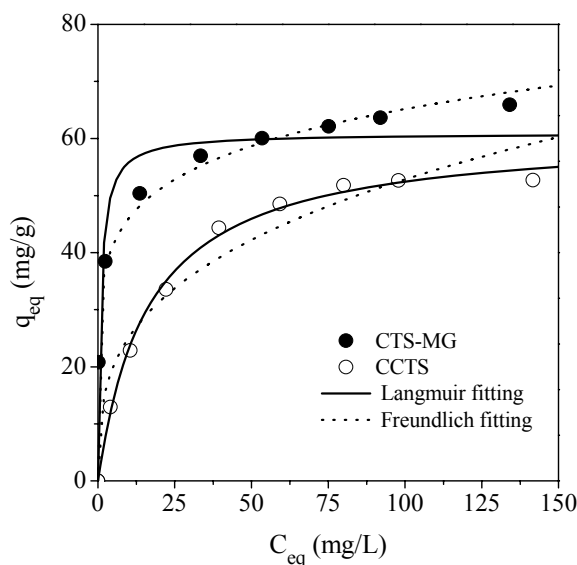


Figure 6.2. Sorption isotherm of arsenate onto CCTS and CTS-MG. Experimental conditions:  $m = 0.5$  g/L,  $\text{pH} = 3$ ,  $T = 293$  K

Table 6.1 Isotherm parameters for arsenate sorption on CCTS and CTS-MG

		<b>CTS-MG</b>	<b>CCTS</b>
<b>Langmuir</b>	$q_{\text{max}}$ (mg/g)	60.893	61.077
	$b$ (L/mg)	1.089	0.061
	$R^2$	0.934	0.996
<b>Freundlich</b>	$K_f$	32.450	11.922
	$1/n$	0.151	0.323
	$R^2$	0.993	0.956

## 6.2 Sorption kinetics under different ionic strength effect

Figure 6.3 shows the arsenate sorption history in the absence and presence of the common electrolyte backgrounds ( $\text{NaClO}_4$ ). Ionic strength was varied by two orders of magnitude, ranging from 0 to 50 mM. It can be found that without influence of ionic strength ( $I = 0$ ), the sorption process follows two steps: rapid sorption occurs in

the first 5 h followed by a slightly slower stage. The total equilibrium time can be achieved within 16 h.

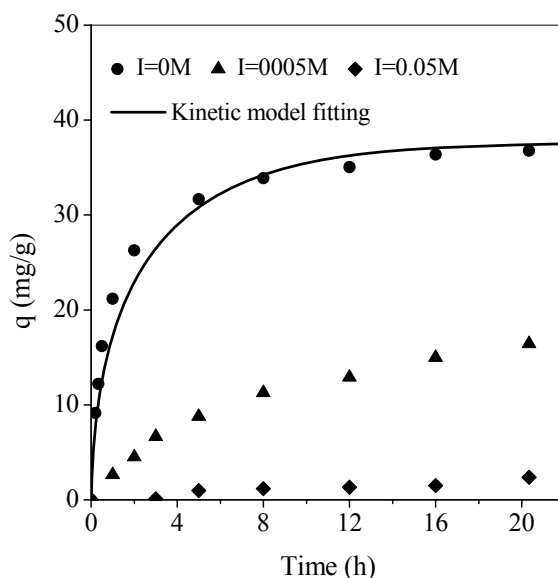


Figure 6.3. Sorption kinetics of arsenate at different ionic strength. Experimental conditions:  $[\text{As(v)}]_0 = 20 \text{ mg/L}$ ,  $m = 0.5 \text{ g/L}$ ,  $\text{pH} = 3$ ,  $T = 293 \text{ K}$

As shown, the rate of arsenate sorption was limited by increasing ionic strength. The higher the  $\text{NaClO}_4$  concentration is, the slower the sorption rate becomes and the longer the equilibrium time requires. Sorption kinetics are usually affected by the availability and accessibility of surface sites, the relative charges of the surface and adsorbing species, and the rate of complexation of the dissolved species with surface sites (Redman et al., 2002). Consequently, the observed extension of equilibrium time with increasing ionic strength may be explained by the following reasons. The influence of ionic strength on the activity coefficient of arsenate possibly reduces its transfer mobility to the sorbent surface (Hamdaoui et al., 2008). Besides, the increase in ionic strength effect can cause a large amount of electrolytes surrounding the

***Chapter 6: Enhanced Sorption of Arsenic onto  
NMDG Modified Chitosan Sorbent (I): Inorganic Arsenic***

---

sorbent surface, and such obstruction hinders the accessibility of arsenate to the active sites of surface. Similar observation was found by Moreira that ionic strength caused a great reduction in the diffusivity for sorption of amino acids with an anion-exchange resin (Moreira and Ferreira, 2005).

On the other hand, the uptake of arsenate is suppressed at higher ionic strength. The sorption capacities at ionic strength of 0.005 and 0.05 M are only 16.4 mg/g and 2.4 mg/g, respectively, much lower than those of NaClO<sub>4</sub> free solution. Under given experimental conditions, the surface of CTS-MG is net positively charged. The negative phenomenon is mainly due to the competition between ClO<sub>4</sub><sup>-</sup> from the salts (present in large concentrations) and arsenic oxyanions, which further diminishes the

number of available binding sites ( $R^*OH_2^+$  or  $R-NH^+-R'$ ). It is consistent with the



prediction that at least the electrostatic interaction plays an important role in sorption process. A similar effect was previously reported by Vijayaraghavan that arsenate sorption onto crab shells declined to a great extent with increasing solution ionic strength (Vijayaraghavan et al., 2009).

Study of ionic strength effect may provide useful information to distinguish between inner-sphere and outer-sphere complexation involved in sorption process (Hayes et al., 1988). In the case of inner sphere complex, covalent bonds forms between the adsorbed ions and the surface functional groups, hence sorption is generally not affected by ionic strength. However, in the case of outer-sphere complexation, the adsorbate is weakly bonded onto the sorbent, which is strongly

## ***Chapter 6: Enhanced Sorption of Arsenic onto NMDG Modified Chitosan Sorbent (I): Inorganic Arsenic***

---

ionic strength dependent. Outer-sphere complex are usually located at the same plane with the background electrolyte ions. The background electrolyte ions can compete with the non-specific sorption ions for available binding sites at the surface. On the other hand, the activity of the adsorbing species can be affected by the variation of the interfacial potential due to the changes of ionic strength (Liu et al., 2008a). As shown in Figure 6.3, the sorption of arsenate onto the CTS-MG sorbent is highly ionic strength dependent, which indicates the formation of outer-sphere surface complexes on the CTS-MG.

Simulation of arsenate sorption kinetics was conducted by the intraparticle diffusion model described in Equation (5.5) to (5.8) in Chapter 5. It can be seen that the model demonstrates a good representation of the kinetics data. The  $k_f$  and  $D_s$  values for arsenate sorption in the absence of  $\text{NaClO}_4$  are  $2.0 \times 10^{-4}$  m/s and  $1.6 \times 10^{-12}$   $\text{m}^2/\text{s}$ , respectively. Our modeling simulation results indicate that the sorption process is mainly controlled by the surface diffusion, while the external mass transfer is less critical.

### **6.3 Simultaneous sorption of arsenate and natural organic matter**

Natural organic matter (NOM) is a ubiquitous substance in groundwater, especially in shallow aquifers. The presence of NOM generally plays a significant role on arsenate sorption behavior (Mak et al., 2009). To develop a better understanding of the performance of CTS-MG, it is therefore necessary to study the influences of NOM on arsenate sorption from natural aqueous environment. pH 7.0 was selected since the majority of actual water supplies normally have a range of

6.5-8.5.

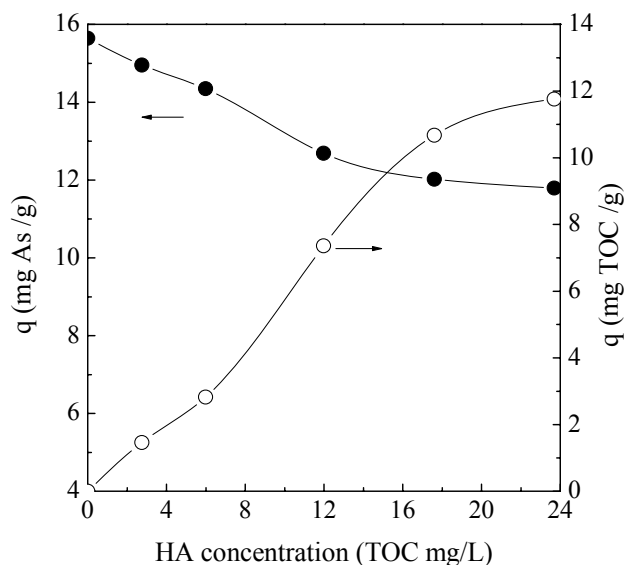


Figure 6.4 Simultaneous sorption of arsenate and HA. Experimental conditions:  $[\text{As(v)}]_0 = 20 \text{ mg/L}$ ,  $m = 0.5 \text{ g/L}$ ,  $\text{pH} = 7$ ,  $T = 293 \text{ K}$ .

Figure 6.4 demonstrates the simultaneous sorption of arsenate and NOM, which is typically represented by HA. As shown, the presence of HA slightly reduces the arsenate sorption onto CTS-MG. In the absence of HA, the sorption amount for arsenic reaches 15.6 mg/g. It further decreases to 11.8 mg/g when the concentration of NOM increases to approximately 25 mg/L (TOC). Meanwhile, good removal of NOM can be found in Figure 6.4. Images in Figure 6.5 also demonstrate the obvious color changes of CTS-MG from white to brown after arsenate sorption in the presence of NOM. Such observations indicate that CTS-MG is effective for both arsenate and organic pollutants removal from multiple-polluted wastewaters.

It is encouraging to note that CTS-MG can achieve simultaneous sorption of both arsenate and HA. HA binding in this study can be attributed to the following reasons:

### ***Chapter 6: Enhanced Sorption of Arsenic onto NMDG Modified Chitosan Sorbent (I): Inorganic Arsenic***

---

the attractive electrostatic interactions between positively charged surface and negatively charged HA; organic complexes formation (e.g.  $-N^+\cdots^-OOC-R'$  or  $-N^+\cdots^-O-R''$ ) between the protonated amine groups and carboxyl / phenolic groups in HA or ligand exchange reaction between surface hydroxyl groups and carboxyl / phenolic groups (Gu et al., 1994; Stumm et al., 1996; Chen et al., 2004).



Figure 6.5. Images of CTS-MG before and after arsenate sorption in the presence of NOM

#### **6.4 Competitive sorption**

Arsenic in contaminated groundwater is usually accompanied with different anions, which may compete with arsenic for the available adsorptive sites. Effects of these co-existing anions were examined to evaluate the efficiency of CTS-MG for arsenate removal. At fixed pH 7.0, the influences of some common anions ( $F^-$ ,  $SO_4^{2-}$ ,  $PO_4^{3-}$ ) at four different concentration levels (0, 0.1, 0.5, 1mM) are illustrated in Figure 6.6.

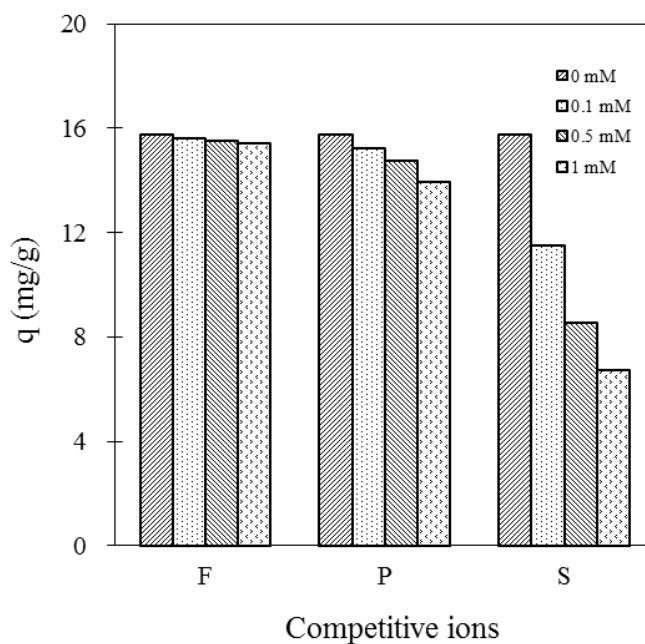


Figure 6.6. Effects of co-existing anions on arsenate removal. Experimental conditions:  $[As(v)]_0 = 20 \text{ mg/L}$ ,  $m = 0.5 \text{ g/L}$ ,  $\text{pH} = 7$ ,  $T = 293 \text{ K}$

As judged from Figure 6.6, the presence of fluoride has no significant effect in arsenic sorption, while sulfate noticeably interferes with the uptake among these three anions. When concentrations of sulfate further increases to 1 mM, the arsenate sorption is only 43 % of the amount in the absence of sulfate. Their effects on sorption exhibit the following descending sequence of: sulfate >> phosphate > fluoride.

Similarly, other researchers also reported that sulfate caused the greatest decrease in arsenate sorption than other competitive anions by a weak-base anion exchange; and anions in solution can exchange with the hydroxyl or other ions around the aminated groups on the surface of sorbent (Awual et al., 2008; Deng et al., 2008). According to electroselectivity, divalent anions take the precedence of monovalent



***Chapter 6: Enhanced Sorption of Arsenic onto  
NMDG Modified Chitosan Sorbent (I): Inorganic Arsenic***

---

anions to be adsorbed by anion exchangers (Awual et al., 2008). Consequently, the anion exchange reaction is probably the involved mechanism for arsenate removal by CTS-MG and subsequently arsenic attaches onto the surfaces through formation of outer-sphere complexes, which is consistent with earlier prediction during ionic strength effect study.

Phosphate and arsenic are located in the same main group and they have the similar molecular structures and chemical properties. Some literature studies showed that phosphate exhibited higher competitive impact on arsenic removal than other co-existing anions (e.g. sulfate) and could form inner-sphere complex with sorbents such as iron-based materials (Zhang et al., 2007c). Such discrepancy is attributed to different mechanisms involved in arsenate sorption.

### **6.5 FTIR analysis**

Figure 6.7 shows the FTIR spectra of the CTS-MG before and after arsenate sorption. For the pristine sorbent, the peaks at  $1084\text{ cm}^{-1}$  and  $881\text{ cm}^{-1}$  corresponds to the C-N stretching vibration in the amine group and C-O stretching vibration in secondary alcohols (Socrates, 2000). After reaction with As(V), the peaks shift to  $1066\text{ cm}^{-1}$  and  $871\text{ cm}^{-1}$ , respectively; which implies the possible involvement of amine and hydroxyl groups in the sorption of arsenate. Simultaneously, two new bands appears at  $833\text{ cm}^{-1}$  and  $906\text{ cm}^{-1}$ , corresponding to the symmetric and asymmetric stretching vibration of As-O bonds, respectively (Goldberg and Johnston, 2001; Zhang et al., 2007c). The peak at  $1384\text{ cm}^{-1}$  is ascribed to the vibration of  $\text{NO}_3^-$   $\text{cm}^{-1}$  as nitric acid was used to adjust solution pH (Zhang et al., 2007c). All these

changes imply that arsenate is adsorbed onto CTS-MG via interaction with both tertiary amine and hydroxyl functional groups.

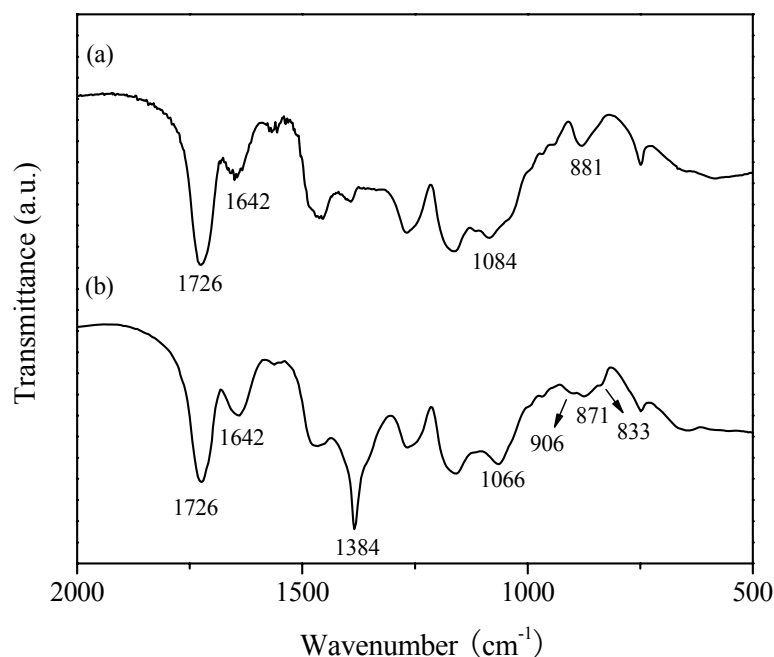


Figure 6.7. FTIR spectra: (a) pristine sorbent and (b) As-loaded sorbent

## 6.6 XPS analysis

To investigate the interactions between arsenic and CTS-MG in the sorption process, XPS analysis of the sorbent before and after arsenic sorption at different pH was performed (Figure 6.8).

As shown, an obvious peak at 45.5 eV is found in the As3d photoelectron spectra of the As-loaded sorbent, indicating the successful attachment of arsenate onto the surface of sorbent (Moulder, 1992). The binding energies at 399.0 eV and 401.8 eV in Figure 6.8b & 6.8c are attributable to the nitrogen atoms in neutral amine ( $\text{-}\underline{\text{N}}$ ) and protonated amine ( $\text{-}\underline{\text{N}}^+$ ) groups, respectively. It can be observed that the proportion of

**Chapter 6: Enhanced Sorption of Arsenic onto  
NMDG Modified Chitosan Sorbent (I): Inorganic Arsenic**

---

the positively charged nitrogen to uncharged nitrogen atoms increases with a decrease in pH. The ratio of  $\text{-N}^+$  to  $\text{-N}$  is 0.27 at pH 7, while it increases to 1.07 at pH 3. More protonated amine groups are consistent with higher sorption amount of arsenic. These results indicate that the tertiary amine groups play an important role for arsenate removal by CTS-MG. Additionally, no detection of As(III) in XPS analysis means no reduction of As(V) occurs during sorption.

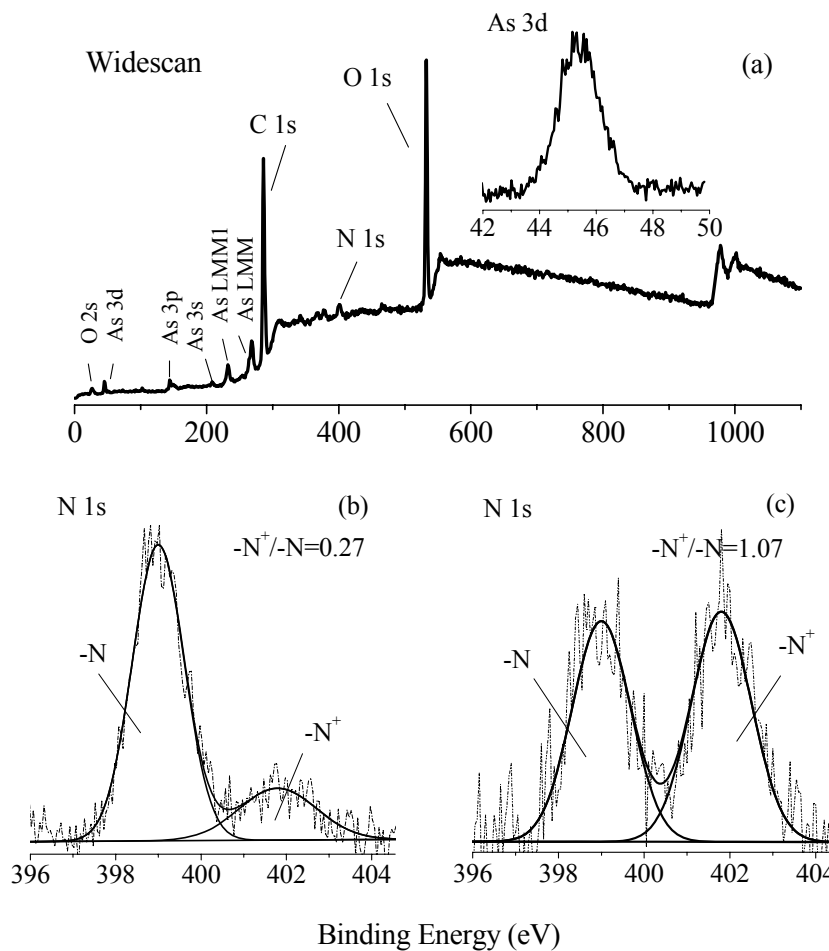


Figure 6.8. XPS of As-loaded sorbent: (a) widescan and As3d core-level; (b) N 1s core-level spectra (pH = 7); and (c) N 1s core-level spectra (pH = 3)

## ***Chapter 6: Enhanced Sorption of Arsenic onto NMDG Modified Chitosan Sorbent (I): Inorganic Arsenic***

---

According to the overall analysis in this study, it can be thus concluded that the protonated amine and hydroxyl groups are responsible for arsenate sorption. On the one hand, the negative arsenate ions can be adsorbed through electrostatic attractive forces with the positively charged amine and hydroxyl groups; on the other hand, the arsenic anions in aqueous solution can exchange with the hydroxyl or other anions around the protonated amine groups on the surface of CTS-MG.

### **6.7 Section summary**

The novel sorbent CTS-MG can be used as an effective sorbent for arsenate removal from aqueous solutions. Results from batch sorption experiments demonstrate that arsenate sorption onto CTS-MG is pH-dependent (with maximum sorption at acidic condition). The sorbent has a high sorption capacity of 69.28 mg/g for arsenate, which is enhanced approximately 13 % in comparison with CTS without chemical modification. Other than that, the affinity constant of CTS-MG is much higher than that of CTS, exhibiting stronger affinity of CTS-MG for arsenate. The kinetic sorption experiment indicates that the sorption equilibrium can be reached within 16 h. The presence of NaClO<sub>4</sub> not only causes higher transfer resistance to arsenate anions, but also competes with arsenate for surface binding sites during sorption. The CTS-MG exhibits great performance for simultaneous removal of arsenate and HA. Among three tested competitive anions, fluoride has no significant effect on arsenate uptake. Sulfate is found to be the greatest competitor with arsenate for available adsorptive sites on the sorbent. Additionally, FTIR and XPS analyses clearly reveal that the tertiary amine and hydroxyl functional groups in CTS-MG

***Chapter 6: Enhanced Sorption of Arsenic onto  
NMDG Modified Chitosan Sorbent (I): Inorganic Arsenic***

---

provide the major binding sites for As(V). Non-specific interactions such as electrostatic attraction and anion exchange between arsenate anions and surface sites play an important role during sorption.

## **CHAPTER 7**

# **ENHANCED SORPTION OF ARSENIC ONTO NMDG MODIFIED CHITOSAN SORBENT (II): METHYLATED ARSENIC**

In addition to inorganic arsenate, other common species of arsenic are methylated arsenic species of MMA and DMA. Methylation of arsenic by various microorganisms ranging from fungi to bacteria can influence the organoarsenic species in the natural systems (Cullen and Reimer, 1989). Methylated arsenic compounds also can be introduced into the environment through industrial and agricultural activities. In the 1990s, MMA and DMA were extensively used as herbicides in the U.S. to control weeds for cotton production and occurred as important contaminants in surface and groundwater (Bednar et al., 2002). U.S. statistics demonstrate that between 2 and 4 million pounds of the sodium salt of MMA were used in the U.S. by industrial, commercial and government sectors during 1999 (Xu et al., 2008).

Quite a number of water sources have been found to be polluted by organic arsenic species. Nearly 24 % of the total dissolved arsenic was detected as the methylated species in the lakes of California and the predominant form was DMA (Pokhrel and Viraraghavan, 2008). Besides, the organic arsenic concentration

accounted for up to 53 - 60 % of the total dissolved arsenic in river and estuarine waters from southwest Spain (Sanchez-Rodas et al., 2005).

Inorganic arsenic species are usually considered more toxic than methylated arsenic; however, the unique toxic properties of organoarsenic have been identified as well. Long-term exposure to DMA can cause DNA damage (Ahmad et al., 1999), chromosomal aberrations, and also demonstrates multi-organ tumor promoting activities including lung, liver, kidney and urinary bladder (Kenyon and Hughes, 2001; Salim et al., 2003; Arnold et al., 2006; Kinoshita et al., 2007). As a consequence, treatment of methylated arsenic is necessary due to their widespread distribution in the environment and potentially adverse impacts to humans. To date, extensive research has been conducted to decontaminate inorganic arsenic from aqueous environmental systems; however, only little information is available for development of novel materials to remove organic arsenic species.

In this chapter, sorption behavior of methylated arsenic species, MMA and DMA onto the polymeric material CTS-MG was conducted and compared with inorganic arsenic. Effects of different experimental parameters, namely solution pH, initial arsenic concentration, contact time, ionic strength, NOM, competitive anions were under investigation. XPS was used to further verify the binding of organic arsenic.

## **7.1 Equilibrium studies**

### **7.1.1 Effect of pH**

**Chapter 7: Enhanced Sorption of Arsenic onto  
NMDG Modified Chitosan Sorbent (II): Methylated Arsenic**

The dependence of sorption capacity to pH varied from one arsenic species to another. MMA and DMA sorption as a function of pH are shown in Figure 7.1.

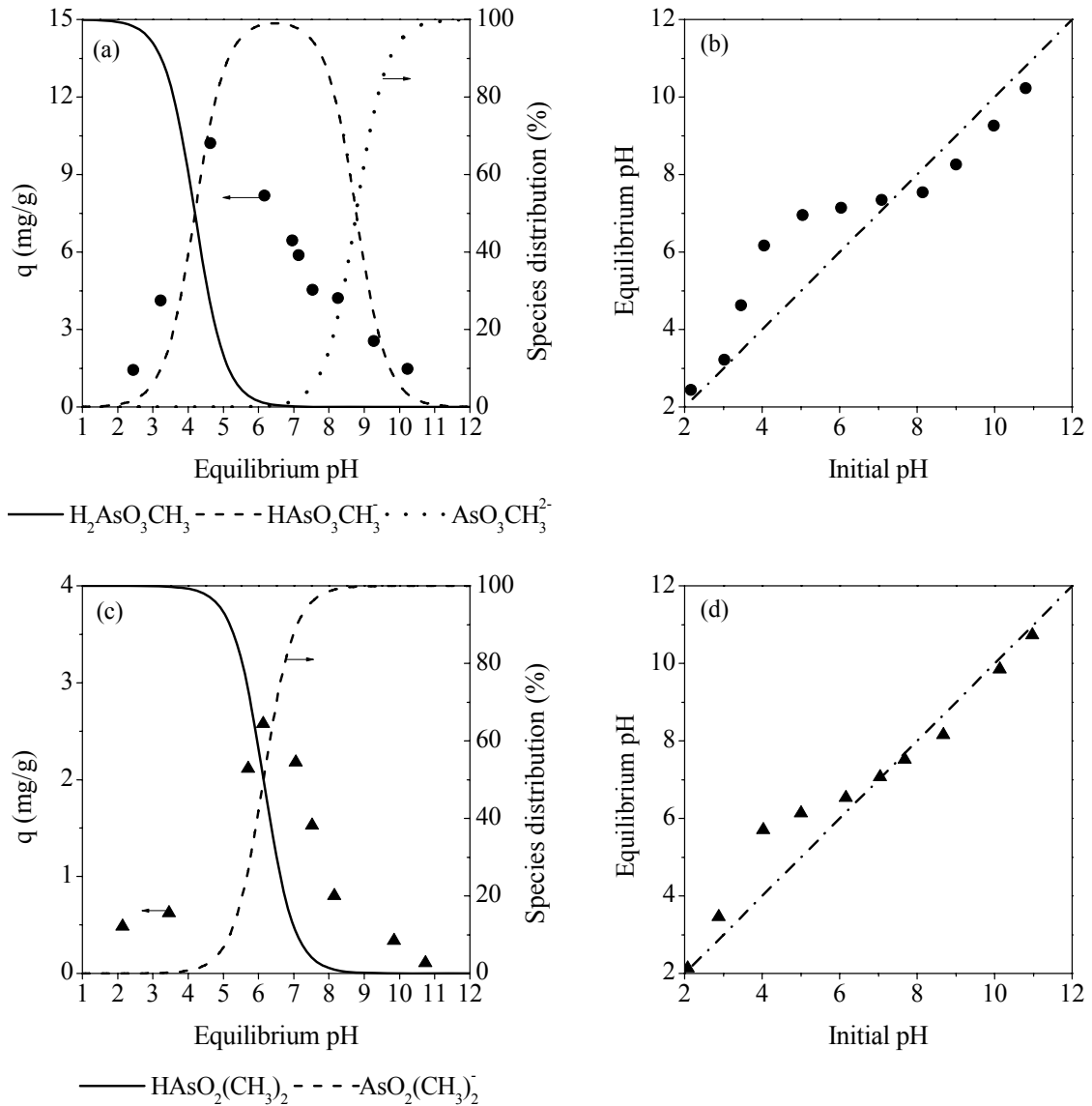


Figure 7.1. (a) Uptake of MMA as a function of pH, (b) Effect of MMA sorption using CTS-MG on solution pH, (c) Uptake of DMA as a function of pH, (d) Effect of DMA sorption using CTS-MG on solution pH. ( $[\text{As}]_0 = 20 \text{ mg/L}$ ;  $m = 0.5 \text{ g/L}$ ;  $T = 293 \text{ K}$ ; contact time = 3 d)

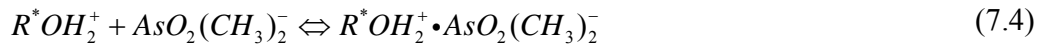
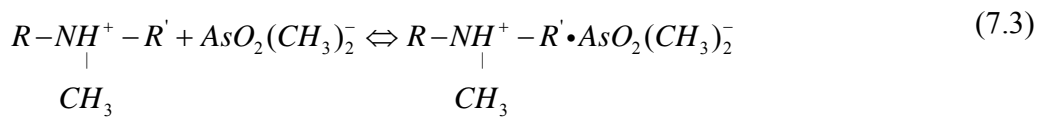
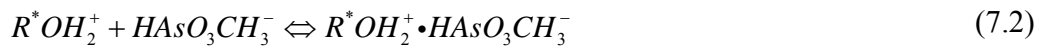
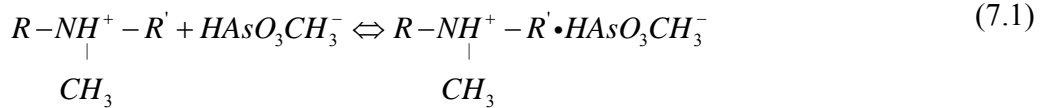


**Chapter 7: Enhanced Sorption of Arsenic onto  
NMDG Modified Chitosan Sorbent (II): Methylated Arsenic**

---

MMA and DMA exhibit similar sorption edge in the pH range of 2 to 11. Besides, DMA is adsorbed in smaller quantities than MMA throughout all pH values. Under acidic condition, the uptake of organic arsenic species is very low. The optimal arsenic removal can be achieved at pH 4 and pH 6 for MMA and DMA, respectively; and then gradually declines with increasing pH.

Such sorption behavior can be further explained by the methylated arsenic speciation as well as the charge property of CTS-MG surface. CTS-MG has a point of zero charge (zpc) of 7.8. According to the species distribution, at extremely low pH, both of the predominant species are neutral species such as  $H_2AsO_3CH_3$  and  $HAsO_2(CH_3)_2$ . The uptake of MMA and DMA nearly approaches to zero, since no electrostatic interaction exists between non-ionic species and the charged surfaces.



where  $R-\underset{\text{CH}_3}{\text{N}}-R'$  and  $R^*OH$  represent the two functional groups on the sorbent

As pH increases, more and more neutral species convert to monovalent arsenic species as  $HAsO_3CH_3^-$  and  $AsO_2(CH_3)_2^-$ . It is favorable for methylated arsenic

sorption by positively charged surfaces of CTS-MG (Equation 7.1 - 7.4). However, with further increase of pH, the number of protonated tertiary amine and hydroxyl groups reduces, and smaller amount of MMA and DMA is adsorbed. The decrease in sorption of MMA and DMA above zpc of CTS-MG is probably attributed to rising competition between hydroxyl ions and arsenic species for active sites. The pH-dependent behavior of MMA and DMA sorption suggests that the non-specific interaction might control the sorption process onto CTS-MG.

A buffering effect is observed for both MMA and DMA sorption (Figure 7.1b & 7.1d). The final pH increases slightly at acidic condition, while it decreases a bit under alkaline solution. Earlier research for inorganic arsenic removal exhibited a similar trend on the same sorbent.

### **7.1.2 Sorption isotherm**

Sorption isotherms of two methylated arsenic species were conducted with initial concentrations ranging from 0 to 125 mg/L (Figure 7.2). Langmuir and Freundlich isotherms were used to analyze the experimental data except DMA uptake by CCTS, in which the sorption can be negligible. Langmuir isotherm indicates homogeneous sorption while Freundlich equation describes sorption on heterogeneous surface. The fitted results are summarized in Table 7.1.

Both Freundlich and Langmuir equations are suitable to describe the sorption behavior of MMA and DMA on modified chitosan. The maximum removal capacities of CTS-MG for MMA and DMA are 15.4 mg/g and 7.1 mg/g, respectively, much

higher than those of CCTS (e.g. 5.9 mg/g for MMA and 0 mg/g for DMA). Chemical modification of CCTS definitely enhances organic arsenic sorption.

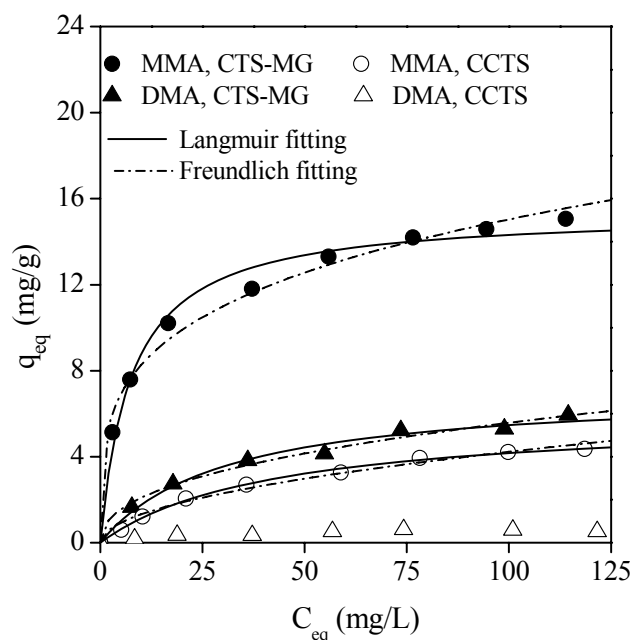


Figure 7.2. Methylated arsenic sorption isotherms onto CTS-MG and CCTS (Experimental conditions:  $m = 0.5$  g/L, pH = 3.4 (MMA), pH = 5 (DMA),  $T = 293$  K, contact time = 3 d)

Table 7.1 Parameters of the isotherm models

		CTS-MG		CCTS	
		MMA	DMA	MMA	DMA
<b>Langmuir</b>	$q_{\max}$ (mg/g)	15.4	7.1	5.9	--
	$b$ (L/mg)	0.132	0.033	0.024	--
	$R^2$	0.988	0.986	0.997	--
<b>Freundlich</b>	$K_f$	4.546	0.784	0.411	--
	$1/n$	0.260	0.426	0.506	--
	$R^2$	0.991	0.987	0.986	--

**Chapter 7: Enhanced Sorption of Arsenic onto  
NMDG Modified Chitosan Sorbent (II): Methylated Arsenic**

---

Compared to inorganic arsenic sorption by CTS-MG in Chapter 6, it was found that substitution of hydroxyl by methyl groups directly affects the sorption behavior. The sorption amount of arsenate is nearly 4-10 times higher than those of methylated arsenic species, respectively. Besides, a decrease in affinity of arsenic species for CTS-MG exhibits similar trends: inorganic As (V) > MMA > DMA. This discrepancy might have been caused by the presence of additional methyl groups of MMA and DMA, which have different molecular geometries as well as different spatial compatibility with surface active sites (Cheng et al., 2005; Ramesh et al., 2007). These trends are also consistent with those reported by Xu et al. for arsenic uptake by TiO<sub>2</sub> (Xu et al., 2007). Sorption performances of various sorbents in literature are summarized in Table 7.2. As judged, CTS-MG exhibits competitive advantages with other materials for methylated arsenic removal from aqueous solution.

Table 7.2 Comparison of methylated arsenic sorption onto several sorbents reported in literature

Sorbent	MMA		DMA		Reference
	pH	q <sub>max</sub> (mg/g)	pH	q <sub>max</sub> (mg/g)	
CTS-MG	3.4	15.396	5	7.134	This work
Calcium alginate encapsulated magnetic sorbent	3-4	8.57	--	--	(Lim et al., 2009)
Iron filings	--	0.65	--	0.02	(Cheng et al., 2005)
Polymeric Al/Fe modified montmorillonite	--	--	6	18.19	(Ramesh et al., 2007)
Degussa P25 TiO <sub>2</sub>	6.8	6.44	6.8	2.77	(Xu et al., 2007)
Iron oxide coated sand	--	--	7.6	0.008	Thirunavukkarasu et al. (2002)

## 7.2 Sorption kinetics under different ionic strength

Sorption kinetics describing the rate of arsenic uptake by CTS-MG is important to evaluate the efficiency of sorption. Figure 7.3 demonstrates the time profile of MMA and DMA sorption onto CTS-MG at two different ionic strengths.

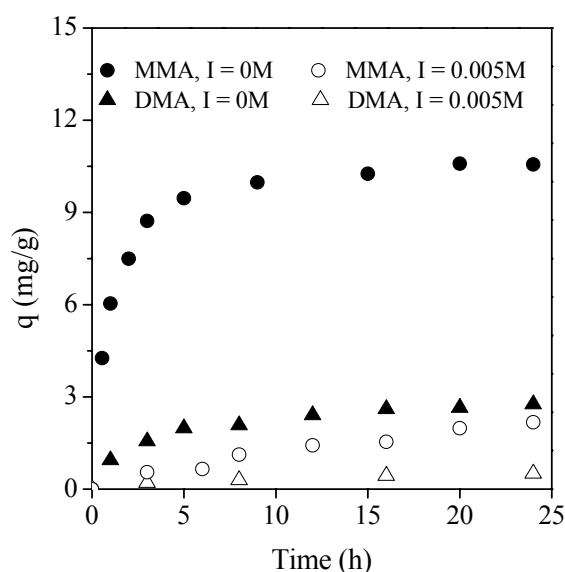


Figure 7.3. Sorption kinetics of MMA and DMA at different ionic strength (Experimental conditions:  $[As]_0 = 20$  mg/L,  $m = 0.5$  g/L, pH = 3.4 (MMA), pH = 5 (DMA),  $T = 293$  K, contact time = 3 d)

Studying the influences of ionic strength is a simple way to distinguish the inner-sphere from outer-sphere sorption. It is found that in the absence of electrolyte backgrounds ( $NaClO_4$ ), over 80 % of MMA and DMA sorption rapidly occurs in the first 8-9 h, and then is followed by a relatively slow process. The equilibrium time is around 20 h.

Besides, the uptake of two methylated arsenic species on CTS-MG obviously exhibits electrolyte dependency. Arsenic removal is inhibited by increasing

concentration of NaClO<sub>4</sub>. Without influences of ionic strength, the sorption capacities for MMA and DMA are around 10.6 mg As/g and 2.7 mg As/g, respectively. When the concentration of NaClO<sub>4</sub> increases to 0.005 M, MMA removal sharply reduces 75 % and DMA sorption approaches to nearly zero. This behavior is an indication of outer-sphere sorption, which assumes the adsorbed ions are distributed at the same plane as the electrolyte ions and increasing solution ionic strength will suppress the removal of non-specifically adsorbed ions (Hayes et al., 1988; Zhang et al., 2007d). Similar trends have also been found for inorganic arsenic sorption onto CTS-MG and the shells of crab (Vijayaraghavan et al., 2009).

Another important finding in this study is that higher ionic strength slows the sorption rate and then extends the equilibrium time. Possible explanation for such negative observation is that the presence of a large amount of background electrolytes interrupts the transfer of adsorbates from bulk solution to the sorbent surface and also limits their accessibility to active sites (Hamdaoui et al., 2008). A similar observation was reported by Moreira that ionic strength led to a significant decrease in the diffusivity for sorption of amino acids with an anion-exchange resin (Moreira and Ferreira, 2005).

### **7.3 Effect of natural organic matter**

Natural organic matter (NOM) is generally present in groundwater, and could potentially affect arsenic species removal through competitive binding. Results for methylated arsenic sorption onto CTS-MG at different concentrations of humic acid

(HA) at pH 7.0 are shown in Figure 7.4.

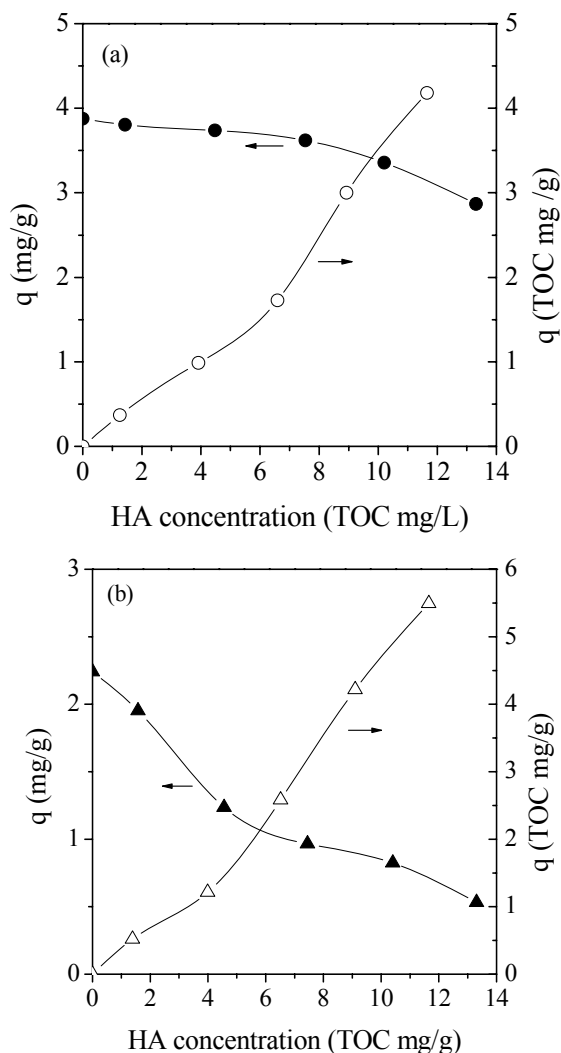


Figure 7.4. Effect of humic acid on the sorption of methylated arsenic: (a) MMA, (b) DMA (Experimental conditions:  $[As]_0 = 20$  mg/L,  $m = 1$  g/L, pH = 7,  $T = 293$  K, contact time = 3 d)

When humic substances are present in the solution, the sorption capabilities become lower for both MMA and DMA. The decrease for MMA sorption is less significant than that for DMA. The sorption amount for DMA reduces up to 76 % when TOC level increase to approximately 14 mg/L.



Figure 7.5. Images of CTS-MG before and after methylated arsenic sorption in the presence of NOM

Simultaneously, uptake of humic substances is observed in this study (Figure 7.4). When HA concentration increases to approximately 12 mg/L (TOC), the sorption capacities of NOM are 4.18 mg/g and 5.49 mg/g in MMA and DMA solution, respectively. Images in Figure 7.5 also show that in the presence of NOM, the color of CTS-MG becomes brown after arsenic sorption. Since humic substances are negatively charged, it can be attracted by positively charged surface of sorbent. Additionally, carboxyl and phenolic groups of HA also can interact with protonated amine functions to form organic complexes (Gu et al., 1994; Stumm et al., 1996; Chen et al., 2004). It can be said that direct competition for binding sites contributes to the decline of organic arsenic removal. HA influences on arsenic uptake increases in the sequence of inorganic As (V) < MMA < DMA. Such observation implies their descending affinities for CTS-MG: As (V) > MMA > DMA, which is consistent with pervious findings from isotherm study.

#### **7.4 Effect of coexisting anions**



***Chapter 7: Enhanced Sorption of Arsenic onto  
NMDG Modified Chitosan Sorbent (II): Methylated Arsenic***

---

Different coexisting anions are usually present in groundwater, which may lead to competitive sorption. Hence, it is important to investigate the potential interference of coexisting anions on the sorption of methylated arsenic. In this study, various concentrations of three common anions including fluoride, phosphate and sulfate were added to arsenic solutions at fixed pH 7.0 and their removal was studied.

As shown in Figure 7.6, at the same concentration level of these three anions, DMA uptake is hindered more remarkably than MMA. When sulfate content increases to 1 mM, arsenic removal capacity reduces nearly 75 % for MMA compared to the amount without addition of sulfate; and almost no sorption is observed for DMA. The degree of the uptake is dependent upon the binding strength of methylated arsenic species onto the sorbent. DMA has much lower affinity for CTS-MG than MMA, and therefore its sorption is hindered more by the coexisting anions.

Besides, among these three competitive anions, the extent of inhibition for arsenic removal demonstrates the following relative trend: sulfate > phosphate > fluoride. Similar adverse effects also have been previously found in inorganic arsenic sorption by CTS-MG as well as by a weak-base anion exchange fibrous sorbent (Awual et al., 2008; Deng et al., 2008). Possible reasons for this behavior might be that organic arsenic species is adsorbed on this polymeric sorbent to form outer-sphere complex through non-specific interaction; and divalent anions are generally preferred to be adsorbed compared to monovalent anions according to the electroselectivity (Awual et al., 2008).

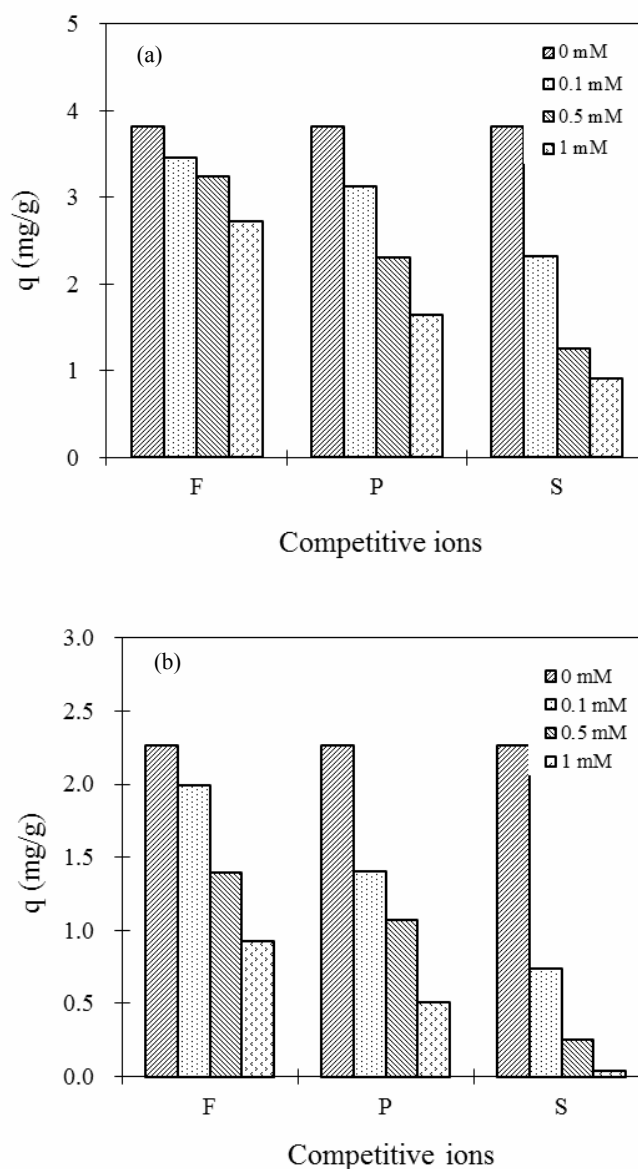


Figure 7.6. Competitive sorption of co-existing anions with methylated arsenic (Experimental conditions:  $[As]_0 = 20$  mg/L,  $m = 1$  g/L,  $pH = 7$ ,  $T = 293$  K, contact time = 3 d)

### 7.5 Spectroscopic analysis

High-resolution spectra of As3d of methylated As-loaded sorbents are illustrated in Figure 7.7, the As3d XPS spectrum at 45.5 eV corresponds to the characteristic

peak of As(V). It confirms the sorption of organic arsenic onto the sorbent. The valence of arsenic remains unchanged during the sorption.

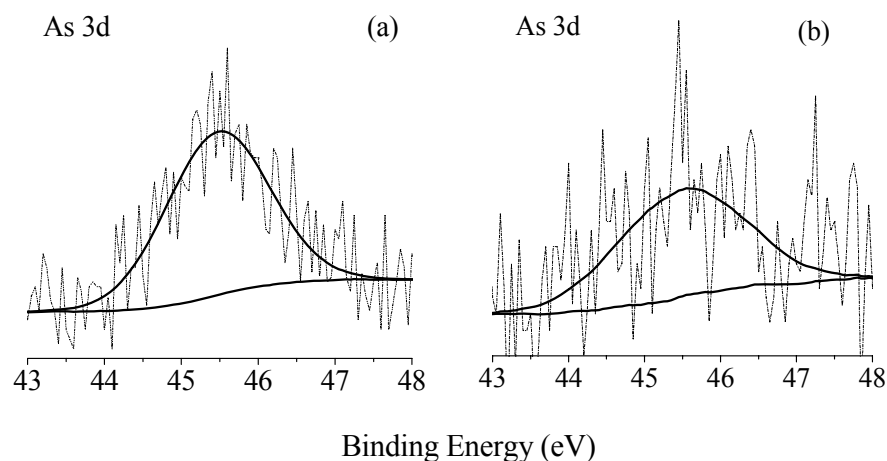


Figure 7.7. XPS (a) As3d core-level spectra of MMA-loaded sorbent, (b) As3d core-level spectra of DMA-loaded sorbent

The decomposition of N 1s spectra of pristine and As-loaded sorbents yields two individual component peaks in Figure 7.8. The peaks at binding energy of 399.0 eV and 401.8 eV can be assigned to the nitrogen atoms in neutral amine (-N) and protonated amine (-N<sup>+</sup>) groups. In comparison with the spectrum of pristine sorbent, the ratios of -N<sup>+</sup>/-N increases from 0.21 to 0.91 at pH 3.4 and 0.36 at pH 5 after MMA and DMA sorption, respectively. Increasing protonated amine groups possibly play an important role for methylated arsenic removal through electrostatic interaction.

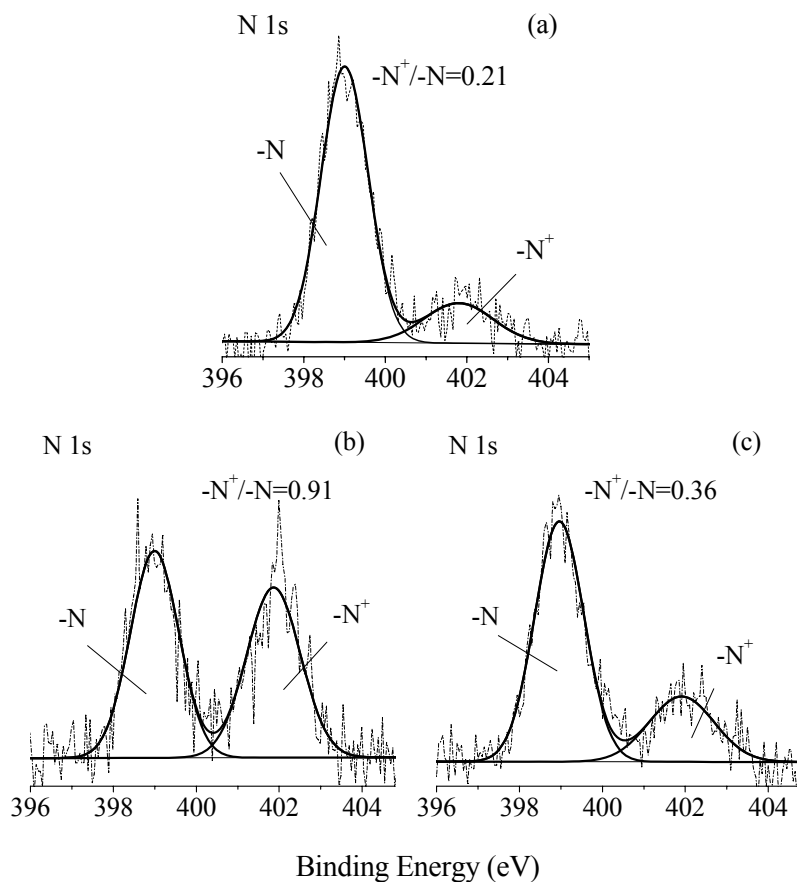


Figure 7.8. N1s core-level spectra of (a) pristine sorbent, (b) MMA-loaded sorbent, (s) DMA-loaded sorbent

### 7.6 Section summary

The present study reveals that MMA and DMA have similar sorption edges in the pH range of 2 to 11. Uptake of methylated arsenic by CTS-MG is pH-dependent and the maximum sorption occurs at acidic solutions. Under optimum pH conditions, the sorption capacities of CTS-MG are 15.396 mg/g for MMA and 7.134 mg/g for DMA, respectively. Surface modification of CCTS is beneficial for arsenic removal as the uptake of MMA by CCTS is only 5.933 mg/g, while almost no DMA sorption is observed. The affinity of different arsenic species to CTS-MG is found to decrease in

***Chapter 7: Enhanced Sorption of Arsenic onto  
NMDG Modified Chitosan Sorbent (II): Methylated Arsenic***

---

the order of inorganic As (V) > MMA > DMA. Substitution of hydroxyl groups with methyl groups makes different molecular geometries and spatial compatibility with surface sites; and thus results in different affinities of arsenic to CTS-MG. Kinetic study shows that equilibrium for MMA and DMA can be achieved within 20 h. The presence of background electrolytes causes a decline in sorption amount as well as extension of total equilibrium time. Coexistence of humic acid, fluoride, phosphate and sulfate inhibits organic arsenic sorption due to the competition for the binding sites. Spectroscopic analyses also confirm the successful uptake of methylated arsenic. Non-specific interaction between the anionic adsorbates and protonated surface sites should be mainly responsible for methylated arsenic removal.

## **CHAPTER 8**

### **FUNCTIONALIZATION OF REGENERATED CELLULOSE MEMBRANES FOR BORON REMOVAL**

In recent years, adsorptive membranes have been emerged as an alternative approach to remove contaminants from aqueous solution. This kind of membranes usually carries specific functional groups on the surfaces, which can reject the contaminants through a series of interaction such as charged neutralization, ion exchange or surface complexation. Therefore, even though the pore size of such membrane is much larger than the size of contaminants, it can still exhibit high retaining efficiency. To some extent, it is also favorable for increasing the permeate flux and meanwhile reducing the energy consumption.

Most research on boron has provided information that vicinal polyalcohol functions are the most efficient ligands for complexation of boron in aqueous solutions (Bicak et al., 2001; Geffen et al., 2006). According to this chemistry, our aim was to prepare a novel adsorptive membrane which possesses this kind of functionality for efficient boron removal.

Due to the presence of hydroxyl groups, regenerated cellulose (RC) membrane is considered to be a versatile platform for surface modification, which can endow the parent materials with desirable functions. Considerable work has been done to functionalize RC membrane surface via ATRP for different applications. For example,

Singh and coworkers prepared a polymeric membrane adsorber, by growing surface-tethered, charged polymer nanolayers from the surfaces of RC membranes. The prepared membranes exhibited high binding capability for lysozyme (Singh et al., 2008). A high-capacity weak anion-exchange membrane was also designed by Bhut and coauthors for protein separation through ATRP. It was found that the protein static sorption capacities increase with increasing polymerization time and finally achieve a plateau value of approximately 66 mg/mL (Bhut et al., 2008). Besides, a *p*-vinylbenzyl sulfobetaine was grafted from RC membranes by Liu and coworkers using ATRP for blood compatibility improvement, and the designed membranes showed improved resistance to nonspecific protein sorption and platelet adhesion (Liu et al., 2009b). However, there has been little research focusing on the surface-initiated ATRP to functionalize RC membranes for boron removal application.

In the present work, a novel adsorptive membrane was prepared by grafting PGMA to RC membranes via ATRP technique, and further ring-opening reactions with NMDG. The chemical functionality, wettability and physical morphology of the pristine and modified membranes were characterized by ATR-FTIR, XPS, WCA and SEM, respectively. Furthermore, the sorption performance as a function of pH, boron initial concentration and ionic strength was investigated. The sorption mechanism was finally studied by ATR-FTIR and XPS. The objective of this study was to obtain highly performed functional membrane and to better understand the underlying mechanism for boron removal.

### **8.1 Membrane surface modification**

Briefly, RC membranes were initially pretreated with methanol in order to remove glycerine; second, surface initiators RC-Br were anchored onto RC membranes through the interaction between surface hydroxyl groups and 2-bromoisobutyrate bromide; third, polymerization of GMA in the presence of ATRP catalyst, and the product is designated as RC-PGMA; finally, NMDG was used to open epoxide rings of the grafted PGMA to introduce the desirable functional groups for boron binding.

## **8.2 Surface characterization**

Surface properties of original membranes and modified membranes were characterized by ATR-FTIR and XPS to elucidate the synthetic reactions.

### **8.2.1 ATR-FTIR analysis**

Figure 8.1 presents typical ATR-FTIR spectra for unmodified RC membranes, RC-PGMA and RC-MG. For the pristine RC membranes (spectrum 8-2a), the broad peak located at  $3370\text{ cm}^{-1}$  is usually due to the -OH stretching vibration (Socrates, 2000). The spectrum also clearly shows the major peaks of the saccharide structure, which include asymmetric stretching of C-O-C at  $1159\text{ cm}^{-1}$  as well as skeletal vibration involving the C-O stretching at  $1062\text{ cm}^{-1}$  and  $1024\text{ cm}^{-1}$  (Liu et al., 2009b; Liu et al., 2010a). The band at  $896\text{ cm}^{-1}$  characterizes the amorphous regions of RC membranes (Cao and Tan, 2006; Liu et al., 2010b). Due to the low content of initiator in comparison to the substrates (RC membranes), characteristic peaks for RC-Br are not visible (data not shown).



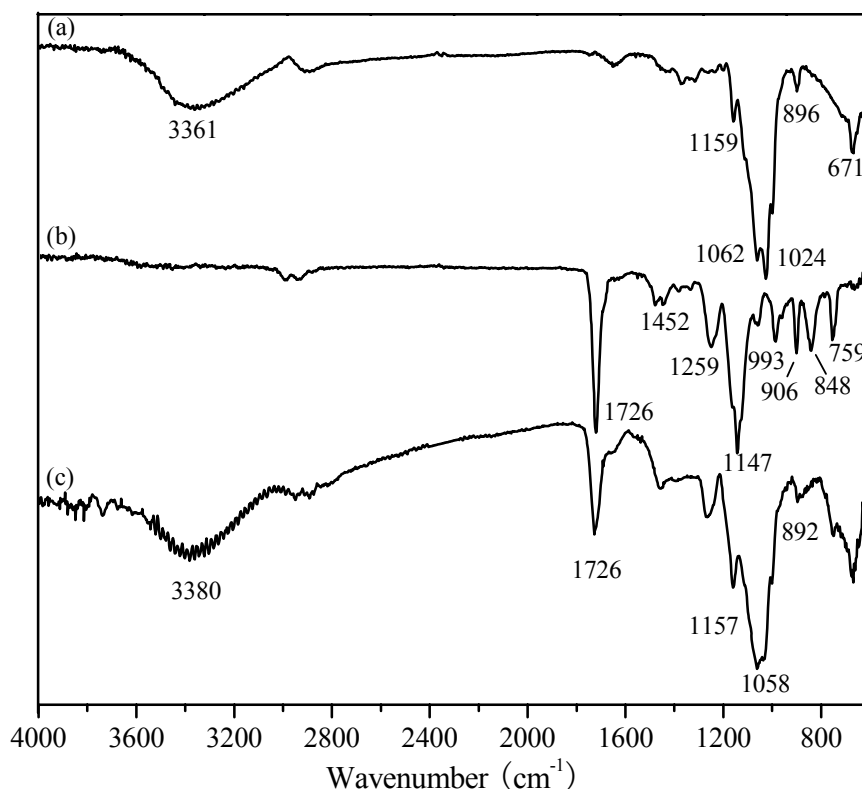


Figure 8.1. ATR-FTIR spectra of (a) RC, (b) RC-PGMA, (c) RC-MG

Following the polymerization, new peak appears at  $1726\text{ cm}^{-1}$  in the RC-PGMA (spectrum 8.1b) which is attributed to the ester  $\text{C}=\text{O}$  stretching vibrations in  $-\text{COO}-$  (Arica et al., 2008; Barringer et al., 2009). The vibration at  $1452\text{ cm}^{-1}$  corresponds to  $-\text{CH}_2$  scissoring band of PGMA (Arica et al., 2008). Three obvious characteristic bands of epoxide groups at  $906\text{ cm}^{-1}$ ,  $848\text{ cm}^{-1}$  and  $759\text{ cm}^{-1}$  are also found in the spectrum (Chan and Gleason, 2005; Ma et al., 2005). Meanwhile, the intensity of hydroxyl characteristic peak at  $3300\text{--}3400\text{ cm}^{-1}$  for RC membranes greatly decreases, which can be explained in two ways. On the one hand, hydroxyl groups are involved in the polymerization; on the other hand, the surface of membrane is covered by a layer of PGMA after polymerization; and both can result in the decreasing intensity of

## *Chapter 8: Functionalization of Regenerated Cellulose Membrane for Boron Removal*

---

-OH. All the above-mentioned changes of spectra support the successful grafting of PGMA from the surface of RC membranes.

Compared spectra 8.1c with spectra 8.1b, it can be found that three typical characteristic peaks for epoxide groups disappears after further functionalization with NMDG, implying the successful conversation of epoxide groups. In addition, new peaks appear at  $1058\text{ cm}^{-1}$  and  $3377\text{ cm}^{-1}$ , which is assigned to the amine C-N stretching vibrations and -OH stretching vibrations, respectively (Socrates, 2000). These results provide evidence for the successful ring-opening reactions to introduce polyhydroxyl and tertiary amine functional groups.

### **8.2.2 XPS analysis**

XPS analysis has been used to characterize the surface composition variations of the pristine and modified RC membrane surfaces qualitatively as well as quantitatively. Table 8.1 summarizes the elemental compositions measured from XPS scans on different surfaces.

Table 8.1 Elemental surface composition of pristine and modified RC membranes determined from XPS

Sample	Element (atom %)			
	C	O	N	Br
RC	55.4	44.6	--	--
RC-Br	57.8	41.6	--	0.6
RC-PGMA	70.2	29.8	--	--
RC-MG	62.9	33.2	3.9	--

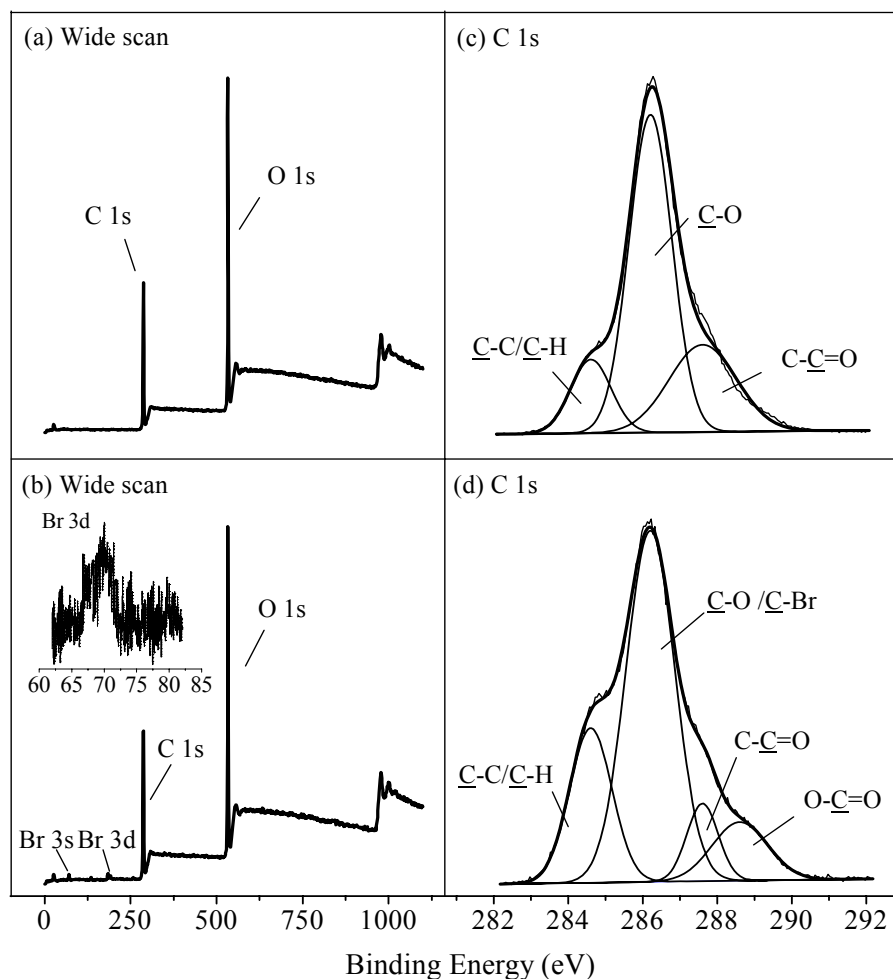


Figure 8.2. XPS spectra of RC (a and c) and RC-Br (b and d)

As shown, after surface initiated reaction, the content of carbon (C 1s) is slightly increased, while the content of oxygen (O 1s) is slightly decreased. Simultaneously, a small amount of bromine (Br 3d, 0.6 %) appeared with a binding energy of around 70 eV (Figure 8.2b) (Pan et al., 2010b).

As for the narrow scan of C 1s in Figure 8.2c and 8.2d, the spectrum of RC and RC-Br can be deconvoluted into three individual component peaks, which come from different groups and overlap each other. The peaks of RC at 284.6, 286.2 and 287.6

## *Chapter 8: Functionalization of Regenerated Cellulose Membrane for Boron Removal*

---

eV, are mainly attributed to  $\underline{\text{C}}\text{-C}/\underline{\text{C}}\text{-H}$ ,  $\underline{\text{C}}\text{-O}$  and  $\text{C-}\underline{\text{C}}\text{=O}$  species, while peaks of RC-Br at 284.6, 286.2, 287.6 and 288.6 eV, can be assigned to  $\underline{\text{C}}\text{-C}/\underline{\text{C}}\text{-H}$ ,  $\underline{\text{C}}\text{-O}$ ,  $\text{C-}\underline{\text{C}}\text{=O}$  and  $\text{O-}\underline{\text{C}}\text{=O}$  groups (Liu et al., 2010a). It is clear that a new peak at 288.6 eV appears in the C 1s of RC-Br. In addition, the content of  $\underline{\text{C}}\text{-C} / \underline{\text{C}}\text{-H}$  species on the CM-Br is obviously higher than that on the pristine RC (22.3 % versus 13.3 %) in Table 8.2. This is because 2-BIB has no  $\underline{\text{C}}\text{-O}$  species but several  $\underline{\text{C}}\text{-C}/\underline{\text{C}}\text{-H}$  species in its structure, and the immobilization of the initiator increases the content of  $\underline{\text{C}}\text{-C}/\underline{\text{C}}\text{-H}$  species and decreases the content of  $\underline{\text{C}}\text{-O}$  species (Liu et al., 2009b). All these changes indicate that the initiator has been successfully anchored on the membrane surface.

After ATRP reaction, the quantity of carbon increases whereas that of oxygen greatly decreases. According to the data in Table 8.1, the C/O atomic ratio is approximately 7:3 (70.2 %: 29.8 %), which agrees well with the corresponding theoretical ratio in GMA. Furthermore, fairly good agreement is also obtained for the  $[\underline{\text{C}}\text{-C}/\underline{\text{C}}\text{-H}]: [\underline{\text{C}}\text{-O}]: [\text{O-}\underline{\text{C}}\text{=O}]$  ratio, which is determined to be 3.2: 3.1: 1 (44.3 %: 42.2 %: 13.5 %) (Table 8.2). The reasonable ratio thus suggests that RC membranes are possibly covered by the grafted PGMA layer.

**Chapter 8: Functionalization of Regenerated Cellulose Membrane  
for Boron Removal**

Table 8.2 Binding energy and relative content of C in pristine and modified RC membranes

Proposed components	Binding energy (eV)	Relative content (%)			
		RC	RC-Br	RC-PGMA	RC-MG
<u>C</u> -C / <u>C</u> -H	284.6	13.3	22.3	44.3	25.7
<u>C</u> -N	285.5	--	--	--	16.9
<u>C</u> -O	286.2	60.7	58.3	42.2	48.6
C- <u>C</u> =O	287.6	26.1	8.3	--	--
O- <u>C</u> =O	288.6	--	11.1	13.5	8.8

With further NMDG functionalization, the content of oxygen remarkably increases to 33.2 %; and the nitrogen content on the surface of RC-MG increases up to 3.9 % while that of RC-PGMA is zero (Table 8.1). Figure 8.3b and 8.3d demonstrates the wide scan and C 1s narrow scan of RC-MG. In comparison with the spectra of RC-PGMA, a new signal of N 1s appears, which originates from amine groups in NMDG. Besides, a new peak component at 288.6 eV, attributed to C-N species, appears in the narrow scan of C 1s in RC-MG (Liu et al., 2010a). The XPS analyses are hence consistent with the ATR-FTIR results and confirm the successful grafting of polyhydroxyl and tertiary amine groups onto RC membranes.

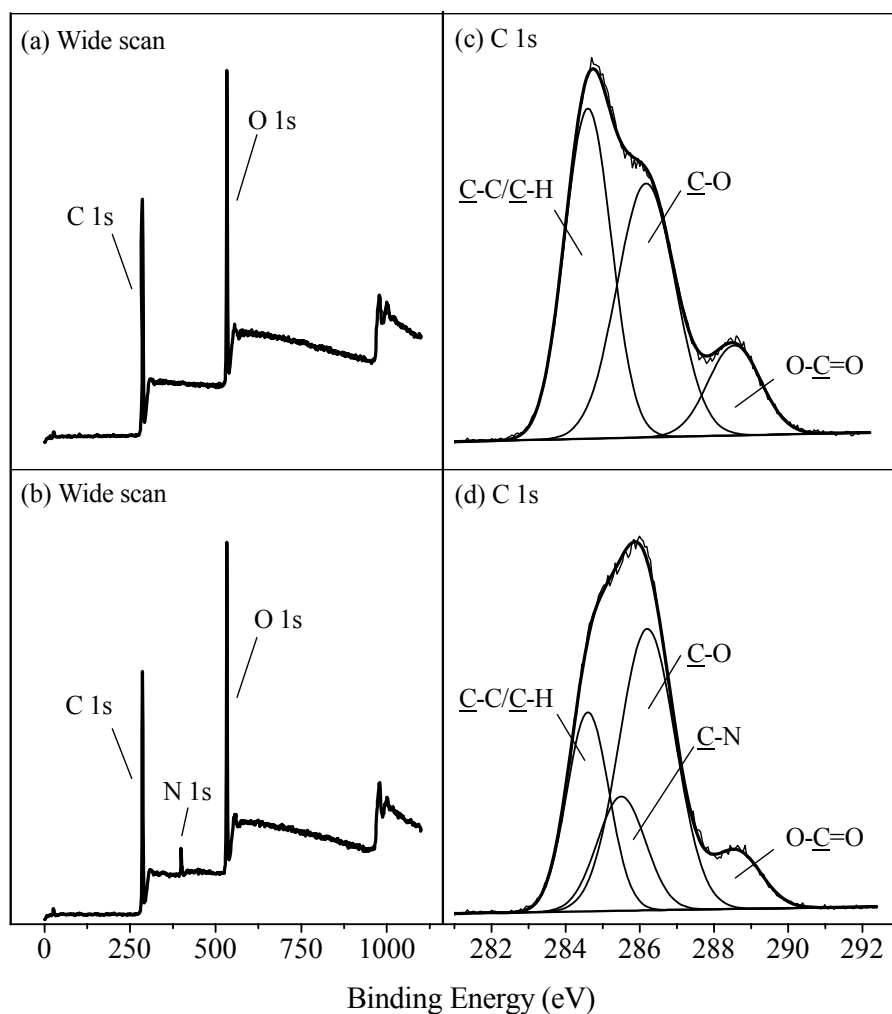


Figure 8.3. XPS spectra of RC-PGMA (a and c) and RC-MG (b and d)

### 8.2.3 Water contact angle analysis

The relative hydrophilicity or hydrophobicity for four surfaces was investigated with a dynamic mode. Figure 8.4 plots the curves of water contact angle as a function of drop age.

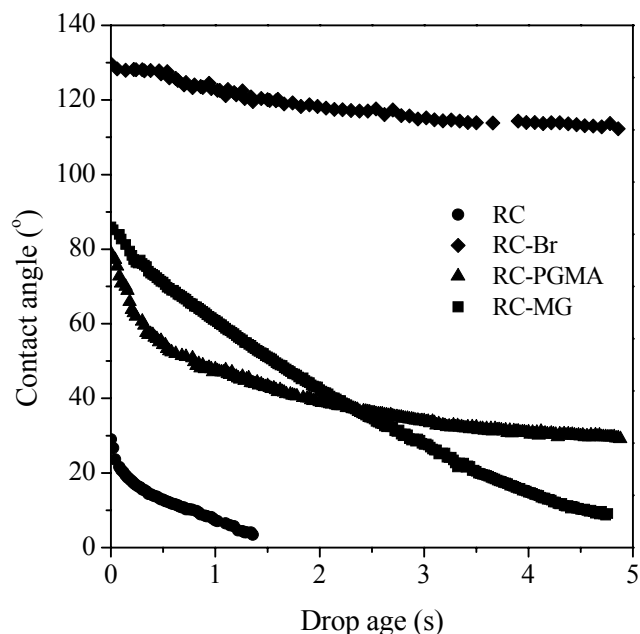


Figure 8.4. Water contact angle versus drop age for pristine and modified RC membranes

As can be seen, due to the presence of massive hydrophilic functional groups in pristine RC membrane, its initial water contact angle is very low and quickly decreases to about  $4^{\circ}$  within 1.3 s. After the anchoring of initiator, the initial water contact angle of RC-Br sharply increases to  $130^{\circ}$ , and the decrease of contact angle with drop age is very slow. These changes imply a transformation from hydrophilic to hydrophobic of membrane surfaces, which is due to the immobilization of hydrophobic initiator.

However, after the ATRP reaction, it can be found that the initial contact angle of these grafted surfaces (RC-PGMA) becomes smaller, and finally declines to nearly  $30^{\circ}$ . With further ring-opening reaction, compared to RC-Br, the attenuation of contact angle with drop age for RC-MG is much faster, which decrease to only  $9^{\circ}$

after 5 s. Such tendency suggests that despite high hydrophobicity of the surface initiators, the containing of hydrophilic hydroxyl groups still brings hydrophilicity to the RC-MG membrane.

#### **8.2.4 Surface morphology of membranes**

Figure 8.5 shows the SEM images of the top and cross-sectional views for pristine and modified RC membranes at different magnification. Compared the top views in Figure 8.5(a-b) with Figure 8.5(e-f), different surface morphology is clearly observed between the virgin and grafted RC substrates. A relatively dense layer forms on the RC membrane surface by grafting NMDG, and less porous structure is observed, which is possibly because the grafted polymer fills the pore spaces of RC membranes (Pan et al., 2010a). Besides, the cross-sectional views in Figure 8.5(c-d) and 8.5 (g-h) show that the thickness of membranes increases significantly after chemical modification. The polymer is grafted from both the membrane outer surface and the pore surfaces within the bulk of the membranes.

The variation in surface structures would affect the flux of membranes. However, due to its nature of controllability in degree of polymerization, the ATRP technique can be used to effectively control the pore sizes and thickness of the prepared membranes in order to achieve the desired performance.



*Chapter 8: Functionalization of Regenerated Cellulose Membrane for Boron Removal*

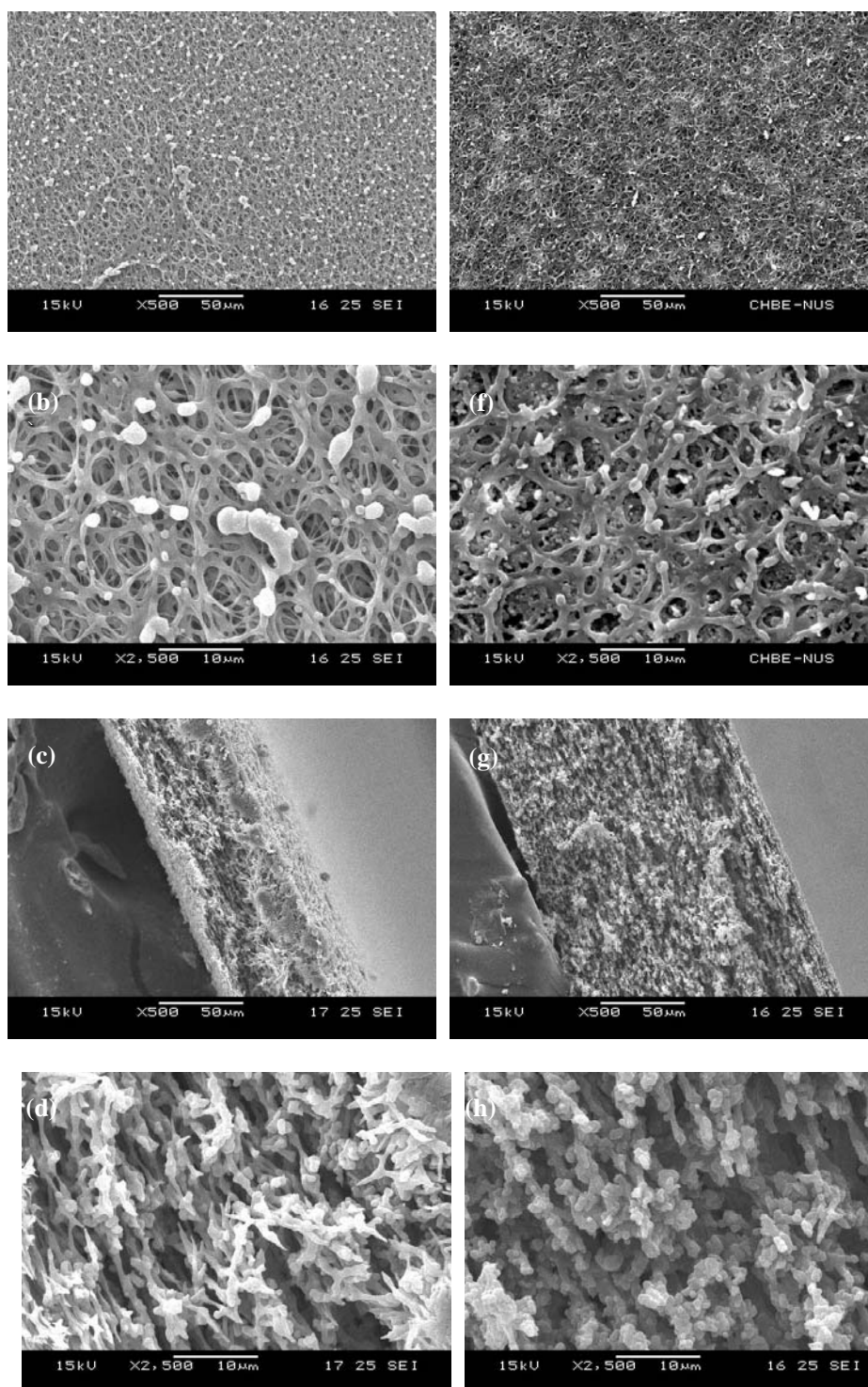


Figure 8.5. SEM images of the top and cross-sectional views of RC (images a-d) and RC-MG membranes (images e-h)

### **8.3 Boron sorption**

#### **8.3.1 Effect of pH**

Figure 8.6 shows the effect of pH on boron sorption. The modified membranes can efficiently remove boron from aqueous solution over a wide range of pH. The sorption capacity of approximately 0.5 mmol/g is maintained between initial pH 4 to 8. Boron uptake starts to decrease from pH 9, and drops over 50 % when pH increases to 11.

It has been reported that below total concentration of 25 mmol boron, the major species would be only  $\text{H}_3\text{BO}_3$  and  $\text{B}(\text{OH})_4^-$  without polyansonic species (Choi and Chen, 1979). When pH is below 8, the neutral forms of boron are mainly present in solution ( $K=5.8 \times 10^{-10}$ ,  $\text{pK}_a = 9.2$  at 25 °C) (Adams, 1964). Boric acid can be adsorbed onto RC-MG through forming complexation with surface functional groups -OH and simultaneously releasing  $\text{H}_2\text{O}$  and/or  $\text{H}^+$  (Su and Suarez, 1995; Simonnot et al., 2000). At higher pH values (e.g.  $\text{pH} > 9$ ), borate anions become the predominant forms. Direct competition between the hydroxyl ions and borate ions results in less boron removal. This observation is consistent with the finding reported by Wang and coworkers (Wang et al., 2007).

It can be found that pH changes during sorption are not very obvious. The equilibrium pH increases a bit in acidic region, which is possibly due to the protonation of tertiary amine and hydroxyl groups on the surface of RC-MG. The optimal pH within a wide range plays an important role for actual application. It

means no pH adjustment is necessary as the majority of water supplies usually have a range of 6.5-8.5.

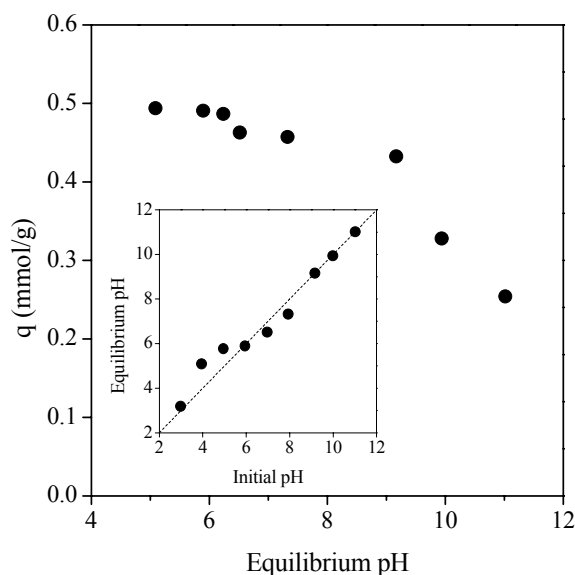


Figure 8.6. Effect of pH on the boron removal by RC-MG (Experimental conditions:  $[B]_0 = 0.46$  mM,  $m = 0.50$  g/L,  $T = 293$  K, contact time = 7 d)

### 8.3.2 Sorption isotherm

Figure 8.7 illustrates the sorption isotherms of pristine and modified membranes. As shown, the sorption capacity of RC can be negligible, whereas RC-MG exhibits a much higher uptake of boron. In other words, surface modification definitely increases the boron removal capability. Direct graphic maximal sorption capacity (corresponding to the isotherm plateau) is determined to be 0.75 mmol/g for RC-MG, which is comparable with those of commercial resins, such as Amberlite IRA 743.

Both Langmuir and Freundlich isotherms described in Chapter 2, were used to analyze the experimental data of RC-MG (only Freundlich type provided). It is found

that Freundlich model is more suitable for describing the sorption behavior of RC-MG, which is possibly due to the heterogeneity of modified membrane surfaces.

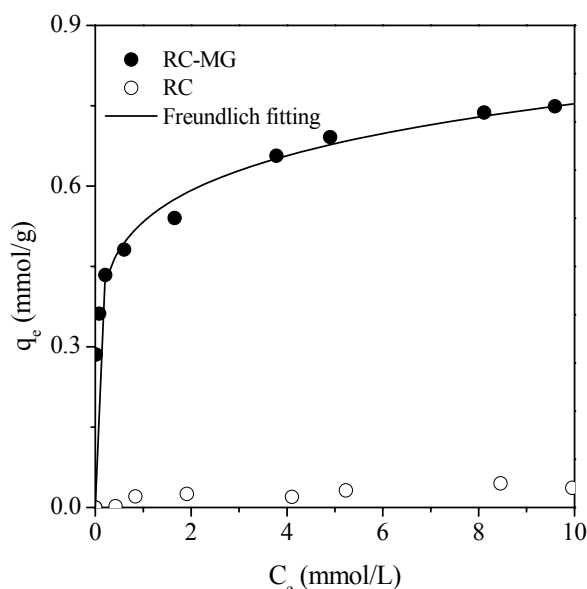


Figure 8.7. Sorption isotherms of boron removal by pristine and modified RC membranes (Experimental conditions: pH = 7,  $m = 0.5$  g/L,  $T = 293$  K, contact time = 7 d)

### 8.3.3 Ionic strength effect

The effect of ionic strength on boron sorption is indicated in Figure 8.8. Ionic strength was varied for two orders of magnitude, from 1 mM to 100 mM  $\text{NaClO}_4$ . As can be seen, the sorption peak is found at pH 6 in the presence of 1 mM  $\text{NaClO}_4$ , but increase in ionic strength leads to a shift in the position of pH edge towards the alkaline region (pH 7 to 8). Besides, at low pH values, boron sorption slightly decreases with increasing ionic strength, while the effect of ionic strength is reversed in the high pH regions. At low pH, the surface is usually positively charged; increasing ionic strength causes decrease of the potential in the plane of sorption and

thus less boron removal; at high pH, increase of ionic strength can provide more cations (e.g.,  $\text{Na}^+$ ) near the negatively charged surface, which are able to increase the potential in the plane of sorption (Goldberg et al., 1993). It is favorable for borate anions uptake and leads to a greater removal. A similar phenomenon was observed by Sabine Goldberg and coworkers, when they studied the sorption of boron on oxides and clays (Goldberg et al., 1993).

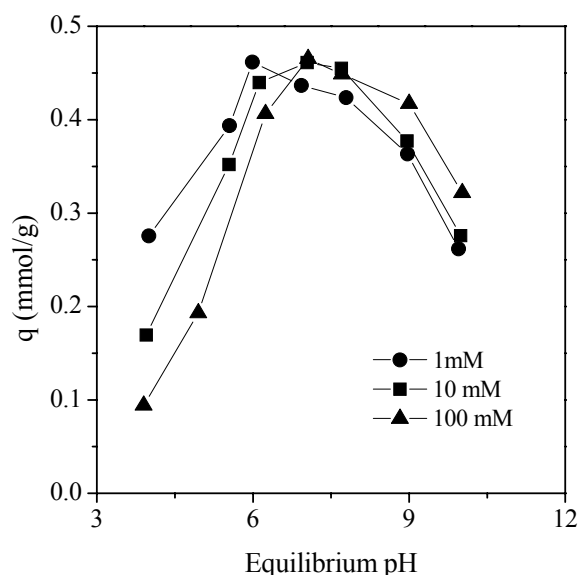


Figure 8.8. Boron sorption as a function of pH and ionic strength in  $\text{NaClO}_4$  solution

Generally, sorption by forming outer-sphere complexes is weakly bonded and highly dependent on ionic strength, since the background electrolyte anions such as  $\text{ClO}_4^-$  also form outer-sphere complexes via charged interaction and directly compete with adsorbed ions for surface binding sites. Conversely, in an inner sphere complex, the sorption shows little sensitivity to ionic strength or responds to higher ionic strength with greater sorption (McBride, 1997). As a consequence, the results imply

that boron may form inner-sphere complexes at the water/solid interface.

#### 8.4 Mechanism study

Figure 8.9 shows the ATR-FTIR spectra of RC-MG before and after boron sorption.

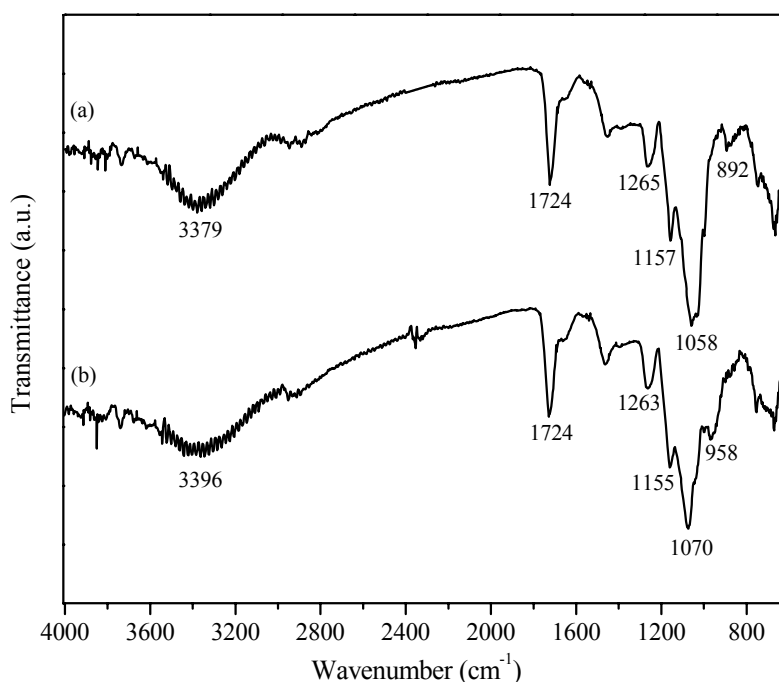


Figure 8.9. ATR-FTIR spectra of RC-MG membranes before and after boron sorption

As shown in spectrum 8.9a, the peak at 892 cm<sup>-1</sup> is attributed to the C-O stretching vibration which originates from secondary alcohols (-CHOH) (Socrates, 2000). After boron sorption (spectrum 8.9b), most observable is that the peak at 892 cm<sup>-1</sup> greatly diminishes, and meanwhile a new peak appears at 958 cm<sup>-1</sup>, assigned to the tetrahedral B asymmetric stretching band (Su and Suarez, 1995; Peak et al., 2003). Besides, a minor peak shift can be found for both -OH and -CN bonds, which shift

from  $3380\text{ cm}^{-1}$  to  $3396\text{ cm}^{-1}$  and from  $1058\text{ cm}^{-1}$  to  $1070\text{ cm}^{-1}$ , respectively. The ATR-FTIR spectra confirm that both polyhydroxyl and tertiary amine groups are involved for boron sorption, and boron is successfully attached to the membrane surface by formation of tetrahedral complexes. XPS analysis also verifies the successful attachment of boron species onto the modified membranes (Figure 8.10).

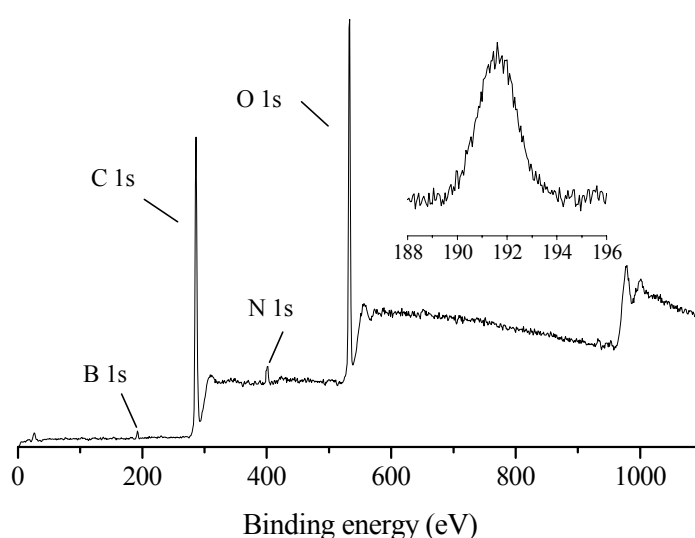


Figure 8.10. XPS spectra of boron-loaded membranes

### 8.5 Section summary

A three-step surface modification of RC membranes involving surface polymerization has been conducted to develop a novel functional membrane with high boron binding capability. The ATR-FTIR and XPS analyses confirm the successful anchoring of surface initiator, grafting of PGMA polymers onto RC membranes as well as further functionalization by NMDG. Dynamic contact angle measurements demonstrate the hydrophilicity of the prepared membranes. SEM

## ***Chapter 8: Functionalization of Regenerated Cellulose Membrane for Boron Removal***

---

observations illustrate that surface modification slightly decreases the porous structure and increases the thickness of membranes. In return, modified membranes show much higher binding capacity for boron relative to pristine RC membranes; and are also comparable with commercially available resins. The optimal initial pH for boron uptake falls in wide range of 4-8; and the maximum sorption capacity achieved is about 0.75 mmol/g at neutral condition. Effect of ionic strength implies that boron may form inner-sphere surface complexes at the water/solid interface. The ATR-FTIR study reveals that polyhydroxyl and tertiary amine groups are mainly responsible for boron removal; tetrahedral boron complex is finally present on the modified membrane surface. XPS also verifies the successful attachment of boron. Therefore, the prepared membrane would have great potential as a novel separation material for boron removal from aqueous solution.



## CHAPTER 9

### CONCLUSIONS AND RECOMMENDATIONS

#### 9.1 Conclusions

The primary objective of this study was to provide an alternative solution for boron and arsenic removal. In order to accomplish this main aim, a range of novel separation materials were designed and synthesized including chitosan-based polymeric sorbent (CTS-MG) and cellulose-based adsorptive membrane (RC-MG). It was found that PGMA is successfully grafted onto the chitosan substrates via surface polymerization technique at room temperature; the desired polyhydroxyl and tertiary amine groups are further obtained through ring-opening reactions. The polymeric sorbent has a mean diameter of 0.6  $\mu\text{m}$ , specific surface area of 16.669  $\text{m}^2/\text{g}$  and  $\text{pH}_{\text{zpc}}$  of 7.8. Compared to unmodified crosslinked chitosan, this sorbent has a rough surface and relatively porous structure. The changes of surface morphology are attributed to chemical modification. Moreover, the surface charges of the sorbent decrease with an increase of pH. The finding is consistent with the observations reported by (Lim et al., 2008).

Equilibrium experiments show that pH changes during boron sorption by CTS-MG are not very significant and the optimal sorption is achieved at initial pH 7. Increasing pH leads to rising sorption capacity under acidic region, whereas decrease of boron removal is observed under alkaline condition. The reason is that boron sorption

is mainly controlled by several factors such as boron speciation, protonation or deprotonation of surface functional groups, as well as complexation reactions. Furthermore, boron removal capability is significantly enhanced after chemical modification. CTS-MG exhibits a considerably high sorption capacity of 2.84 mmol/g, which is much higher than those of commercial resin Amberlite IRA-743 and most sorbents previously reported. These findings are of crucial importance in terms of practical application for boron removal. On one hand, high sorption capability and selectivity are appealing aspects to end-users. On the other hand, the optimal removal at neutral pH makes the sorbent applicable in the majority of water supplies without pH adjustment; slight changes of pH during sorption can avoid further pH balancing at the post-treatment as well.

Kinetic studies demonstrate that up to 90 % of boron is removed within 8 hours and the sorption kinetics is well described by an intraparticle surface diffusion model. The presence of background electrolytes such as sodium chloride and sodium nitrate does not affect boron removal, suggesting formation of inner-sphere surface complexes on the sorbent. It is in good agreement with the findings reported by Goldberg et al. (1993, 2005). Boron removal from simulated seawater was also conducted to investigate the potential efficiency of CTS-MG for natural water bodies. At dose of 1.2 g/L, boron removal efficiency is as high as 90 % and boron level in the effluent is below 0.5 mg/L. If substituting a second stage RO with the sorption unit, the dose of sorbent can be reduced to about 0.3 g/L. As such, the overall capital, operational cost and low recovery problems can be significantly reduced in comparison with an “all RO” strategy.

Boron sorption chemistry was analyzed by FT-IR and XPS studies. The appearance of B-O bonds in the FT-IR spectrum indicates the successful attachment of boron to the sorbent. It was found that secondary alcohols (-CHOH) and tertiary amine (-CN) groups of CTS-MG play an important role in boron binding. Boric acid initially attaches to polyhydroxyl functional groups and bound water through Lewis acid/base pairing, which continues to be stabilized by hydrogen bonding. A proton or water is then released, and trigonal boric acid is converted to tetrahedral boron complexes on the surface of sorbent.

Effects of different experimental parameters, namely solution pH, initial arsenic concentration, contact time, ionic strength, natural organic matter (NOM), and competitive anions were carried out in order to investigate sorption behaviors of both inorganic and organic arsenic onto the polymeric sorbent. Batch experiments show that arsenate and methylated arsenic sorption are pH dependent and have similar sorption edges in the pH range of 2 to 11. The maximum sorption capacities of arsenic are 69.3 mg/g for arsenate (pH 3), 15.4 mg/g for MMA (pH 3.4) and 7.1 mg/g for DMA (pH 5), respectively. This sorbent outperforms the unmodified chitosan in terms of both sorption capacity and affinity for arsenic. It was found that the affinity of different arsenic species to CTS-MG decreases in the order of inorganic As (V) > MMA > DMA. It is likely that substitution of hydroxyl groups with methyl groups makes different molecular geometries and spatial compatibility with surface sites; and thus results in such discrepancy. Moreover, the sorption equilibrium can be reached within 16 hours for arsenate and 20 hours for organic arsenic species, respectively. As for inorganic arsenic, modeling sorption kinetics by intraparticle diffusion model is

successfully conducted where the equilibrium relationship is based on Freundlich equation. It was found that the sorption process is mainly controlled by surface diffusion, while external mass transfer is less critical. Existence of background electrolytes as sodium perchlorate not only greatly affects the sorption amount, but also retards the transfer rate of arsenate and methylated arsenic onto the surface of sorbent. Such strong ionic strength dependence indicates the formation of outer-sphere surface complexes on CTS-MG.

Coexistence of natural organic matter is found to compete with arsenic for binding sites. Such direct competition is possibly due to the interaction of HA with protonated amine or hydroxyl functions include electrostatic attraction, organic complexes formation or ligand exchange reaction. During competitive studies, effects of three anions on arsenate uptake exhibit the following descending sequence of: sulfate > phosphate > fluoride, which is similar to the observation reported by Awual et al. (2008). Possible reasons for this behavior can be that arsenic species is adsorbed on this polymeric sorbent to form outer-sphere complex through electrostatic interaction or ion exchange; divalent anions are usually preferred to be adsorbed compared to monovalent anions according to the electroselectivity. In addition, the FT-IR and XPS studies show that both tertiary amine and hydroxyl functional groups in CTS-MG are involved in arsenic sorption. Non-specific interactions are mainly responsible for both inorganic and organic removal.

A novel adsorptive membrane RC-MG with high boron binding capability was also successfully prepared by ATRP method and NMDG further functionalization. SEM observations reveal that RC membrane is covered by a dense layer with little

porosity, which is possibly due to the filling of pore spaces by the grafted polymer (Pan et al., 2010a) Surface modification contributes to higher boron binding capability. At neutral pH, the maximum sorption capacity of boron is 0.75 mmol/g, which is comparable with those of commercial resins, such as Amberlite IRA 743. Studies of ionic strength show that at low pH regions, boron sorption slightly decreases with increasing ionic strength, while the effect of ionic strength is reversed in the high pH values. It is in agreement with the observation reported by Sabine Goldberg et al. (2003) when they studied the sorption of boron on oxides and clays. This finding suggests that boron may form inner-sphere surface complexes at the water/solid interface. Both ATR-FTIR and XPS analyses confirm the successful attachment of boron. Both hydroxyl and amine functionalities are involved in boron removal by RC-MG.

## **9.2 Recommendations**

Based on the investigations and findings of this study, a few recommendations are proposed below for future work:

1. In laboratory scale experimental studies, these two separation materials have demonstrated its good capability for boron and arsenic removal. Application of these materials in column / filtration studies as well as its regeneration would be of practical importance.
2. In this present study, chitosan-based polymeric sorbent exhibits high sorption capacity for both inorganic and organic arsenic species; however, it does not show

specific selectivity toward arsenic as competition from background ions can greatly affect arsenic removal. To address this issue, metal or its compounds can be incorporated into this material due to their high affinity towards arsenic.

3. Although Langmuir and Freundlich isotherm equations provide good fitting results for experimental data, these models are “mathematical functions” and hardly reflect the actual sorption mechanism. Actually, mathematical modeling of sorption is a great challenge due to the highly complex sorption system. Therefore, development of new sorption models based on ion exchange, surface complex formation should provide more scientific understanding of the process.

## REFERENCES

Anirudhan, T.S., Rijith, S., Tharun, A.R. 2010. Adsorptive removal of thorium(IV) from aqueous solutions using poly(methacrylic acid)-grafted chitosan/bentonite composite matrix: Process design and equilibrium studies. *Colloids and Surfaces A: Physicochemical and Engineering Aspects* 368, 13-22.

Adams, R.M.e., 1964. Boron, metallo-boron compounds, and boranes. Interscience Publishers, New York.

Ahmad, S., Anderson, W.L., Kitchin, K.T., 1999. Dimethylarsinic acid effects on DNA damage and oxidative stress related biochemical parameters in B6C3F1 mice. *Cancer Letters* 139, 129-135.

Alexandratos, S.D., 2007. New polymer-supported ion-complexing agents: Design, preparation and metal ion affinities of immobilized ligands. *Journal of Hazardous Materials* 139, 467-470.

Altundogan, H.S., Tumen, F., 2003. As(V) removal from aqueous solutions by coagulation with liquid phase of red mud. *Journal of Environmental Science and Health Part a-Toxic/Hazardous Substances & Environmental Engineering* 38, 1247-1258.

Amin, M.N., Kaneco, S., Kitagawa, T., Begum, A., Katsumata, H., Suzuki, T., Ohta, K., 2006. Removal of arsenic in aqueous solutions by adsorption onto waste rice husk. *Industrial & Engineering Chemistry Research* 45, 8105-8110.

Andreae, M.O., 1980. Arsenic in Rain and the Atmospheric Mass Balance of Arsenic. *Journal of Geophysical Research-Oceans and Atmospheres* 85, 4512-4518.

Argust, P., 1998. Distribution of boron in the environment. *Biological Trace Element Research* 66, 131-143.

Arica, M.Y., Akyol, A.B., Bayramoglu, G., 2008. Adsorption of trypsin onto magnetic ion-exchange beads of poly(glycidylmethacrylate-co-ethyleneglycoldimethacrylate). *Journal of Applied Polymer Science* 107, 2810-2819.

- Arnold, L.L., Eldan, M., Nyska, A., van Gemert, M., Cohen, S.M., 2006. Dimethylarsinic acid: Results of chronic toxicity/oncogenicity studies in F344 rats and in B6C3F1 mice. *Toxicology* 223, 82-100.
- Awual, M.R., Urata, S., Jyo, A., Tamada, M., Katakai, A., 2008. Arsenate removal from water by a weak-base anion exchange fibrous adsorbent. *Water Research* 42, 689-696.
- Banasiak, L.J., Schafer, A.I., 2009. Removal of boron, fluoride and nitrate by electrodialysis in the presence of organic matter. *Journal of Membrane Science* 334, 101-109.
- Barringer, J.E., Messman, J.M., Banaszek, A.L., Meyer, H.M., Kilbey, S.M., 2009. Immobilization of biomolecules on poly(vinylidimethylazlactone)-containing surface scaffolds. *Langmuir* 25, 262-268.
- Basha, C.A., Selvi, S.J., Ramasamy, E., Chellammal, S., 2008. Removal of arsenic and sulphate from the copper smelting industrial effluent. *Chemical Engineering Journal* 141, 89-98.
- Bayramoglu, G., Yavuz, E., Senkal, B.F., Arica, M.Y., 2009. Glycidyl methacrylate grafted on p(VBC) beads by SI-ATRP technique: Modified with hydrazine as a salt resistance ligand for adsorption of invertase. *Colloids and Surfaces a-Physicochemical and Engineering Aspects* 345, 127-134.
- Bednar, A.J., Garbarino, J.R., Ranville, J.F., Wildeman, T.R., 2002. Presence of organoarsenicals used in cotton production in agricultural water and soil of the southern United States. *Journal of Agricultural and Food Chemistry* 50, 7340-7344.
- Bektas, N., Oncel, S., Akbulut, H.Y., Dimoglo, A., 2004. Removal of boron by electrocoagulation. *Environmental Chemistry Letters* 2, 51-54.
- Bencko, V., 1977. Carcinogenic, Teratogenic, and Mutagenic Effects of Arsenic. *Environmental Health Perspectives* 19, 179-182.
- Bhakat, P.B., Gupta, A.K., Ayoob, S., Kundu, S., 2006. Investigations on arsenic(V) removal by modified calcined bauxite. *Colloids and Surfaces a-Physicochemical and Engineering Aspects* 281, 237-245.



Bhut, B.V., Wickramasinghe, S.R., Husson, S.M., 2008. Preparation of high-capacity, weak anion-exchange membranes for protein separations using surface-initiated atom transfer radical polymerization. *Journal of Membrane Science* 325, 176-183.

Bicak, N., Bulutcu, N., Senkal, B.F., Gazi, M., 2001. Modification of crosslinked glycidyl methacrylate-based polymers for boron-specific column extraction. *Reactive & Functional Polymers* 47, 175-184.

Bicak, N., Gazi, M., Bulutcu, N., 2003. N,N-bis(2,3-dihydroxypropyl) octadecylamine for liquid-liquid extraction of boric acid. *Separation Science and Technology* 38, 165-177.

Bicak, N., Ozbelge, H.O., Yilmaz, L., Senkal, B.F., 2000. Crosslinked polymer gels for boron extraction derived from N-glucidol-N-methyl-2-hydroxypropyl methacrylate. *Macromolecular Chemistry & Physics* 201, 577-584.

Bicak, N., Senkal, B.F., 1998. Sorbitol-modified poly(N-glycidyl styrene sulfonamide) for removal of boron. *Journal of Applied Polymer Science* 68, 2113-2119.

Biswas, B.K., Inoue, K., Ghimire, K.N., Kawakita, H., Ohto, K., Harada, H., 2008. Effective removal of arsenic with lanthanum(III)- and cerium(III)-loaded orange waste gels. *Separation Science and Technology* 43, 2144-2165.

Borah, D., Satokawa, S., Kato, S., Kojima, T., 2008. Surface-modified carbon black for As(V) removal. *Journal of Colloid and Interface Science* 319, 53-62.

Brunauer, S., Emmett, P.H., Teller, E., 1938. Adsorption of gases in multimolecular layers. *Journal of the American Chemical Society* 60, 309-319.

Bursali, E.A., Cavas, L., Seki, Y., Bozkurt, S.S., Yurdakoc, M., 2009. Sorption of boron by invasive marine seaweed: *Caulerpa racemosa* var. *cylindracea*. *Chemical Engineering Journal* 150, 385-390.

Butterwick, L., Oude, N., Raymond, K., 1989. Safety assessment of boron in aquatic and terrestrial environments. *Ecotoxicology and Environmental Safety* 17, 339-371.

Calmon, C., 1973. Trace heavy metal removal by ion exchange. *Traces of heavy metals in water: Removal processes and monitoring*, EPA - 902.

- Canamero, P.F., de la Fuente, J.L., Madruga, E.L., Fernandez-Garcia, M., 2004. Atom transfer radical polymerization of glycidyl methacrylate: A functional monomer. *Macromolecular Chemistry & Physics* 205, 2221-2228.
- Cao, Y., Tan, H.M., 2006. Preparation and properties of microporous cellulose membranes from novel cellulose/aqueous sodium hydroxide solutions. *Journal of Applied Polymer Science* 102, 920-926.
- Cengeloglu, Y., Tor, A., Arslan, G., Ersoz, M., Gezgin, S., 2007. Removal of boron from aqueous solution by using neutralized red mud. *Journal of Hazardous Materials* 142, 412-417.
- Chan, K., Gleason, K.K., 2005. Photoinitiated chemical vapor deposition of polymeric thin films using a volatile photoinitiator. *Langmuir* 21, 11773-11779.
- Chen, J.P., 1997. Sorption of metal ions from aqueous solutions: Equilibrium and kinetics, and transport. Thesis (PhD), Georgia Institute of Technology, Atlanta, GA.
- Chen, J.P., Lin, M.S., 2001a. Equilibrium and kinetics of metal ion adsorption onto a commercial H-type granular activated carbon: Experimental and modeling studies. *Water Research* 35, 2385-2394.
- Chen, J.P., Lin, M.S., 2001b. Surface charge and metal ion adsorption on an H-type activated carbon: experimental observation and modeling simulation by the surface complex formation approach. *Carbon* 39, 1491-1504.
- Chen, J.P., Tendeyong, F., Yiacoumi, S., 1997. Equilibrium and kinetic studies of copper ion uptake by calcium alginate. *Environmental Science & Technology* 31, 1433-1439.
- Chen, J.P., Wu S.N., 2004. Simultaneous adsorption of copper ions and humic acid onto an activated carbon. *Journal of Colloid and Interface Science* 280, 334-342.
- Chen, J.P., Wei, Y.T., Zheng, Y.M. Chemically-modified chitosan beads. US provisional patent No. 61/355,057. Filing Date: June 15, 2010

Chen, J.P., Yang, L., 2005. Chemical modification of *Sargassum* sp for prevention of organic leaching and enhancement of uptake during metal biosorption. *Industrial & Engineering Chemistry Research* 44, 9931-9942.

Cheng, R.C., Wang, H.C., Beuhler, M.D., 1994. Enhanced coagulation for arsenic removal. *Journal American Water Works Association* 86, 79-90.

Cheng, Z.Q., Van Geen, A., Louis, R., Nikolaidis, N., Bailey, R., 2005. Removal of methylated arsenic in groundwater with iron filings. *Environmental Science & Technology* 39, 7662-7666.

Chetelat, B., Gaillardet, J., 2005. Boron isotopes in the Seine River, France: A probe of anthropogenic contamination. *Environmental Science & Technology* 39, 2486-2493.

Choi, J.W., Choi, N.C., Lee, S.J., Kim, D.J., 2007. Novel three-stage kinetic model for aqueous benzene adsorption on activated carbon. *Journal of Colloid and Interface Science* 314, 367-372.

Choi, W.W., Chen, K.Y., 1979. Evaluation of boron removal by adsorption on solids. *Environmental Science & Technology* 13, 189-196.

Choong, T.S.Y., Chuah, T.G., Robiah, Y., Koay, F.L.G., Azni, I., 2007. Arsenic toxicity, health hazards and removal techniques from water: an overview. *Desalination* 217, 139-166.

Coughlin, J.R., 1998. Sources of human exposure - Overview of water supplies as sources of boron. *Biological Trace Element Research* 66, 87-100.

Cullen, W.R., Reimer, K.J., 1989. Arsenic speciation in the environment. *Chemical Reviews* 89, 713-764.

Cussler, E.L., 1997. *Diffusion : mass transfer in fluid systems*. Cambridge University Press, New York.

Dambies, L., Salinaro, R., Alexandratos, S.D., 2004. Immobilized N-methyl-D-glucamine as an arsenate-selective resin. *Environmental Science & Technology* 38, 6139-6146.

- Deng, S.B., Li, Z.J., Huang, J., Yu, G., 2010. Preparation, characterization and application of a Ce-Ti oxide adsorbent for enhanced removal of arsenate from water. *Journal of Hazardous Materials* 179, 1014-1021.
- Deng, S.B., Yu, G., Xie, S.H., Yu, Q., Huang, J., Kuwaki, Y., Iseki, M., 2008. Enhanced adsorption of arsenate on the aminated fibers: Sorption behavior and uptake mechanism. *Langmuir* 24, 10961-10967.
- Di Natale, F., Erto, A., Lancia, A., Musmarra, D., 2008. Experimental and modelling analysis of As(V) ions adsorption on granular activated carbon. *Water Research* 42, 2007-2016.
- Dutta, P.K., Ray, A.K., Sharma, V.K., Millero, F.J., 2004. Adsorption of arsenate and arsenite on titanium dioxide suspensions. *Journal of Colloid and Interface Science* 278, 270-275.
- Dyer, S.D., Caprara, R.J., 1997. A method for evaluating consumer product ingredient contributions to surface and drinking water: Boron as a test case. *Environmental Toxicology & Chemistry* 16, 2070-2081.
- Edwards, M., 1994. Chemistry of arsenic removal during coagulation and Fe-Mn oxidation. *Journal American Water Works Association* 86, 64-78.
- Egneus, B., Uppstrom, L., 1973. Extraction of boric-acid with aliphatic 1,3-diols and other chelating-agents. *Analytica Chimica Acta* 66, 211-229.
- Eguez, H.E., Cho, E.H., 1987. Adsorption of arsenic on activated-charcoal. *Journal of Metals* 39, 38-41.
- Emiroglu, O., Cicek, A., Arslan, N., Aksan, S., Ruzgar, M., 2010. Boron concentration in water, sediment and different organisms around large borate deposits of Turkey. *Bulletin of Environmental Contamination & Toxicology* 84, 427-431.
- Figoli, A., Cassano, A., Criscuoli, A., Mozumder, M.S.I., Uddin, M.T., Islam, M.A., Drioli, E., 2010. Influence of operating parameters on the arsenic removal by nanofiltration. *Water Research* 44, 97-104.
- Garcia-Soto, M.D.D., Camacho, E.M., 2005. Boron removal by processes of

chemisorption. *Solvent Extraction Ion Exchange* 23, 741-757.

Garcia-Soto, M.D.D., Camacho, E.M., 2006. Boron removal by means of adsorption with magnesium oxide. *Separation and Purification Technology* 48, 36-44.

Gazi, M., Bicak, N., 2007. Selective boron extraction by polymer supported 2-hydroxyethylamino propylene glycol functions. *Reactive & Functional Polymers* 67, 936-942.

Gazi, M., Galli, G., Bicak, N., 2008. The rapid boron uptake by multi-hydroxyl functional hairy polymers. *Separation and Purification Technology* 62, 484-488.

Gazi, M., Senkal, B., Bicak, N., 2004. Modification of crosslinked poly(styrene) based polymers for boron-specific extraction. *Macromolecular Symposia* 217, 215-221.

Geffen, N., Semiat, R., Eisen, M.S., Balazs, Y., Katz, I., Dosoretz, C.G., 2006. Boron removal from water by complexation to polyol compounds. *Journal of Membrane Science* 286, 45-51.

Gemici, U., Tarcan, G., 2002. Distribution of boron in thermal waters of western Anatolia, Turkey, and examples of their environmental impacts. *Environmental Geology* 43, 87-98.

Gemici, U., Tarcan, G., Helvacı, C., Somay, A.M., 2008. High arsenic and boron concentrations in groundwaters related to mining activity in the Bigadic borate deposits (Western Turkey). *Applied Geochemistry* 23, 2462-2476.

Gerente, C., Andres, Y., McKay, G., Le Cloirec, P., Removal of arsenic(V) onto chitosan: From sorption mechanism explanation to dynamic water treatment process. *Chemical Engineering Journal* 158, 593-598.

Ghimire, K.N., Inoue, K., Makino, K., Miyajima, T., 2002. Adsorptive removal of arsenic using orange juice residue. *Separation Science and Technology* 37, 2785-2799.

Glenn, S.M., Lester, L.J., 2010. An analysis of the relationship between land use and arsenic, vanadium, nitrate and boron contamination in the Gulf Coast aquifer of Texas.

Journal of Hydrology 389, 214-226.

Glueckstern, P., Priel, M., 2003. Optimization of boron removal in old and new SWRO systems. *Desalination* 156, 219-228.

Goldberg, S., 2005. Inconsistency in the triple layer model description of ionic strength dependent boron adsorption. *Journal of Colloid and Interface Science* 285, 509-517.

Goldberg, S., Forster, H.S., Heick, E.L., 1993. Boron adsorption mechanisms on oxides, clay-minerals, and soils inferred from ionic-strength effects. *Soil Science Society of America Journal* 57, 704-708.

Goldberg, S., Johnston, C.T., 2001. Mechanisms of arsenic adsorption on amorphous oxides evaluated using macroscopic measurements, vibrational spectroscopy, and surface complexation modeling. *Journal of Colloid and Interface Science* 234, 204-216.

Gomes, J.A.G., Daida, P., Kesmez, M., Weir, M., Moreno, H., Parga, J.R., Irwin, G., McWhinney, H., Grady, T., Peterson, E., Cocke, D.L., 2007. Arsenic removal by electrocoagulation using combined Al-Fe electrode system and characterization of products. *Journal of Hazardous Materials* 139, 220-231.

Gu, B.H., Schmitt, J., Chen, Z.H., Liang, L.Y., McCarthy, J.F., 1994. Adsorption and desorption of natural organic-matter on iron-oxide - Mechanisms and models. *Environmental Science & Technology* 28, 38-46.

Gu, Z.M., Fang, J., Deng, B.L., 2005. Preparation and evaluation of GAC-based iron-containing adsorbents for arsenic removal. *Environmental Science & Technology* 39, 3833-3843.

Guo, H.M., Li, Y., Zhao, K., 2010. Arsenate removal from aqueous solution using synthetic siderite. *Journal of Hazardous Materials* 176, 174-180.

Gupta, A., Chauhan, V.S., Sankararamkrishnan, N., 2009. Preparation and evaluation of iron-chitosan composites for removal of As(III) and As(V) from arsenic contaminated real life groundwater. *Water Research* 43, 3862-3870.

- Hamdaoui, O., Saoudi, F., Chiha, M., Naffrechoux, E., 2008. Sorption of malachite green by a novel sorbent, dead leaves of plane tree: Equilibrium and kinetic modeling. *Chemical Engineering Journal* 143, 73-84.
- Hameed, B.H., El-Khaiary, M.I., 2008. Batch removal of malachite green from aqueous solutions by adsorption on oil palm trunk fibre: Equilibrium isotherms and kinetic studies. *Journal of Hazardous Materials* 154, 237-244.
- Harisha, R.S., Hosamani, K.M., Keri, R.S., Nataraj, S.K., Aminabhavi, T.M., 2010. Arsenic removal from drinking water using thin film composite nanofiltration membrane. *Desalination* 252, 75-80.
- Hassan, K.M., Fukuhara, T., Hai, F.I., Bari, Q.H., Islam, K.M.S., 2009. Development of a bio-physicochemical technique for arsenic removal from groundwater. *Desalination* 249, 224-229.
- Hayes, K.F., Papelis, C., Leckie, J.O., 1988. Modeling Ionic-Strength Effects on Anion Adsorption at Hydrous Oxide Solution Interfaces. *Journal of Colloid and Interface Science* 125, 717-726.
- Hering, J.G., Chen, P.Y., Wilkie, J.A., Elimelech, M., 1997. Arsenic removal from drinking water during coagulation. *Journal of Environmental Engineering-Asce* 123, 800-807.
- Hilal, N., Kim, G.J., Somerfield, C., 2010. Boron removal from saline water: A comprehensive review. *Desalination In Press, Corrected Proof*.
- Ho, Y.S., McKay, G., 1999. Pseudo-second order model for sorption processes. *Process Biochemistry* 34, 451-465.
- Howe, P.D., 1998. A review of boron effects in the environment. *Biological Trace Element Research* 66, 153-166.
- Hristovski, K.D., Westerhoff, P.K., Moller, T., Sylvester, P., 2009. Effect of synthesis conditions on nano-iron (hydr)oxide impregnated granulated activated carbon. *Chemical Engineering Journal* 146, 237-243.
- Inukai, Y., Tanaka, Y., Matsuda, T., Mihara, N., Yamada, K., Nambu, N., Itoh, O., Doi,

- T., Kaida, Y., Yasuda, S., 2004. Removal of boron(III) by N-methylglucamine-type cellulose derivatives with higher adsorption rate. *Analytica Chimica Acta* 511, 261-265.
- Itakura, T., Sasai, R., Itoh, H., 2005. Precipitation recovery of boron from wastewater by hydrothermal mineralization. *Water Research* 39, 2543-2548.
- Jacob, C., 2007. Seawater desalination: Boron removal by ion exchange technology. *Desalination* 205, 47-52.
- Jain, C.K., Ali, I., 2000. Arsenic: Occurrence, toxicity and speciation techniques. *Water Research* 34, 4304-4312.
- Jeong, Y., Fan, M., Singh, S., Chuang, C.L., Saha, B., van Leeuwen, H., 2007. Evaluation of iron oxide and aluminum oxide as potential arsenic(V) adsorbents. *Chemical Engineering and Processing* 46, 1030-1039.
- Jin, Y.Z., Gao, C., Kroto, H.W., Maekawa, T., 2005. Polymer-grafted carbon spheres by surface-initiated atom transfer radical polymerization. *Macromolecular Rapid Communications* 26, 1133-1139.
- Jing, C.Y., Meng, X.G., Calvache, E., Jiang, G.B., 2009. Remediation of organic and inorganic arsenic contaminated groundwater using a nanocrystalline TiO<sub>2</sub>-based adsorbent. *Environmental Pollution* 157, 2514-2519.
- Kabay, N., Arar, O., Acar, F., Ghazal, A., Yuksel, U., Yuksel, M., 2008a. Removal of boron from water by electrodialysis: effect of feed characteristics and interfering ions. *Desalination* 223, 63-72.
- Kabay, N., Guler, E., Bryjak, M., 2010. Boron in seawater and methods for its separation - A review. *Desalination* 261, 212-217.
- Kabay, N., Sarp, S., Yuksel, M., Kitis, M., Koseoglu, H., Arar, O., Bryjak, M., Semiat, R., 2008b. Removal of boron from SWRO permeate by boron selective ion exchange resins containing N-methyl glucamine groups. *Desalination* 223, 49-56.
- Kaftan, O., Acikel, M., Eroglu, A.E., Shahwan, T., Artok, L., Ni, C.Y., 2005. Synthesis, characterization and application of a novel sorbent, glucamine-modified



MCM-41, for the removal/preconcentration of boron from waters. *Analytica Chimica Acta* 547, 31-41.

Kanel, S.R., Greneche, J.M., Choi, H., 2006. Arsenic(V) removal from groundwater using nano scale zero-valent iron as a colloidal reactive barrier material. *Environmental Science & Technology* 40, 2045-2050.

Karahan, S., Yurdakoc, M., Seki, Y., Yurdakoc, K., 2006. Removal of boron from aqueous solution by clays and modified clays. *Journal of Colloid and Interface Science* 293, 36-42.

Karakaplan, M., Tural, S., Tural, B., Turgut, Y., Hosgoren, H., 2004. The solvent extraction of boron with synthesized aliphatic 1,3-diols: Stripping and extraction behavior of boron by 2,2,5-trimethyl-1,3-hexanediol. *Solvent Extraction Ion Exchange* 22, 897-911.

Kenyon, E.M., Hughes, M.F., 2001. A concise review of the toxicity and carcinogenicity of dimethylarsinic acid. *Toxicology* 160, 227-236.

Kinoshita, A., Wanibuchi, H., Morimura, K., Wei, M., Nakae, D., Arai, T., Minowa, O., Noda, T., Nishimura, S., Fukushima, S., 2007. Carcinogenicity of dimethylarsinic acid in Ogg1-deficient mice. *Cancer Science* 98, 803-814.

Kluczka, J., Ciba, J., Trojanowska, J., Zolotajkin, M., Turek, M., Dydo, P., 2007a. Removal of boron dissolved in water. *Environmental Progress* 26, 71-77.

Kluczka, J., Trojanowska, J., Zolotajkin, M., Ciba, J., Turek, M., Dydo, P., 2007b. Boron removal from wastewater using adsorbents. *Environmental Technology* 28, 105-113.

Kostal, J., Yang, R., Wu, C.H., Mulchandani, A., Chen, W., 2004. Enhanced arsenic accumulation in engineered bacterial cells expressing ArsR. *Applied and Environmental Microbiology* 70, 4582-4587.

Kosutic, K., Furac, L., Sipos, L., Kunst, B., 2005. Removal of arsenic and pesticides from drinking water by nanofiltration membranes. *Separation and Purification Technology* 42, 137-144.

- Lafferty, B.J., Loeppert, R.H., 2005. Methyl arsenic adsorption and desorption behavior on iron oxides. *Environmental Science & Technology* 39, 2120-2127.
- Lakshmipathiraj, P., Prabhakar, S., Raju, G.B., 2010. Studies on the electrochemical decontamination of wastewater containing arsenic. *Separation and Purification Technology* 73, 114-121.
- Lazaridis, N.K., Asouhidou, D.D., 2003. Kinetics of sorptive removal of chromium(VI) from aqueous solutions by calcined Mg-Al-CO<sub>3</sub> hydrotalcite. *Water Research* 37, 2875-2882.
- Lim, S.F., Chen, J.P., 2007. Synthesis of an innovative calcium-alginate magnetic sorbent for removal of multiple contaminants. *Applied Surface Science* 253, 5772-5775.
- Lim, S.F., Zheng, Y.M., Chen, J.P., 2009. Organic arsenic adsorption onto a magnetic sorbent. *Langmuir* 25, 4973-4978.
- Lim, S.F., Zheng, Y.M., Zou, S.W., Chen, J.P., 2008. Characterization of copper adsorption onto an alginate encapsulated magnetic sorbent by a combined FT-IR, XPS and mathematical modeling study. *Environmental Science & Technology* 42, 2551-2556.
- Liu, G.J., Zhang, X.R., McWilliams, L., Talley, J.W., Neal, C.R., 2008a. Influence of ionic strength, electrolyte type, and NOM on As(V) adsorption onto TiO<sub>2</sub>. *Journal of Environmental Science and Health Part a-Toxic/Hazardous Substances & Environmental Engineering* 43, 430-436.
- Liu, H.N., Ye, X.S., Li, Q., Kim, T., Qing, B.J., Guo, M., Ge, F., Wu, Z.J., Lee, K., 2009a. Boron adsorption using a new boron-selective hybrid gel and the commercial resin D564. *Colloids and Surfaces a-Physicochemical and Engineering Aspects* 341, 118-126.
- Liu, P.S., Chen, Q., Liu, X., Yuan, B., Wu, S.S., Shen, J., Lin, S.C., 2009b. Grafting of Zwitterion from Cellulose Membranes via ATRP for Improving Blood Compatibility. *Biomacromolecules* 10, 2809-2816.
- Liu, P.S., Chen, Q., Wu, S.S., Shen, J., Lin, S.C., 2010a. Surface modification of cellulose membranes with zwitterionic polymers for resistance to protein adsorption

and platelet adhesion. *Journal of Membrane Science* 350, 387-394.

Liu, S.L., Zeng, J.A., Tao, D.D., Zhang, L.N., 2010b. Microfiltration performance of regenerated cellulose membrane prepared at low temperature for wastewater treatment. *Cellulose* 17, 1159-1169.

Liu, Y., Gaskell, K.J., Cheng, Z.H., Yu, L.L., Payne, G.F., 2008b. Chitosan-coated electrodes for bimodal sensing: Selective post-electrode film reaction for spectroelectrochemical analysis. *Langmuir* 24, 7223-7231.

Lorenzen, L., Vandeventer, J.S.J., Landi, W.M., 1995. Factors affecting the mechanism of the adsorption of arsenic species on activated carbon. *Minerals Engineering* 8, 557-569.

Lyday, P.A. 2000. Boron. U.S. Geological Survey.

Ma, Z.Y., Guan, Y.P., Liu, H.Z., 2005. Synthesis and characterization of micron-sized monodisperse superparamagnetic polymer particles with amino groups. *Journal of Polymer Science Part a-Polymer Chemistry* 43, 3433-3439.

Mak, M.S.H., Rao, P.H., Lo, I.M.C., 2009. Effects of hardness and alkalinity on the removal of arsenic(V) from humic acid-deficient and humic acid-rich groundwater by zero-valent iron. *Water Research* 43, 4296-4304.

Mandal, B.K., Suzuki, K.T., 2002. Arsenic round the world: a review. *Talanta* 58, 201-235.

Mao, Y., Gleason, K.K., 2004. Hot filament chemical vapor deposition of poly(glycidyl methacrylate) thin films using tert-butyl peroxide as an initiator. *Langmuir* 20, 2484-2488.

Matsumoto, M., Kondo, K., Hirata, M., Kokubu, S., Hano, T., Takada, T., 1997. Recovery of boric acid from wastewater by solvent extraction. *Separation Science and Technology* 32, 983-991.

Matsumoto, M., Matsui, T., Kondo, K., 1999. Adsorption mechanism of boric acid on chitosan resin modified by saccharides. *Journal of Chemical Engineering of Japan* 32,

190-196.

McBride, M.B., 1997. A critique of diffuse double layer models applied to colloid and surface chemistry. *Clays & Clay Minerals* 45, 598-608.

Melitas, N., Conklin, M., Farrell, J., 2002. Electrochemical study of arsenate and water reduction on iron media used for arsenic removal from potable water. *Environmental Science & Technology* 36, 3188-3193.

Mellor, J.W., 1922. A comprehensive treatise on inorganic and theoretical chemistry. Longmans, Green, London, New York.

Mohan, D., Pittman, C.U., 2007. Arsenic removal from water/wastewater using adsorbents - A critical review. *Journal of Hazardous Materials* 142, 1-53.

Molina, L., Sanchez-Martos, F., Pulido-Bosch, A., Vallejos, A., 2003. Origin of boron from a complex aquifer in southeast of Spain. *Environmental Geology* 44, 301-307.

Mondal, P., Majumder, C.B., Mohanty, B., 2008. Growth of three bacteria in arsenic solution and their application for arsenic removal from wastewater. *Journal of Basic Microbiology* 48, 521-525.

Moreira, M.J., Ferreira, L.M., 2005. Kinetic studies for sorption of amino acids using a strong anion-exchange resin - Effect of ionic strength. *Journal of Chromatography A* 1092, 101-106.

Moulder, J.F.S., W. F.; Sobol, P. E.; Bomben, K. D., 1992. Handbook of X-ray photoelectron spectroscopy: a reference book of standard spectra for identification and interpretation of XPS data. Perkin-Elmer Corporation, Physical Electronics Division, Eden Prairie, Minn.

Muetterties, E.L., 1967. The chemistry of boron and its compounds. John Wiley & Sons, Inc: New York.

Naday, N., 1999. Boron removal from seawater reverse osmosis permeate utilizing selective ion exchange resin. *Desalination* 124, 131-135.

- Ning, R.Y., 2002. Arsenic removal by reverse osmosis. *Desalination* 143, 237-241.
- Nriagu, J.O., Bhattacharya, P., Mukherjee, A.B., Bundschuh, J., Zevenhoven, R., Loeppert, R.H., 2007. Arsenic in soil and groundwater: an overview. *Trace Metals and other Contaminants in the environment* 9, 3-60.
- Onyango, M.S., Kojima, Y., Aoyi, O., Bernardo, E.C., Matsuda, H., 2004. Adsorption equilibrium modeling and solution chemistry dependence of fluoride removal from water by trivalent-cation-exchanged zeolite F-9. *J. Colloid Interface Sci.* 279, 341-350.
- Oo, M.H., Song, L.F., 2009. Effect of pH and ionic strength on boron removal by RO membranes. *Desalination* 246, 605-612.
- Oren, Y., Linder, C., Daltrophe, N., Mirsky, Y., Skorka, J., Kedem, O., 2006. Boron removal from desalinated seawater and brackish water by improved electrodialysis. *Desalination* 199, 52-54.
- Ozturk, N., Kavak, D., 2004. Boron removal from aqueous solutions by adsorption on waste sepiolite and activated waste sepiolite using full factorial design. *Adsorption-Journal of the International Adsorption Society* 10, 245-257.
- Pan, B.C., Du, W., Zhang, W.M., Zhang, X., Zhang, Q.R., Pan, B.J., Lv, L., Zhang, Q.X., Chen, J.L., 2007. Improved adsorption of 4-nitrophenol onto a novel hyper-cross-linked polymer. *Environmental Science & Technology* 41, 5057-5062.
- Pan, K., Zhang, X.W., Cao, B., 2010a. Surface-initiated atom transfer radical polymerization of regenerated cellulose membranes with thermo-responsive properties. *Polymer International* 59, 733-737.
- Pan, K., Zhang, X.W., Ren, R.M., Cao, B., 2010b. Double stimuli-responsive membranes grafted with block copolymer by ATRP method. *Journal of Membrane Science* 356, 133-137.
- Parga, J.R., Cocke, D.L., Valenzuela, J.L., Gomes, J.A., Kesmez, M., Irwin, G., Moreno, H., Weir, M., 2005. Arsenic removal via electrocoagulation from heavy metal contaminated groundwater in La Comarca Lagunera Mexico. *Journal of Hazardous Materials* 124, 247-254.

- Parks, J.L., Edwards, M., 2005. Boron in the environment. *Critical Reviews in Environmental Science and Technology* 35, 81-114.
- Parschova, H., Mistova, E., Matejka, Z., Jelinek, L., Kabay, N., Kauppinen, P., 2007. Comparison of several polymeric sorbents for selective boron removal from reverse osmosis permeate. *React. Funct. Polym.* 67, 1622-1627.
- Peak, D., Luther, G.W., Sparks, D.L., 2003. ATR-FTIR spectroscopic studies of boric acid adsorption on hydrous ferric oxide. *Geochim. Cosmochim. Acta* 67, 2551-2560.
- Pedersen, A.J., Kristensen, I.V., Ottosen, L.M., Ribeiro, A.B., Villumsen, A., 2005. Electrodialytic remediation of CCA-treated waste wood in pilot scale. *Engineering Geology* 77, 331-338.
- Pena, M.E., Korfiatis, G.P., Patel, M., Lippincott, L., Meng, X.G., 2005. Adsorption of As(V) and As(III) by nanocrystalline titanium dioxide. *Water Research* 39, 2327-2337.
- Peraniemi, S., Hannonen, S., Mustalahti, H., Ahlgren, M., 1994. Zirconium-loaded activated-charcoal as an adsorbent for arsenic, selenium and mercury. *Fresenius Journal of Analytical Chemistry* 349, 510-515.
- Pokhrel, D., Viraraghavan, T., 2006. Arsenic removal from an aqueous solution by a modified fungal biomass. *Water Research* 40, 549-552.
- Pokhrel, D., Viraraghavan, T., 2008. Organic arsenic removal from an aqueous solution by iron oxide-coated fungal biomass: An analysis of factors influencing adsorption. *Chemical Engineering Journal* 140, 165-172.
- Prats, D., Chillon-Arias, M.F., Rodriguez-Pastor, M., 2000. Analysis of the influence of pH and pressure on the elimination of boron in reverse osmosis. *Desalination* 128, 269-273.
- Qi, T., Sonoda, A., Makita, Y., Kanoh, H., Ooi, K., Hirotsu, T., 2002. Synthesis and borate uptake of two novel chelating resins. *Industrial & Engineering Chemistry Research* 41, 133-138.

Qiu, H., Lv, L., Pan, B.C., Zhang, Q.J., Zhang, W.M., Zhang, Q.X., 2009. Critical review in adsorption kinetic models. *Journal of Zhejiang University-Science A* 10, 716-724.

Rajakovic, L.V., Ristic, M.D., 1996. Sorption of boric acid and borax by activated carbon impregnated with various compounds. *Carbon* 34, 769-774.

Rakhmatullina, E., Manton, A., Burgi, T., Malinova, V., Meier, W., 2009. Solid-supported amphiphilic triblock copolymer membranes grafted from gold surface. *Journal of Polymer Science Part a-Polymer Chemistry* 47, 1-13.

Ramesh, A., Hasegawa, H., Maki, T., Ueda, K., 2007. Adsorption of inorganic and organic arsenic from aqueous solutions by polymeric Al/Fe modified montmorillonite. *Separation and Purification Technology* 56, 90-100.

Redman, A.D., Macalady, D.L., Ahmann, D., 2002. Natural organic matter affects arsenic speciation and sorption onto hematite. *Environmental Science & Technology* 36, 2889-2896.

Remy, P., Muhr, H., Plasari, E., Ouerdiane, I., 2005. Removal of boron from wastewater by precipitation of a sparingly soluble salt. *Environmental Progress* 24, 105-110.

Ristic, M.D., Rajakovic, L.V., 1996. Boron removal by anion exchangers impregnated with citric and tartaric acids. *Separation Science and Technology* 31, 2805-2814.

Rodriguez-Lopez, G., Marcos, M.D., Martinez-Manez, R., Sancenon, L., Soto, J., Villaescusa, L.A., Beltran, D., Amoros, P., 2004. Efficient boron removal by using mesoporous matrices grafted with saccharides. *Chemical Communications*, 2198-2199.

Ruthven, D.M., 1984. *Principles of adsorption and adsorption processes*. Wiley, New York.

Sabarudin, A., Oshita, K., Oshima, M., Motomizu, S., 2005. Synthesis of cross-linked chitosan possessing N-methyl-D-glucamine moiety (CCTS-NMDG) for adsorption/concentration of boron in water samples and its accurate measurement by ICP-MS and ICP-AES. *Talanta* 66, 136-144.

- Salameh, Y., Al-Lagtah, N., Ahmad, M.N.M., Allen, S.J., Walker, G.M., 2010. Kinetic and thermodynamic investigations on arsenic adsorption onto dolomitic sorbents. *Chemical Engineering Journal* 160, 440-446.
- Salentine, C.G., 1983. High-field B-11 NMR of alkali borates - aqueous polyborate equilibria. *Inorganic Chemistry* 22, 3920-3924.
- Salim, E.I., Wanibuchi, H., Morimura, K., Wei, M., Mitsuhashi, M., Yoshida, K., Endo, G., Fukushima, S., 2003. Carcinogenicity of dimethylarsinic acid in p53 heterozygous knockout and wild-type C57BL/6J mice. *Carcinogenesis* 24, 335-342.
- Sanchez-Rodas, D., Gomez-Ariza, J.L., Giraldez, I., Velasco, A., Morales, E., 2005. Arsenic speciation in river and estuarine waters from southwest Spain. *Science of the Total Environment* 345, 207-217.
- Scott, K.N., Green, J.F., Do, H.D., McLean, S.J., 1995. Arsenic removal by coagulation. *Journal American Water Works Association* 87, 114-126.
- Senkal, B.F., Bicak, N., 2003. Polymer supported iminodipropylene glycol functions for removal of boron. *Reactive & Functional Polymers* 55, 27-33.
- Simonnot, M.O., Castel, C., Nicolai, M., Rosin, C., Sardin, M., Jauffret, H., 2000. Boron removal from drinking water with a boron selective resin: Is the treatment really selective? *Water Research* 34, 109-116.
- Singh, N., Wang, J., Ulbricht, M., Wickramasinghe, S.R., Husson, S.M., 2008. Surface-initiated atom transfer radical polymerization: A new method for preparation of polymeric membrane adsorbers. *Journal of Membrane Science* 309, 64-72.
- Smedley, P.L., Kinniburgh, D.G., 2002. A review of the source, behaviour and distribution of arsenic in natural waters. *Applied Geochemistry* 17, 517-568.
- Smith, B.M., Todd, P., Bowman, C.N., 1995. Boron removal by polymer-assisted ultrafiltration. *Separation Science and Technology* 30, 3849-3859.
- Socrates, G., 2000. Infrared and Raman characteristic group frequencies: tables and



charts. Wiley, New York.

Stumm, W., Morgan, J.J., 1996. Aquatic chemistry: Chemical equilibria and rates in natural waters, 3<sup>rd</sup> ed., Wiley.

Su, C.M., Puls, R.W., 2001. Arsenate and arsenite removal by zerovalent iron: Kinetics, redox transformation, and implications for in situ groundwater remediation. *Environmental Science & Technology* 35, 1487-1492.

Su, C.M., Suarez, D.L., 1995. Coordination of adsorbed boron - A FTIR spectroscopic study. *Environmental Science & Technology* 29, 302-311.

Subramanian, R., Sukumar, A., 1988. Biological Reference Materials and analysis of toxic elements. *Fresenius Zeitschrift Fur Analytische Chemie* 332, 623-626.

Tang, F., Zhang, L.F., Zhu, J., Cheng, Z.P., Zhu, X.L., 2009. Surface functionalization of chitosan nanospheres via surface-initiated AGET ATRP mediated by iron catalyst in the presence of limited amounts of air. *Industrial & Engineering Chemistry Research* 48, 6216-6223.

Teclu, D., Tivchev, G., Laing, M., Wallis, M., 2008. Bioremoval of arsenic species from contaminated waters by sulphate-reducing bacteria. *Water Research* 42, 4885-4893.

Thirunavukkarasu, O.S., Viraraghavan, T., Subramanian, K.S., Tanjore, S., 2002. Organic arsenic removal from drinking water. *Urban Water* 4, 415-421.

Tien, C., 1994. Adsorption calculations and modeling. Butterworth-Heinemann, Boston.

Tseng, C.H., Huang, Y.K., Huang, Y.L., Chung, C.J., Yang, M.H., Chen, C.J., Hsueh, Y.M., 2005. Arsenic exposure, urinary arsenic speciation, and peripheral vascular disease in blackfoot disease-hyperendemic villages in Taiwan. *Toxicology and Applied Pharmacology* 206, 299-308.

Vaclavikova, M., Gallios, G.P., Hredzak, S., Jakabsky, S., 2008. Removal of arsenic from water streams: An overview of available techniques. *Clean Technologies and Environmental Policy* 10, 89-95.

Vasudevan, S., Sheela, S.M., Lakshmi, J., Sozhan, G., 2010. Optimization of the process parameters for the removal of boron from drinking water by electrocoagulation - a clean technology. *Journal of Chemical Technology & Biotechnology* 85, 926-933.

Vijayaraghavan, K., Arun, M., Joshi, U.M., Balasubramanian, R., 2009. Biosorption of As(V) onto the shells of the crab (*Portunus sanguinolentus*): Equilibrium and kinetic studies. *Industrial & Engineering Chemistry Research* 48, 3589-3594.

Walker, M., Seiler, R.L., Meinert, M., 2008. Effectiveness of household reverse-osmosis systems in a Western US region with high arsenic in groundwater. *Science of the Total Environment* 389, 245-252.

Wang, L., Qi, T., Gao, Z., Zhang, Y., Chu, J., 2007. Synthesis of N-methylglucamine modified macroporous poly(GMA-co-TRIM) and its performance as a boron sorbent. *Reactive & Functional Polymers* 67, 202-209.

Wang, L., Qi, T., Zhang, Y., 2006. Novel organic-inorganic hybrid mesoporous materials for boron adsorption. *Colloids and Surfaces a-Physicochemical and Engineering Aspects* 275, 73-78.

Wang, S.L., Zhao, X.Y., 2009. On the potential of biological treatment for arsenic contaminated soils and groundwater. *Journal of Environmental Management* 90, 2367-2376.

Wasay, S.A., Haron, J., Tokunaga, S., 1996. Adsorption of fluoride, phosphate, and arsenate ions on lanthanum impregnated silica gel. *Water Environment Research* 68, 295-300.

World Health Organization, 2004. *Guidelines for drinking-water quality*, vol. 1, 3rd ed. World Health Organization, Geneva.

Wu, H.X., Tong, R., Qiu, X.Q., Yang, H.F., Lin, Y.H., Cai, R.F., Qian, S.X., 2007. Functionalization of multiwalled carbon nanotubes with polystyrene under atom transfer radical polymerization conditions. *Carbon* 45, 152-159.

Xu, D.N., Peak, D., 2007. Adsorption of boric acid on pure and humic acid coated

am-Al(OH)(3): A boron K-edge XANES study. *Environmental Science & Technology* 41, 903-908.

Xu, F.J., Cai, Q.J., Kang, E.T., Neoh, K.G., 2005. Covalent graft polymerization and block copolymerization initiated by the chlorinated SiO<sub>2</sub> (SiO<sub>2</sub>-Cl) moieties of glass and oriented single crystal silicon surfaces. *Macromolecules* 38, 1051-1054.

Xu, R.J., Xing, X.R., Zhou, Q.F., Jiang, G.B., Wei, F.S., 2010. Investigations on boron levels in drinking water sources in China. *Environmental Monitoring and Assessment* 165, 15-25.

Xu, T.L., Cai, Y., O'Shea, K.E., 2007. Adsorption and photocatalyzed oxidation of methylated arsenic species in TiO<sub>2</sub> suspensions. *Environmental Science & Technology* 41, 5471-5477.

Xu, Y., Jiang, J.Q., 2008. Technologies for boron removal. *Industrial & Engineering Chemistry Research* 47, 16-24.

Xu, Z.H., Jing, C.Y., Li, F.S., Meng, X.G., 2008. Mechanisms of photocatalytical degradation of monomethylarsonic and dimethylarsinic acids using nanocrystalline titanium dioxide. *Environmental Science & Technology* 42, 2349-2354.

Xue, B., Sun, Y., 2001. Protein adsorption equilibria and kinetics to a poly(vinyl alcohol)-based magnetic affinity support. *Journal of Chromatography A* 921, 109-119.

Yazicigil, Z., Oztekin, Y., 2006. Boron removal by electro dialysis with anion-exchange membranes. *Desalination* 190, 71-78.

Yilmaz, A.E., Boncukcuoglu, R., Kocakerim, M.M., 2007. A quantitative comparison between electrocoagulation and chemical coagulation for boron removal from boron-containing solution. *Journal of Hazardous Materials* 149, 475-481.

Yilmaz, A.E., Boncukcuoglu, R., Kocakerim, M.M., Keskinler, B., 2005. The investigation of parameters affecting boron removal by electrocoagulation method. *Journal of Hazardous Materials* 125, 160-165.

Yilmaz, A.E., Boncukcuoglu, R., Kocakerim, M.M., Yilmaz, M.T., Paluluoglu, C., 2008. Boron removal from geothermal waters by electrocoagulation. *Journal of*

Hazardous Materials 153, 146-151.

Yoon, K.R., Ramaraj, B., Lee, S., Yu, J.S., Choi, I.S., 2009. Surface-initiated atom-transfer radical polymerization of 3-O-methacryloyl-1,2:5,6-di-O-isopropylidene-alpha-D-glucofuranoside onto gold surface. *Journal of Biomedical Materials Research Part A* 88A, 735-740.

Yu, W.H., Kang, E.T., Neoh, K.G., 2004. Controlled grafting of well-defined epoxide polymers on hydrogen-terminated silicon substrates by surface-initiated ATRP at ambient temperature. *Langmuir* 20, 8294-8300.

Yu, W.H., Kang, E.T., Neoh, K.G., Zhu, S.P., 2003. Controlled grafting of well-defined polymers on hydrogen-terminated silicon substrates by surface-initiated atom transfer radical polymerization. *Journal of Physical Chemistry B* 107, 10198-10205.

Yuksel, S., Yurum, Y., 2010. Removal of Boron from aqueous solutions by adsorption using fly ash, zeolite, and demineralized lignite. *Separation Science Technology* 45, 105-115.

Yurdakoc, M., Seki, Y., Karahan, S., Yurdakoc, K., 2005. Kinetic and thermodynamic studies of boron removal by Siral 5, Siral 40, and Siral 80. *Journal of Colloid and Interface Science* 286, 440-446.

Zhang, F., Shi, Z.L., Chua, P.H., Kang, E.T., Neoh, K.G., 2007a. Functionalization of titanium surfaces via controlled living radical polymerization: From antibacterial surface to surface for osteoblast adhesion. *Industrial & Engineering Chemistry Research* 46, 9077-9086.

Zhang, G.S., Liu, H.J., Liu, R.P., Qu, J.H., 2009. Removal of phosphate from water by a Fe-Mn binary oxide adsorbent. *Journal of Colloid and Interface Science* 335, 168-174.

Zhang, G.S., Qu, J.H., Liu, H.J., Cooper, A.T., Wu, R.C., 2007b. CuFe<sub>2</sub>O<sub>4</sub>/activated carbon composite: A novel magnetic adsorbent for the removal of acid orange II and catalytic regeneration. *Chemosphere* 68, 1058-1066.

Zhang, G.S., Qu, J.H., Liu, H.J., Liu, R.P., Wu, R.C., 2007c. Preparation and evaluation of a novel Fe-Mn binary oxide adsorbent for effective arsenite removal.

Water Research 41, 1921-1928.

Zhang, J.S., Stanforth, R.S., Pehkonen, S.O., 2007d. Effect of replacing a hydroxyl group with a methyl group on arsenic (V) species adsorption on goethite ( $\alpha$ -FeOOH). *Journal of Colloid and Interface Science* 306, 16-21.

Zhang, O.L., Gao, N.Y., Lin, Y.C., Xu, B., Le, L.S., 2007e. Removal of Arsenic(V) from aqueous solutions using iron-oxide-coated modified activated carbon. *Water Environment Research* 79, 931-936.

Zhang, S.J., Li, X.Y., Chen, J.P., 2010a. Preparation and evaluation of a magnetite-doped activated carbon fiber for enhanced arsenic removal. *Carbon* 48, 60-67.

Zhang, S.X., Niu, H.Y., Cai, Y.Q., Zhao, X.L., Shi, Y.L., 2010b. Arsenite and arsenate adsorption on coprecipitated bimetal oxide magnetic nanomaterials:  $\text{MnFe}_2\text{O}_4$  and  $\text{CoFe}_2\text{O}_4$ . *Chemical Engineering Journal* 158, 599-607.

Zhang, Y., Yang, M., Dou, X.M., He, H., Wang, D.S., 2005. Arsenate adsorption on an Fe-Ce bimetal oxide adsorbent: Role of surface properties. *Environmental Science & Technology* 39, 7246-7253.

Zheng, G.D., Stover, H.D.H., 2003. Formation and morphology of methacrylic polymers and block copolymers tethered on polymer microspheres. *Macromolecules* 36, 1808-1814.

Zheng, Y.M., Lim, S.F., Chen, J.P., 2009. Preparation and characterization of zirconium-based magnetic sorbent for arsenate removal. *Journal of Colloid and Interface Science* 338, 22-29.

Zhou, Y., Sun, T., Chan, M., Zhang, J., Han, Z.Y., Wang, X.W., Toh, Y., Chen, J.P., Yu, H., 2005. Scalable encapsulation of hepatocytes by electrostatic spraying. *Journal of Biotechnology* 117, 99-109.

## **PUBLICATIONS**

### **Patents**

Chen, J.P., **Wei, Y.T.**, Zheng, Y.M., Chemically-modified chitosan beads.

US provisional patent No. 61/355,057

Filing Date: June 15, 2010

### **Journal Articles**

- **Wei Y.T.**, Zheng Y.M., Chen J.P., “Uptake of methylated arsenic by a polymeric adsorbent: process performance and adsorption chemistry”, *Water Res.* 2011, 45(6), 2290-2296. (5-Year Impact Factor: 4.828)
- **Wei Y.T.**, Zheng Y.M., Chen J.P., “Design and fabrication of an innovative and environmental friendly adsorbent for boron removal”, *Water Res.* 2011, 45(6), 2297-2305. (5-Year Impact Factor: 4.828)
- **Wei Y.T.**, Zheng Y.M., Chen J.P., “Functionalization of regenerated cellulose membrane via surface initiated atom transfer radical polymerization for boron removal from aqueous solution”, *Langmuir* 2011, 27 (10), 6018-6025. (5-Year Impact Factor: 4.363)
- **Wei Y.T.**, Zheng Y.M., Chen J.P., “Enhanced adsorption of arsenate onto a natural polymer-based sorbent by surface atom radical polymerization”, *J. Colloid Interf. Sci.* 2011, 356 (1), 234-239. (5-Year Impact Factor: 3.172)
- **Wei Y.T.**, Zheng Y.M., Flora J.R.V., Chen J.P., “Surface modification of crosslinked chitosan beads via atom transfer radical polymerization technology for effective boron removal: A combined FT-IR, XPS, and quantum modeling study”. (in review)

### **Conference proceedings**

- **Wei Y.T.**, Zheng Y.M., Chen J.P., “Adsorption of arsenate onto a chitosan based polymeric adsorbent”, AICHE Annual Meeting, Salt Lake City, United States of America, 2010. (presentation)
- **Wei Y.T.**, Zheng Y.M., Chen J.P., “Synthesis and characterization of novel sorbent for boron removal”, AICHE Annual Meeting, Philadelphia, United States of America, 2008. (presentation)
- Zou S.W., Zheng Y.M., Lim S.F., **Wei Y.T.**, Chen J.P. “Preparation of Zr(IV)-loaded membranes for decontamination of As(V) from aqueous solutions”, AICHE Annual Meeting, Philadelphia, United States of America, 2008. (poster)

**Book Chapter**

Nadeeshani Nanayakkara, K.G., **Wei, Y.T.**, Zheng, Y.M., Chen, J.P., 2008. Food Industry Wastewater Treatment, Handbook of Industrial and Hazardous Wastes Treatment - II, Chapter 30, Taylor and Francis & CRC Press.

Chen, J.P., Mou, H.H., Wang, L.K., Matsuura, T., **Wei, Y.T.**, 2010. Membrane Separation: Basics and Applications, Handbook of Environmental Engineering 13, Chapter 7, Humana Press.